ALLOY DESIGN FOR ELECTROSLAG WELDED RAILROAD RAIL

Milton R. Scholl
B.S., California Polytechnic State University, 1979

A thesis submitted to the faculty
of the Oregon Graduate Center
in partial fulfillment of the
requirements for the degree
Master of Science
in
Materials Science and Engineering

November, 1981

The thesis "Alloy Design for Electroslag Welded Railroad Rail" by Milton R. Scholl has been examined and approved by the following Examination Committee:

William E. Wood
Professor
Thesis Research Advisor

Jack H. Devletian
Associate Professor

Nicholas G. Eror
Associate Professor

Douglas F. Barofsky
Associate Professor

ACKNOWLEDGMENTS

I would like to express my appreciation for the help and guidance of my thesis advisors, Dr. W. E. Wood and Dr. J. H. Devletian; and to the rest of my thesis committee, Dr. N. G. Eror and Dr. D. Barofsky. I would like to thank Mr. R. C. Wiley, Chairman of the Metallurgical and Welding Engineering Department at the California Polytechnic State University, San Luis Obispo, for pointing me in the right direction from the start.

I would like to thank the Southern Pacific Transportation Company and W. E. Thomford for their assistance and support of this research project.

I would also like to thank S. Venkataraman for his help in understanding the electroslag welding process. Lastly I would like to thank my colleague-in-arms, Mr. Robert Turpin, for his help and for the long discussions on the hows and whys of electroslag welding of railroad rail.

TABLE OF CONTENTS

TABLE OF CONTENTS (cont.)

TABLE OF CONTENTS (cont.)

LIST OF TABLES

LIST OF FIGURES

LIST OF FIGURES (cont.)

LIST OF FIGURES (cont.)

LIST OF FIGURES (cont.)

LIST OF FIGURES (cont.)

ABSTRACT

Alloying of Electroslag Welded Railroad Rail

Milton R. Scholl, M.S.
Oregon Graduate Center, 1981

Supervising Professor: William E. Wood

In the last fifty years railroads have increasingly installed continuously welded rail (CWR) in mainline track, although at current installation rates there will not be significant amounts in secondary lines until the year 2000. CWR is welded in the plant using the flash-butt or oxy-acetylene welding processes and field welded using the thermit welding process. The latter is the only process presently used for repair welding rail. The chief disadvantage to the thermit welding process is its high failure rate due to inherent susceptibility to defects. Recently the electroslag welding process has been adapted to weld railroad rail. This investigation entailed the development of suitable weld metal alloys for the electroslag welding of railroad rail.

Alloys were selected according to their ability to achieve a 24 Rockwell C minimum hardness at the rail head given the weld cooling rate. Alloying elements were added via the filler wire and/or the consumable guide tube. Welds were made on 136 lb/yd standard carbon railroad rail and then sectioned for various mechanical property tests and microscopic examination.

Two alloys were developed which matched or bettered rail steel mechanical properties. A 2¼Cr-1Mo filler wire and a mild steel guide tube produced a bainitic weld metal deposit at the same strength level and a higher dynamic fracture toughness than the rail steel. A weld metal deposit produced by a high carbon (0.65 C) filler wire and a composite guide tube produced a weld whose strength was slightly less than the rail steel, but whose dynamic fracture toughness was much higher. This filler metal produced a fine pearlitic microstructure both at the rail head and at the rail base.

OBJECTIVE

Between 1933 and 1971, 36,030 miles of continuously welded rail were laid in the United States (1). The quarter-mile long rail segments are usually joined in the field by the thermit welding process which uses the strong exothermic reactivity of iron oxide and aluminum to produce the heat necessary for welding. The process is also used for field repair welding. The thermit welding process is essentially a casting process containing inherent defects which lower weld properties below those of the rail; consequently the failure rate of thermit welds is significantly higher than that of the plant welding processes, flash-butt and gas-pressure welding, even though there are more of the latter in the field than there are thermit welds (2). As an alternative to the thermit process for field welding, the electroslag welding process has been adapted for joining of railroad rail. The purpose of this investigation was the development of suitable filler metals which result in weld properties that match or better those of the rail.

CHAPTER 1

INTRODUCTION

1.1 Rail Development

Today's railroad rail has progressed a long way from the flat cast iron straps of 1767 (Figure 1). Rails of cast iron and malleable iron were used through the 1820's, at which time rolled rails were introduced. The first tee rails, forerunners of today's rail, were rolled in 1831 but the design was abandoned until the period of 1858 to 1868 when there was a resurgence in the use of tee rails (3). Rail design evolved in response to increasingly heavier rolling stock and more powerful locomotives. Early rolling stock weight was negligible compared to today's 100 and 120 ton capacity rail cars. Locomotives have similarly evolved from a few horsepower to over 5000 horsepower. Train speeds have increased from a few miles per hour to the 130 mph Tokiado Shinkansen (4) in Japan and the 230 mph T.G.V. train in France.

Rail design and composition has been governed by three important factors. First, the rail must have adequate bending strength to survive the deflection caused by the car trucks passing over it. Second, the rail must have a running surface whose low wear rate provides a long service life; and the rail must have adequate strength and properties to prevent shelling-type rail head flaws due to today's high wheel loads from forming. Shelling-type flaws form under and parallel to the rail running surface and can eventually propagate

transversely causing total failure of the rail section. Third, the rail section must have a wide base and an adequate bearing surface in order to remain stable under load on straight as well as curved track (5). Of these three factors the first two deal with rail metallurgy (composition and microstructure), and the last deals with the shape of the rail cross-section.

Rail chemistry has progressed from cast and malleable irons to a variety of steels. Today commercial rails range from simple carbon and manganese steel to rails with high silicon contents and rails alloyed with chromium, molybdenum, and sometimes vanadium. The alloys have been designed to extend the rail life by reducing wear rates under heavy loads, particularly on curves, and to minimize failure due to shelling-type flaws.

1.2 Standard Rail Joining Techniques

The primary means for joining rail has been to bolt them together. Figure 2 depicts the typical rail joint bolted together with fish-plates (6). Until early this century this was the only means of joining rail lengths. It is still widely used today even with the push towards continuous welded rail (CWR). There are currently about 80×10^6 bolted joints in U.S. track today, half of these in mainline track Bolted joints have significant drawbacks, particularly with today's high speeds and high tonnages. For one, the joint stiffness, or resistance to bending, is never as great as that of the rail, even when newly installed with highly torqued bolts. As the bolts loosen

under the flexing of the joint under traffic, the rail ends and the rail heads begin to incur damage in the form of battering. The bolt holes themselves are a source of cracks and must be regularly maintained, needing periodic tightening and lubrication of joint bars. One advantage to bolted joints is that they are easy to install in the field, with minimum equipment and expertise.

An alternative to mechanical joints is to weld the rail lengths together to form a continuous string, or rather continuous welded rail (CWR). Railroads are installing CWR as mainline track today, but at present rates of installation there will be no significant amounts in secondary lines before the year 2000 (7). CWR almost eliminates joint maintenance.

Several welding processes are used in CWR. Flash-butt welding, gas-pressure welding, and thermit welding have the greatest use in the U.S. The Europeans, Japanese, and Russians also use a variety of other types of processes such as combining both submerged-arc and electroslag welding (7,8,9) and enclosed-arc welding (11,12). These processes are not utilized in the U.S. to any great extent.

Flash-butt welding uses high currents and low voltages (20,000-100,000 amps, 5-10 volts) to heat and melt the ends of rails at which time the rails are forced together either under constant pressure or by impact loading of 60-65 tons. No filler metal is used in making the weld. The process is not sensitive to the surface condition of the rail ends as molten metal is produced and expelled

by the flashing process, cleaning the rail ends of oxides and debris. There is no cast structure reported in the weld metal due to the expulsion of the molten material. An upset about 3/8 inch is formed during the welding process which is usually sheared off mechanically and then the weld is ground to the rail contour. Flash-butt welding is usually done in-plant where rates of up to 100-160 welds per 8 hour shift have been reached. Portable flash-butt welders for field work are in use but are rather large and built on a rail car. One of the first of these in use in the U.S. was built by the Soviet Union.

Gas-pressure welding is similar to flash-butt welding, using torch flames instead of electrical current for a heat source. In gas-pressure welding, oxy-acetylene torches preheat the rail ends to 2000°F at which time upsetting begins with forces on the order of 10 tons. The upset produced, as in flash-butt welding, must be sheared off. The gas-pressure weld must also undergo subsequent normalization at 1550°F, again using oxy-acetylene torches. Because there is no material melted or expelled during the welding process as in flash-butt welding, the gas-pressure weld's integrity is sensitive to the cleanliness of the rail ends. In-plant welds at the rate of 120 per 8 hour shift can be made (6). Gas-pressure welding has not been as widely used since the advent development of the flash-butt welding process. As with flash-butt welding, portable gas-pressure welding systems exist but are rather large and bulky, having to be transported by rail car.

As stated previously, both flash-butt welding and gas-pressure welding require large machines to produce the weld and to shear off the subsequent upset. Both processes have been adapted to field use, but require one or several rail cars. An in-track flash-butt welder can produce 50 to 60 welds per 8 hour shift while in-track gas-pressure welding can produce 40 to 50 welds per 8 hour shift (6). Currently in the U.S. the thermit process is used almost exclusively for field repair welding and for joining long rail strings when laying CWR.

The thermit process is essentially a casting process using aluminum's strong exothermic reactivity with oxygen as a source of energy. Goldschmidt developed the commercial process in the 1890's, using fine aluminum powder and iron oxide as the reactants, ignited by a barium peroxide fuse (5,12). He was granted a patent in 1897 and later used the process to weld two pieces of iron together. Since that time at the turn of the century the thermit welding process has been adapted to weld oil field equipment; join castings and for equipment restoration in steel mills (5); join reinforcing steel in the construction industry; and of course, to join railroad rail.

The thermit process, as currently used, uses more than just aluminum and iron oxide as the reactants. Table I illustrates some of the reactants used. The weld filler metal is provided by the iron produced in the reaction and by prealloyed steel shot which is included in the mixture of reactants and which is melted by the heat

of their reaction, which can theoretically reach 5600°F. Actual temperatures do not reach quite that high due to losses in the crucible and in melting the iron charge (shot). In the case of rail welding, the alloyed shot contains carbon, manganese, and silicon, formulated such that the resulting weld metal's microstructure is similar to that of the rail.

The basic welding procedure is to first prepare and preheat the rail joint using an oxy-fuel torch with a refractory mold around the joint. Some adaptations to the process do not require preheating by torch but use the molten metal to preheat the joint. A crucible is placed over the rail joint to be welded and the thermit reactants ignited. After the reaction is completed and slag has floated to the top, the crucible is either manually tapped or a present number of steel discs located in the bottom melt automatically.

The result is a casting, with attendant casting features such as risers and runouts. These are usually chiseled off while hot, after which the now-welded joint is ground to match the rail head contour and to facilitate visual inspection.

1.3 Welded Rail Joint Properties

Although the flash-butt welding process, the gas-pressure welding process, and the thermit process enjoy popularity of use, they all have limitations. Equipment limitations notwithstanding, these three welding processes do not consistently produce welds which have mechanical properties close to those of the rail steel.

In the American railroad industry, two tests are performed to check weld quality: the 12 inch or 33 inch stroke rolling load test and the slow-bend test. Figures 3 and 4, respectively, show the loading and fixture arrangements for these tests. Base rail as well as welded and bolted joints are tested. The American Railway Engineering Association (AREA) reports test results annually for both tests. Figure 5 shows the results of several years of rolling load tests for various weld types. Although not noted, the welded joints were from a variety of rail section sizes; generally the higher the wheel load, the larger the section size. 2×10^6 cycles was considered a runout, a non-failure, on the rolling load tests. Of eight flash-butt welds tested, two broke--a 25% failure rate. Sixteen gas-pressure welds were tested and only one failed, a 6% failure rate. Of 23 thermit welds tested, 11 broke, yielding a 48% failure rate for a process which is about the only field repair welding process in use in the United States.

In the slow-bend tests a tentative criteria of 1½ inch deflection with a 140 ksi modulus of rupture was suggested (13). As can be seen in Figure 6, not many welded joints could meet this criteria, though all rail sections do. In percent figures, 67% of flash-butt welds, 16% of the gas-pressure welds, and none of the thermit welds met the criteria. The slow-bend and rolling load tests are the only mechanical property data available for welded rail joints.

In 1962 the AREA (American Railway Engineering Association) began to request data from the railroads on butt weld failures as

well as the number of welded joints in service. Figure 7 shows the accumulated number of welds by type, per year. All three are increasing as the move to install CWR accelerates. With the increasing number of welds, failure rates are increasing, shown in Figure 8. Figure 9 shows the average age of the thermit welds decreasing significantly compared to gas pressure and flash-butt welding. These two figures reflect the increasing popularity of flash-butt welding for making rail strings and the increased use of the thermit process for joining the strings together.

The failure rate per 100 weld years, shown in Figure 10, shows that failure rate of thermit welds is almost a thousand times higher than that of flash-butt and gas-pressure welds while the number of thermit welds in service is a hundred times less.

Until recently there have been no alternatives to thermit in terms of portability and speed for field repair use. The thermit process is used almost exclusively for making field repairs and to join continuous rail strings. Other portable welding systems do exist and are used, but cost and field portability considerations of the flash-butt and gas-pressure welding systems presently result in the use of thermit process to join quarter-mile-long strings in the field.

1.4. Electroslag Rail Joining

Recently at the Oregon Graduate Center the electroslag welding process has been adapted to weld railroad rails as an alternative to

the thermit process. Electroslag welding has been used to join railroad rail by the Soviet Union and the Japanese in the past (6-9,14-16) but little detailed information is available. The Soviets, particularly, have reported using electroslag welding to join crane rail which has a squatter, more square cross-section than railroad rail.

Electroslag welding was developed in Russia in the 1950's. Europeans refined the process through the 1950's-1960's. Significant use of the process in the U.S. did not begin until the mid-sixties (17). The electroslag welding process in one in which a current-carrying electrode, a wire or a plate, is fed into a hot conductive slag bath (Figure 11). The resistive (I^2R) heating of the slag bath melts the electrode as it is continuously fed into the slag bath. There are two variations of electroslag welding (ESW), one which uses a consumable guide tube for the wire electrode, and the other which uses a nonconsumable guide tube for the electrode (Figures 12 and 13, respectively). In the latter, the guide tube moves upward with the slag bath as the weld progresses, maintaining a constant distance between the end of the guide tube and the top of the slag bath. In consumable guide tube ESW, the guide tube remains stationary, being melted off as the slag bath moves upward. ESW is commonly used to weld plate from 3/4 inch to over 20 inches thick.

The electroslag welding process as adapted at the Oregon Graduate Center for the welding of railroad rail uses a consumable guide tube and specially designed copper molds to contain the hot slag and molten metal baths (18) (Figure 14). With a consumable guide tube and

filler wire there are two means by which the weld metal may be alloyed to meet rail properties. One uses an alloyed guide tube which, when melted and diluted by the rail steel and the filler wire, yields a weld metal chemistry and microstructure whose properties match the rail steel mechanical properties. The other uses an alloyed filler wire along with a mild steel guide tube, which after dilution with the melted rail steel and the guide tube material, results in a weld metal whose properties match the rail properties. Both methods were pursued in this project to develop suitable alloy weld metal chemistries and microstructures for the electroslag welding of railroad rail.

1.5 Rail and Electroslag Weld Metal Alloy Design and Microstructures

Rail

Today ingots to be rolled into railroad rails are produced by two steelmaking processes: the basic oxygen process and the electric arc furnace which only one U.S. rail producer is using (19). In 1969 there were only five U.S. rail producers, compared to 69 in 1874 (20). All rail steel ingots in the U.S. are cast into big-end-down molds. Hot topping of these killed ingots is not a common practice among U.S. rail producers, which can lead to a large shrinkage cavity in the top of the ingot. The first rail to be rolled from the top of the ingot is designated the "A" rail and is closest to the shrinkage cavity and has the greatest potential for internal problems.

The 136 lb/yd standard carbon railroad rail is essentially a 1080 steel containing 0.80 wt.% carbon and 0.70-1.00 wt.% manganese. Fully heat-treated rails, head hardened rails, and alloy rails for use in high tonnage lines and on high wear curves are produced in lesser quantities than the standard carbon rail. Standard carbon rails are also "control-cooled"; that is, they are slow cooled between 725 and 300°F after rolling such that the lower temperature is not reached for seven hours (20). This practice was first instituted on a production basis in 1937 as an effort to reduce the hydrogen content of the rail. The slow cooling is to allow hydrogen diffusion out of the rail. If the hydrogen was not otherwise removed, shatter-cracks and hydrogen-induced flaking would form within the rail and could eventually cause rail failure.

The standard carbon rail (as well as the Cr-Mo and Cr-V rails) has a pearlitic microstructure. The alloy rails have a finer, more transitional pearlite than the carbon rails. The fine pearlite reportedly has more favorable wear properties over coarse pearlite and other structures of equivalent hardness (19).

Currently there are no mechanical property specifications for railroad rail other than a 24 HRC minimum and a requirement for a survival from the impact of a one-ton tup dropped from 17 to 22 feet, depending on the section size. There are no mechanical property, chemistry, or microstructure specifications on the rail butt welds. Only tentative criteria are recommended by the AREA; these are (a) a 1½ inch deflection and a 140 ksi modulus of rupture in a slow

bend test; and (b) runouts of 2×10^6 cycles on a rolling load test machine. However, these are not even required tests. Therefore, it was decided to develop compositions and microstructures that would result in a weld which would meet a 24 Rockwell C minimum hardness and match or better the standard carbon rail steel mechanical properties such as tensile and yield strength, ductility, CVN impact toughness, and fracture toughness.

Electroslag Welds

Both flash-butt and gas-pressure welding processes use no filler metals; therefore the weld zone consists of the heat-affected zone in each rail end and a single fusion line. Post-weld heat treatment eliminates detrimental microstructures and determines the final microstructure and mechanical properties of the weld zone. In the case of flash-butt welding, heat treatment is usually performed by sending a current through the now-joined rail. Air cooling and residual heat of the rail slows the cooling rate such that predominantly pearlite is formed in the weld zone. Gas-pressure welds are normalized at 1550°F using oxy-fuel torches in an effort to minimize detrimental weld zone microstructures.

The thermit and electroslag welding processes use filler materials but require no subsequent heat treatment, residual heat of the rail and air cooling act to promote a generally pearlitic microstructure in the thermit weld. The thermit process uses a prealloyed steel shot as a filler material while in electroslag welding either alloyed wires or alloyed guide tubes may be used. Thermit weld metal has been

developed such that the weld microstructure and composition are similar to that of the rail steel. As in the rail, the primary alloying element in the thermit weld is carbon.

Since most of the electroslag weld metal is added by either the guide tube or the filler wire, it is possible to alloy the weld and to develop a wide range of alloy compositions.

Almost all alloying elements act to increase the hardenability of plain carbon steel. This is easily dramatized by examining the effect of adding an alloying element such as carbon, one of the most potent hardening agents, on the Continuous Cooling Transformation (CCT) diagram. The CCT diagram is developed by austenitizing small steel specimens and cooling them at constant rates in a dilatometer. The expansion and contractions which occur at phase changes, such as austenite to ferrite, are measured by the dilatometer and plotted versus temperature and time. By using a number of different cooling rates, a CCT diagram is generated which shows the times and temperatures at which various microstructures form given different cooling rates. The effect of most alloying elements is to shift these curves to the right, decreasing the cooling rate needed to form a particular microstructure. Figure 15 shows the CCT diagrams for a 1020 and a 1080 steel, illustrating the strong effect of carbon on the position of the curves.

There were two options available to develop a suitable weld metal microstructure: one was to add carbon to match the rail's microstructure and chemistry; the other was to use other alloying elements

without additional carbon to increase the weld metal hardenability to a point such that a 24 HRC minimum hardness was attained, not necessarily through a pearlitic microstructure.

Using the microstructure of a 1020 steel as a base, alloying elements were selected which shifted the CCT curves far enough to the right to avoid pearlite formation, promoting bainite instead. The martensite transformation range was avoided as well because of the large amounts of alloying elements required at the cooling rates involved, and due to hardness considerations.

While carbon is one of the most potent alloying elements in steel for delaying the start of transformations and for lowering the bainite start temperature (B_s), molybdenum, chromium, and manganese, in that order, are almost as potent. Statistical treatments and multiple regression analysis give quantitative equations which relate the effects of alloying elements on the B_s temperature and on the time to start of transformation (21). An equation developed by Stevens and Haynes (21) quantitatively reveals the strong effect of carbon and the similar effects of molybdenum, chromium and manganese on the B_s temperature (Equation 1).

$$B_s\ (C) = 830 - 170C - 90Mn - 70Cr - 83Mo \qquad (1)$$

$$\text{Log } C_f = 3.288C - 0.168Si + 1.068Mn + 1.266Cr + 2.087Mo + 0.300Ni - 0.626Cu - 1.931 \qquad (2)$$

where C_f is the time to cool between A_{c3} and 500°C.

Kunitake and Ohtani (21) developed a quantitative expression of the effect of alloying elements on the time to cool between the A_{c3} and 500°C in order to suppress the ferrite-pearlite reaction and form bainite (Equation 2). The equation shows that chromium, molybdenum and manganese play a larger role than carbon in promoting the bainitic reaction, especially when considered in conjunction with one another in commonly added amounts. These alloys in particular were examined as alternatives to alloying with just carbon.

Carbon as a single alloying addition promotes the formation of pearlite at low cooling rates. As carbon contents are increased from very low amounts, the bainitic and martensitic transformation ranges begin to appear and expand; the ferrite-pearlite transformation, however, is not significantly delayed, since pearlite is a lamellar eutectoid composed of ferrite and iron carbide (Fe_3C). In the slow air cooling of standard carbon rail steel and of carbon alloyed weld metal, a ferrite-pearlite microstructure is almost inevitable.

Addition of chromium results in retardation of the ferrite-pearlite transformation and extends the bainitic transformation range such that bainite will form at slower cooling rates than otherwise. The martensite transformation range expands as the B_s increases and transformation ranges lengthen as the chromium content is increased. Molybdenum additions act to retard diffusion transformations, encouraging the beinitic transformation. With increasing molybdenum content the B_s temperature gradually drops and the ferrite-pearlite transformation region begins to separate from the bainitic transformation region.

Together chromium and molybdenum act to lower the B_s temperature twice as fast with increasing alloy additions, as well as extending the time for bainite transformation to occur.

By itself manganese has a small effect on the hardenability of a plain carbon steel, unless large amounts are added. The ferrite-pearlite transformation dominates; only at the highest cooling rates may bainite and martensite form. When molybdenum is added along with manganese, a synergistic action occurs; the B_s temperature is lowered, the ferrite-pearlite transformation delayed, and wider ranges of shear-type reactions are produced than would be the case with only manganese addition (22).

Chromium-molybdenum and manganese-molybdenum alloys both are widely used in industry and consequently filler wires containing them are available. Required amounts of alloy additions were established through analysis of CCT diagrams for carbon-chromium-molybdenum and carbon-manganese-molybdenum alloys, after which a commercially available wire nearest to that composition was obtained. Transfer of alloying elements through the slag bath was assumed initially to be the same as that through a welding arc.

CHAPTER 2

EXPERIMENTAL PROCEDURE

2.1 Alloy Additions

Alloying elements were added to the electroslag weld metal by two means. The first used alloy guide tubes. A cast iron guide tube and a guide tube which was half rail steel were tried. Alloying elements were also added by using commercially available filler wires of suitable composition. 2¼Cr-1Mo, 2Mn-½Mo, and 0.65wt.% C wires were used. Generally the alloyed guide tubes were used with a mild steel filler wire and the alloyed wires were used with a mild steel guide tube. The exception was when the 0.65wt.% C wire was used along with a guide tube constructed such that the top half was made out of rail steel.

2.2 Welding Procedure

The experimental procedure involved constructing the consumable guide tube from the necessary materials, then setting up and making an electroslag weld on two sections of 136 lb/yd standard carbon railroad rail. The guide tube, which is constructed of half-inch plate and half-inch round commercial guide tube material, is shown in Figure 16. The welding equipment set-up and fixturing is shown in Figure 17.

The basic welding procedure follows:

1. Rails with saw-cut ends were set up in a fixture with a 1¼ inch gap. The wire feeder was placed on the rail.

2. The starting block was aligned under rail base gap and then cooling shoes and runouts were installed. Electrode power leads, ground leads and control cables were connected.

3. The starting block and rail base were preheated to 400-600°F using an oxy-acetylene torch with a rosebud tip.

4. The weld was started and both strip chart recorder and automatic metered flux addition started at the same time. Hobart PF-201 running flux was used. Voltage and amperage were maintained at 31 V and 1100 A respectively.

5. The cooling water recirculator was started 2½ to 3 minutes after the weld began.

6. When the slag bath reached the top of the runout, welding was stopped and after 15 to 30 sec. the slag was drained from the runout. The runouts, cooling shoes, and starting block were then removed. The weld air-cooled to ambient after which time sectioning was performed.

2.3 Specimen Preparation

Once the weld was completed and had cooled to ambient, sectioning for various specimens commenced. At least two welds were made with each alloy chemistry to get all mechanical property specimens and both macro- and micro-metallographic specimens. Sectioning was carried out on a Marvel Model 8 bandsaw fitted with a one-inch blade.

Specimens needing surface grinding were ground on a Thompson Model B5 2 × 14 inch automatic surface grinder.

Sulfur Printing

Sulfur prints, which give a qualitative view of the amount of sulfur present in the steel, were performed on all heats of rail steel received as well as on some of the welds. Sulfur prints were made from surface ground transverse sections of rail steel. Weld metal sulfur prints were made from longitudinal and transverse surface ground sections. The sulfur printing procedure used, as recommended in Kehl (23), follows:

1. The surface to be sulfur printed was ground and then thoroughly cleaned.

2. Bromide photographic paper was soaked in a 2% H_2SO_4/water solution for 3 to 4 minutes. The entire procedure was carried out in room light.

3. The photographic paper was removed from the H_2SO_4 solution, drained and then the emulsion side placed in intimate contact with the ground surface, squeegeed to remove air bubbles and excess solution.

4. After 2 minutes the photographic paper was removed, washed thoroughly to remove residual H_2SO_4, and fixed for 10 minutes in photographic paper fixer. Steps 2, 3 and 4 were repeated three times.

5. After fixing, the sulfur print was washed in running water for 60 minutes and then dried on a print drying drum.

Macro-Metallographic Weld Specimens

Sections for macro-etching were taken through the electroslag weld in both transverse and longitudinal directions, vertical to the rail axis (Figure 18). The specimens were surface ground and then etched in 10% Nital (10 ml nitric acid to 90 ml methanol). These were then examined for grain size and grain orientation, and for weld defects such as lack of fusion, porosity, inclusions, and cracking. Each etched section was photographed. Some of the longitudinal vertical sections were used for hardness traverses.

Dilution Measurements

Calculations of the percent dilution of the weld metal by the amount rail steel melted, the guide tube contribution, and the filler wire added, were made using data obtained from a weld using the standard electroslag rail welding procedure with a mild steel filler wire and a mild steel guide tube. Two welds were made, though not consecutively; one with a 1 inch gap and the other with a 1¼ inch gap, using essentially the same welding parameters. Because of machining problems encountered with 1 inch gap weld, the 1¼ inch gap weld was heat-treated at 1500°F for 8 hours and then furnace cooled in order to soften the weld and heat-affected zone microstructures as an aid to bandsawing. Sectioning was in the longitudinal horizontal plane with sections about ¼ inch thick, as shown in Figure 19. After sectioning each slab was measured for thickness, surface ground, and then etched in 10% Nital. It was then photographed with a Polaroid MP-3 copy stand camera using Kodak Royal Pan 4 × 5 film. These photographs were

then enlarged to actual size and the outline of the section and the weld traced on graph paper. With the tracing it was then possible to calculate the amount of dilution. By plotting the dilution measurements versus height above the rail base a representation of the changing dilution versus the rail cross-section was obtained.

Metallographic Specimens

Specimens taken from the rail head of each weld for comparisons between the various alloy chemistries were examined using a Ziess Ultraphot II optical microscope and a JEOL JSM-35 scanning electron microscope (SEM) equipped with an Ortec energy dispersive x-ray (EDAX) analyzer. Figure 20 depicts the location of these specimens, which were usually taken from the weld sectioned for macroscopic examination. Specimens from the rail base area of the weld were also taken to examine the microsctructures of the weld and the HAZ in the region of the weld starting reinforcement.

Hardness Measurements

Hardness measurements were made using the Rockwell "C" scale (Diamond Brale indenter, 150 kg load) on a Rockwell hardness tester. Traverses across the weld metal were made at the rail head height on the longitudinal vertical plane near the rail-weld centerline. Some traverses were performed vertically down along the weld axis to check the hardness variation between the starting reinforcement and the runout.

Chemical Analysis

A sample was cut from the weld near the rail head surface for spark spectro-analysis. Analysis was performed at ESCO Corporation. Carbon analysis using a LECO Model 750-100 70-second carbon analyzer was also performed on certain welds as a traverse vertically along the weld centerline to examine the effects of changing weld metal dilution.

Chemical analysis of the filler wires used was made by making a button of the wire. This was achieved by cutting short pieces of wire and loading them into a 1¼ inch diameter, 3 inch long quartz crucible. Three of these crucibles were then placed into a larger graphite crucible. This was loaded into a graphite element Model 580-C BREW furnace. The cut wire samples were heated under helium at near atmospheric pressure to 3000°F, held there for a few minutes, and then cooled. One surface of the resulting button was then ground flat and used for spark spectro-analysis.

Mechanical Property Specimens

Specimens of the rail steel and of the alloyed weld metals were taken for tensile, fracture toughness and impact tests. Figure 21 shows the locations and orientations of the specimens taken from the as-received rail steel. Figure 22 shows the locations and orientations of specimens taken from the alloyed electroslag rail welds.

Blanks were machined to yield a ASTM standard .505 inch diameter tensile bar (24). Tests were performed on a Tinius Olsen 120,000 lb

capacity universal testing machine. Fracture toughness data was obtained through two methods for the rail steel. Standard Compact Tension specimens were made according to ASTM STP 399 (25) and tested on a 20,000 lb Instron dynamic testing machine at room temperature for static fracture toughness, K_{Ic}. Dynamic fracture toughness data, K_{Id}, was also obtained by using fatigue-precracked Charpy V-notch specimens, tested at room temperature. These were tested on an automated instrumented impact system at Battelle Northwest Laboratories.

For weld metal fracture toughness, only fatigue-precracked Charpy V-notch specimens were used, primarily due to the dimensional constraints of the electroslag rail weld configuration. These were tested at Battelle Northwest Laboratories using their instrumented impact system.

Standard Charpy V-notch specimens were taken from three different orientations in the rail steel (see Figure 17). All were tested at room temperature on a 265 ft-lb Tinius Olsen pendulum type instrumented impact testing system located at Battelle Northwest Laboratories. Specimens from the alloyed electroslag weld metal were tested in the same manner. One alloyed weld was tested at higher temperature, 300°F, to measure toughness variations vertically along the weld axis.

CHAPTER 3

RESULTS

3.1 Alloy Additions

In order to establish the necessary weld metal alloy additions, the weld cooling rate was measured at the rail head, and was found to be 175°F per minute at 1333°F. With these data and CCT diagrams three alloyed wires were chosen to be studied: 2¼Cr-1Mo, 2Mn-½Mo, and 0.65 wt.% C. The undiluted as-deposited compositions of these three are shown in Table II, along with the button analyses.

A weld using a guide tube made employing cast iron for carbon addition was used to generate data for calculation of carbon transfer through the slag bath. A guide constructed such that the top half was rail steel and the lower mild steel was also used in conjunction with the 0.65wt.% C wire.

3.2 Chemical Analysis

Rail Steel

Results of the chemical analyses of the rail steels used in this investigation are shown in Table III, along with the AREA and ASTM specifications for 136 lb/yd standard carbon "tee" rails. All rail sections used were near or within specifications. Two rail sections, No. 003 and 004, turned out to be Cr-Mo rails with about 0.60 Cr and 0.17 Mo (all compositions in weight percent). This is within the Cr-Mo rail steel composition seen in commercial American-made rail, which

is 0.60 Cr and 0.20 Mo (46). Two other sections, No. 001 and 002, showed high silicon contents as analyzed which corresponded to the silicon content of 0.70 Si seen in commercial American-made Hi-Silicon railroad rail (47).

Electroslag Weld Metal

Analytical results of the various weld metal alloy compositions are shown in Table IV. Welds made using the 2¼Cr-1Mo filler wire and a mild steel guide tube had compositions of 0.14-0.20wt.% C, 0.56-0.59wt.% Mn, 1.45-1.82wt.% Cr, and 0.65-0.75wt.% Mo at the rail head. The 2Mn-½Mo filler wire with a mild steel guide tube yielded a 0.11 wt.% C, 0.90wt.% Mn, and 0.19wt.% Mo weld metal deposit. The 0.65 wt.% C filler wire with a mild steel guide tube produced 0.514wt.% C, 0.63wt.% Mn deposit at the rail head. By using the 0.65wt.% C filler wire and a guide tube constructed such that the top half was rail steel and the lower mild steel, the carbon content was increased to 0.60 with 0.77wt.% Mn. For comparison a thermit weld was analyzed as well, yielding 0.50wt.% C, 1.09wt.% Mn at the rail head. Silicon and aluminum contents were higher in the thermit weld than in the electroslag welds, with 0.37wt.% and 0.37wt.% respectively. With the exception of the 2Mn-½Mo weld, silicon contents in the electroslag welds were on the order of 0.15-0.19wt.%. The silicon content of the 2Mn-½Mo weldment was 0.39wt.%. Aluminum contents for all the electroslag welds were below 0.006wt.%.

Filler Wire Analysis

In order to determine amounts of alloying elements transferred through the electroslag slag bath, the filler wires were melted and analyzed. The results are shown in Table II. These results were used in concert with the rail weld analyses and dilution measurements to calculate the percentage of element transfer across the electroslag slag bath.

Carbon Analysis of the Rail Welds

Carbon analysis traverses were made on three electroslag rail welds: No. 68, 94 and 96. Weld No. 68 was made using mild steel tubular filler wire with a low carbon content along with a mild steel guide tube. Weld No. 94 was made using the 0.65wt.% C filler wire with a mild steel guide tube. Weld No. 96 was made using the 0.65wt.% C filler wire also, but with a guide tube constructed such that the top half was rail steel and the lower half was mild steel (Figure 23). The carbon content was measured at half-inch intervals vertically along a transverse section. Results are shown in Figures 24, 25 and 26 for welds No. 68, 94 and 96, respectively.

Weld No. 68 varied between 0.20wt.% C at the top of the rail head to 0.40wt.% C in the starting reinforcement. The carbon content just below the rail head was 0.30wt.% and was 0.22wt.% in the rail web. Weld No. 94 contained 0.54wt.% C at the rail head, 0.59wt.% C just below the rail head, 0.52wt.% C in the web and 0.46wt.% C in the starting reinforcement. Weld No. 96 started at 0.62wt.% C at the

rail head, went to 0.66wt.% C just below the rail head, then to 0.52 wt.% C in the web and 0.43wt.% C in the starting reinforcement.

3.3 Macro-Metallography

Sulfur Prints

Representative sulfur prints of transverse sections of as-received rail steel are shown in Figure 27. Sulfur prints of electroslag rail welds for both longitudinal vertical sections are shown in Figure 28. A thermit weld sulfur print, from a transverse section, is shown in Figure 29 for comparison.

Transverse Weld Sections

The transverse section gives an overall view of the weld metal solidification pattern, grain structure and a view of macroscopic defects. Photographs of the macroetched sections are shown in Figure 30. Overall, the grain size is finer than that seen in normal mild steel electroslag plate welds, an example of which is shown in Figure 31.

Longitudinal Vertical Weld Sections

Macroetched longitudinal vertical weld sections, taken at the weld/rail centerline show the shape and depth of fusion and of the heat-affected zone. Examples are shown in Figure 32.

Longitudinal Horizontal Weld Sections

Longitudinal horizontal sections through the weld were taken in order that the dilution of the weld metal might be determined. This was done for welds with a 1 inch gap and for a 1¼ inch gap. The data from calculation of rail steel dilution versus the vertical location on the rail are shown in Figures 33 (1 inch gap) and 34 (1¼ inch gap).

3.4 Micro-Metallography

Each weld's microstructure, in the etched condition, was examined and photographed using both optical and scanning electron microscopes. The same was done for the as-received rail steel and for a thermit weld as well.

Unetched specimens of rail steel, thermit weld metal, and electroslag weld metal were used for inclusion counts at 100× and for size distribution characterization at higher magnifications.

Rail Steel

Photomicrographs of the as-received rail steel are shown in Figure 35, along with the unetched rail steel at 100×. The microstructure was almost 100% fine pearlite with manganese sulfide inclusion stringers running parallel to the rail axis. Energy dispersive x-ray (EDAX) analysis confirmed the inclusion chemistry (Figure 36). Small amounts of ferrite were visible only around some of the inclusion stringers.

Thermit Weld

A thermit weld was examined for comparison to the electroslag rail weldments. Photomicrographs in the rail head area showed a 90-95% pearlitic microstructure (Figure 37). Ferrite was present as veins between the prior austenite grains and as lenses surrounding inclusions. The fineness of the weld's pearlite was equivalent to the rail steel. The base section of the thermit weld was bainitic in contrast to the pearlitic microstructure at the rail head (Figure 38).

There were a variety of inclusions seen in the thermit welds, from mixtures of aluminum oxide to Ti-Mn-Al-S inclusions. Examples are shown in Figure 39, with both photomicrographs and x-ray maps of the inclusions.

Electroslag Rail Weld (ESRW)--Mild Steel Filler Wire and Mild Steel Guide Tube

Mild steel filler wire and mild steel guide tubes were used in the initial electroslag rail welding process development. Photomicrographs of the rail head area of one of these welds are shown in Figure 40. The microstructure was basically ferrite and contained a small amount of fine pearlite.

ESRW--2¼Cr-1Mo Filler Wire and Mild Steel Guide Tube

The first alloy composition evaluated utilized a 2¼Cr-1Mo filler wire and a mild steel guide tube. The rail head microstructure (Figure 41) was a mixture of lower and upper bainite, both in an

"over-tempered" condition, with large carbides visible. Free ferrite was not found other than that present in the bainite plates. Inclusions in the weld metal were predominantly manganese sulfide spheres as SEM and EDAX analysis revealed (Figure 42). These are typical of inclusions found in all electroslag rail welds made using alloyed filler wires. The microstructure at the rail base was the same as that at the rail head (Figure 43), unlike the thermit weldments.

ESRW--2Mn-½ Mo Filler Wire and Mild Steel Guide Tube

Photomicrographs of the rail head region of the weld metal resulting from using the 2Mn-½ Mo filler wire and a mild steel guide tube are shown in Figure 44. The microstructure was similar to welds with a mild steel filler wire, consisting of bainitic ferrite and a ferrite/carbide aggregate. Inclusions were of the same type as in the 2¼Cr-1Mo weldment.

ESRW--0.65wt.% C Filler Wire and Mild Steel Guide Tube

In order to produce a microstructure similar to that of the rail steel, i.e., a fine pearlite, a 0.65wt.% C filler wire was used with a mild steel guide tube. The microstructure produced by such an alloy was 80-90% pearlite with 10-20% proeutectoid ferrite present, usually at the grain boundaries in either polygonal or Widmannstätten morphologies (Figure 45). The pearlite was finer than that in the rail steel, as shown in comparison in Figure 46. Inclusions were again like those in the 2¼Cr-1Mo weldment.

ESRW--0.65C Filler Wire and Half Rail Steel Guide Tube

In order to increase the hardness of the rail head of a weld with a pearlitic microstructure, additional carbon was added to the weld metal through the use of a guide tube constructed such that the top half was made of rail steel. The rest of the guide was fabricated of mild steel since the extra carbon was not needed in areas other than the rail head. The microstructure was one of fine transitional pearlite with some ferrite present in grain boundaries (Figure 47). The pearlite was transitional in the sense that the cementite plates were not fully continuous.

Inclusion Size and Distribution

Inclusions were counted and measured on randomly selected 1000× fields on the Ziess microscope. This was performed on the thermit and electroslag weld metal deposits as well as the parent rail steel. The results are shown graphically in Figures 48-53. The electroslag weld metal deposits contained fewer large inclusions (greater than 0.0002 in. in largest dimension) than the rail steel or the thermit weld metal. The thermit weld metal and rail steel each had large numbers of inclusions. The thermit weld metal had the greatest amount of inclusions of all the samples examined.

3.5 Mechanical Testing

Hardness Measurement

Hardness traverses were made across the weld metal at the rail head. Figure 54 depicts the traverse of the mild steel filler wire/ mild steel guide tube weld. This weld attained a hardness of 20 HRC at the weld centerline, about one inch below the top of the rail head. Closer to the top of the rail head the hardness was below the lower end of the Rockwell "C" scale (less than 10 HRC). The unaffected rail steel was consistently 25-26 HRC in all welds.

The weldment using a 2¼Cr-1Mo filler wire and a mild steel guide tube attained a hardness of 26 HRC at the rail head. The traverse is shown in Figure 55. Using a 2Mn-½Mo filler wire with a mild steel guide tube yielded a hardness less than 10 HRC. The traverse for this weld is shown in Figure 56.

The 0.65wt.% C filler wire and mild steel guide tube yielded a hardness of 26 HRC at the weld centerline of the rail head. The weld using the same wire but with a guide tube constructed such that the upper half was rail steel and the lower was mild steel, yielded a 24 HRC at the weld centerline of the rail head. Traverses for each of these are shown in Figures 57 and 58, respectively.

A hardness traverse across a thermit weld at the rail head is shown in Figure 59. A hardness of 32 HRC was attained at the rail head.

Tensile Properties

Tensile properties from the various electroslag rail welds and for the as-received rail sections are shown in Table V. Thermit weld properties are shown as well.

CVN Impact Toughness

The Charpy V-notch impact toughness weld centerline specimens at room temperature of the rail steels, rail welds, and a thermit weld are shown in Table V. The values of the weld toughness are averages since the impact toughness varies vertically through the weld. Figure 60 illustrates the changes in impact toughness of specimens from a 2¼Cr-1Mo weld seen at room temperature. By increasing weld ductility by testing at higher temperatures, a greater range of values was seen, as is depicted in Figure 61. This weld also used the 2¼Cr-1Mo filler wire. Results of the rest of the impact tests are shown in Figures 62 and 63.

Fracture Toughness

Static fracture toughness of the rail steel was measured using plane strain compact tension specimens as per ASTM STP 399, and dynamic fracture toughness by using fatigue-precracked Charpy V-notch specimens, both tests being conducted at room temperature. Dynamic fracture toughness of the weld metals was obtained through the use of fatigue-precracked Charpy V-notch specimens. Dynamic fracture toughness was

used predominantly due to its extensive use in railway literature. These results as well as those for the rail steel are shown in Table V. Figures 64-67 graphically show the results of the fracture toughness tests on the electroslag rail welds.

CHAPTER 4

DISCUSSION

4.1 Alloying Element Transfer

In the electroslag welding process, the molten neutral slag bath provides the heat needed to melt the weld filler materials. The slag bath is a mixture of oxides and calcium fluoride which, when melted, becomes electrically conductive and forms a liquid which is of lesser density than molten steel, and floats on top. The composition of the flux used to develop the slag bath is shown in Table VI. The molten slag's electrical resistance generates heat by I^2R heating. Temperatures in the slag bath reach 4000°F. This intense heat melts the filler wires as they move into the slag bath. Plate guide tubes melt at or just below the surface of the slag bath. In either case there is a steady stream of molten metal droplets moving down through the slag bath to the molten metal pool below.

The slag-metal reactions which occur during the weld are very complex, responding to a steady state set up once the slag bath is established. Due to the slag-metal interactions, total transfer of alloying elements through the slag bath is not always possible. Some proportion of the alloying element added may remain in the slag bath. Large amounts of alloying elements can drastically change the slag bath composition as well as the temperature at which it is molten.

The running flux used to produce the slag bath was an oxide based flux containing calcium fluoride for fluidity and conductivity. Oxides present in large proportions were calcium oxide, manganese oxide, and silicon dioxide. Other oxides were present in only small quantities. The oxides break down to their ionic states in the high temperature environment of the slag bath and as ions react with the molten metal. Chemical reactions between the slag and the metal occur as the molten metal droplets fall through the slag bath. Reactions between the slag bath and the base material are reported to be minimal (27). Since the slag system is oxide based, oxidation occurs to metals prone to it, causing their subsequent loss to the slag bath and decreasing the concentration in the weld metal. Paton (27) reported that the loss occurs as the weld progresses, causing a slight variation in the weld metal concentration of such elements as carbon, silicon, and manganese from the weld start to the runout. Changes in weld metal composition were seen in the electroslag rail welds but were attributed to the changing weld metal dilution by the rail steel (Figure 68).

Paton attributes the loss partially to the electrical characteristics of the D.C. reverse polarity (electrode positive) welding setup by considering the slag bath as a mixture of anions and cations from the dissociated oxides which under a direct current produces an electrolytic reaction. Electrolytic deposition occurs at the cathode (the weld metal pool) as the cations combine with electrons to form metal atoms. At the anode (the electrode wire or plate), oxygen is liberated.

The liberated oxygen reacts with the surfaces of the newly formed droplets of metal from the electrode, causing intense oxidation reactions with such elements as manganese and carbon. Paton also reports that the welding current has an effect on slag bath alloy transfer by speeding up the metal droplet transfer through the slag bath. Droplet speed through the slag bath is not increased by increased welding current. Droplet size, on the other hand, is increased with an increase in welding current.

Molybdenum, as a pure elemental wire fastened to the guide tube, exhibited only a 50% transfer rate through the slag bath, while if present as an element in filler wire it showed an 80-100% transfer rate. Carbon in the form graphite and pearlite in a grey cast iron plate guide tube yielded an 80-85% transfer rate, while carbon in a filler wire maintained a 90-100% transfer rate. Chromium, manganese, and a molybdenum all exhibited transfer rates of 80-100% when included in a filler wire.

These alloy transfer characteristics, as well as considerationof the dilution characteristics of the electroslag rail weld, must be taken into account when designing weld metal alloys. Together, the necessary wire and/or guide tube composition can be developed so as to produce a certain weld metal composition. The final weld metal chemistry depends on the weld cooling rate and the properties and microstructures desired.

4.2 Fracture Toughness of Railroad Rails and Electroslag Rail Welds

Standard carbon railroad rail is brittle at room temperature, exhibiting a totally transgranular cleavage fracture mode. Cleavage facets have been shown to traverse the entire prior austenite grain, not being influenced by pearlite colony size (ref. Hyzak, Bernstein & Stone, Report R-168 AAR). The ductile to brittle transition temperature is on the order of 300°F. Impact toughnesses of only 2-3 foot-pounds are obtained from CVN specimens. Static fracture toughness (K_{Ic}) is only about 35-38 ksi$\sqrt{in}$. Dynamic fracture toughness (K_{Id}), from instrumented precracked CVN specimens is about 10 ksi$\sqrt{in}$ lower than the static test values (28). In this investigation dynamic fracture toughness was used almost exclusively for fracture toughness determination of the electroslag rail welds.

Specimen size constraints notwithstanding, dynamic fracture toughness tests yield data which relates closer to the actual loading the railroad rail sees under rail traffic. High impact loads occur in tens of milliseconds under rail traffic, which is similar to the loading seen in a DVN impact test.

Another constraint to the fracture toughness measurement of the electroslag rail welds was the composition geometry of the weld metal. The weld metal composition was not constant from the rail base to the rail head, even if constant filler wire and plate guide tube composition was maintained. Due to the changing rail cross-section and weld contour, dilution of the weld metal by the rail steel caused the carbon content to vary from the rail base to the rail head. Likewise the

alloy composition varied from the rail base to the rail head for the same reason--the changing weld contour. The composition changes occurred over fairly short distances. A large specimen, such as the standard compact tension specimen, with the notch oriented vertically would then cover a wide range of compositions in the weld metal. Charpy-sized specimens were therefore used. Also more specimens would be obtained from a single weld when using the standard-sized Charpy bars. Statically testing for fracture toughness using the CVN specimen is possible; however, the results would not be as meaningful as the results from dynamic fracture toughness testing using an instrumented fatigue-precracked CVN test, especially when considering the rail/wheel interactions.

4.3 Effect of Microstructure on the Electroslag Rail Welds

Alloying the electroslag rail welds was predominantly carried out by means of alloyed filler wires with some welds alloyed by means of the guide tube. Alloys were chosen on their ability to produce a 24 HRC minimum hardness at the weld cooling rate indicated by the CCT diagrams. With this hardness requirement, martensitic microstructures were not feasible without subsequent tempering operations and large amounts of alloying elements. Alloyed wires produced bainitic deposits while welds alloyed with only carbon produced pearlitic weld metal deposits.

Pearlitic Microstructures

Welds made using high carbon (0.65wt.% C) filler wire produced pearlitic microstructures whose interlamellar spacing was as fine or finer than that of the rail steel. Two variations of alloying with the high carbon wire were made; one alloying with the high carbon wire and a mild steel guide tube; the other alloying with the high carbon wire and a guide tube whose upper half was rail steel. In the latter, the rail steel in the upper portion of the guide tube raised the carbon content of the weld metal making it slightly harder.

In electroslag welding the slag bath melts the rail steel about one inch above the molten metal pool, and as the base material melts, it flows down into the molten metal pool. The important point is that solidification of this molten metal occurs about an inch below the area from which it was melted. At the head of an electroslag welded rail there is a large degree of penetration into the rail steel on each side of the weld. This would mean that the rail contributes a large amount of carbon to the weld metal; but since the molten metal is solidified an inch below where the melting was taking place, the carbon content at the top of the rail head is much lower than the rest of the weld. The peak in carbon content is below the rail head. The weld metal at the rail head comes almost solely from the filler wire and guide tube. It was this reason that the guide tube's upper half was made of rail steel, to compensate for the lack of carbon addition by rail steel dilution.

Both welds using the high carbon wire resulted in pearlite microstructures, with a small amount of proeutectoid ferrite at the prior austenite grain boundaries at the rail head. The amount of ferrite in each was about the same. The extra carbon due to rail steel in the guide tube did not promote the formation of more pearlite, but rather refined the pearlite that was present. The small amount of extra carbon slightly increased the weld metal hardenability. This increase was enough to extend the time to the start of transformation such that at the weld cooling rate, transformation oddurred at a lower temperature, producing a finer more transitional pearlite with the same amount of proeutectoid ferrite present as the weld without the rail steel in the guide tube. Still further increases of carbon at the rail head would further retard transformation times, eventually precluding pearlite formation at the given weld cooling rate and promoting the formation of an upper bainitic microstructure. The proeutectoid ferrite would disappear, possibly being replaced with proeutectoid cementite.

The strength of pearlite is almost completely dependent on the interlamellar spacing of the ferrite and cementite plates. The relationship is almost linear in 100% pearlite steels (Figure 69). Basically as the interlamellar spacing of the pearlite decreases, the yield strength increases. At very small interlamellar spacings, which correspond to low transformation temperatures, the cooperative growth mechanism of pearlite begins to deteriorate, forming a degenerate pearlite with broken or discontinuous lamella of cementite. If transformation temperature decreases further shear type transformation

products, bainites (which differ in property/microstructure relationships) begin to form instead of pearlite.

Alloying elements can be used to refine pearlite without the necessity of increasing cooling rates. Chromium-molybdenum rail steels were developed to maintain a 100% pearlite microstructure with superior properties to the standard carbon rail steels by decreasing the interlamellar spacing to the point of degeneracy through the use of alloying elements. The small interlamellar spacing enabled the alloy rail steel to reach a yield strength of 120 ksi, versus 70 ksi for standard carbon rail; with a dynamic fracture toughness of 36-44 ksi$\sqrt{in}$ versus 26 ksi$\sqrt{in}$ for standard carbon rail (29,30).

Both pearlitic weld metal deposits had hardnesses slightly less than the rail steel. The tensile properties were less as well. CVN impact values were about the same as rail steel. The dynamic fracture toughness, K_{Id}, however, was higher than the rail steel's 26 ksi $\sqrt{in}$; with values of 30 ksi$\sqrt{in}$ in the plain high carbon wire weld, and about 35 ksi$\sqrt{in}$ in the high carbon wire weld with the added rail steel. These test results were at the rail head. At the rail base K_{Id} values ranged from 40-45 ksi$\sqrt{in}$. The increase in fracture toughness of the weld deposits with respect to the rail steel could be attributed to the cleanliness of the weld deposit relative to the rail steel and also to the small amount of proeutectoid ferrite present in the prior austenite grain boundaries of the weld metal deposit. At room temperature it had been shown that the fracture toughness increases with decreasing volume fraction of pearlite (Figure 70) (55). The

increase in fracture toughness in the rail head region of the high carbon weld with rail steel plate guide tube additions compared to the welds without the extra carbon may be due to the increased fineness of the pearlite, since the same amount of proeutectoid ferrite is present in each case.

Bainitic Microstructures

The two alloy wires used, 2¼Cr-1Mo and 2Mn-½Mo, both promoted bainitic microstructures. The 2Mn-½Mo wire with a mild steel guide tube resulted in a weld deposit with a low hardness (about 15 HRC) at the rail head with a bainitic ferrite microstructure. The 2¼Cr-1Mo wire, on the other hand, produced an adequately hard (at least 24 HRC) weld metal deposit at the rail head with a microstructure consisting of both upper and lower bainite. The 2Mn-½Mo weld metal deposit was lower in tensile strength than the rail steel, but possessed greater ductility; an 85.2 ksi ultimate with 28% elongation in two inches versus a 135 ksi ultimate with 12% elongation for rail steel. Fracture toughness was also the highest of the alloys tested, 55-60 ksi $\sqrt{in}$.

The 2¼Cr-1Mo weld metal deposit matched the rail steel in tensile strength but with higher ductility, 16% elongation in two inches. Its fracture toughness was also better than the rail steel's 26 ksi$\sqrt{in}$ at about 35 ksi$\sqrt{in}$.

The bainitic ferrite deposit of the 2Mn-½Mo filler wire was able to attain a higher ductility and fracture toughness because of the

large amount of ferrite present. Ferrite/carbide aggregates were confined to separate grains; no dispersed carbides were seen within the ferrite plates. The ferrite, however, decreased the tensile properties and the weld metal hardness, two important properties at the rail head. Increasing the alloy content would likely increase the tensile strength and hardness at the expense of the ductility and the fracture toughness.

In contrast to the 2Mn-½Mo weld metal, the 2¼Cr-1Mo weld metal deposit consisted totally of upper and lower bainite. Typically, upper bainite exhibited carbide precipitates on and parallel to the grain or plate boundaries while in lower bainite the precipitates form at an angle to the plate boundary. There was no free ferrite present in the 2¼Cr-1Mo weld metal. The uniform dispersion of carbides in the ferrite matrix allowed the structure to reach a hardness of at least 24 HRC at the rail head. The chromium and molybdenum acted together to lengthen the transformation times such that the pearlite nose on the CCT curve was bypassed. Molybdenum in particular acts to suppress the cooperative growth mechanism of the austenite to pearlite transformation which lengthens the transformation times.

By increasing the chromium-molybdenum alloy composition, transformation times could be increased to allow a 100% lower bainite microstructure to form, without large increases in tensile strength or hardness. A 100% lower bainite microstructure would be advantageous because of the superior toughness properties compared to a mixed or totally upper bainitic microstructure. The long continuous carbide films in upper bainite provide a longer fracture path than the carbide

films in lower bainite, which lowers upper bainite's fracture toughness. Tensile strength and hardness would not be appreciably increased in a 100% lower bainite microstructure, mostly due to the slow cooling rate of the weld.

The slow cooling rate of the electroslag rail weld due to the retained heat in the rails after welding promoted a "self-tempering" action. The weld cooling rate was such that 100% pearlite was formed in the heat-affected zone in the reaustenitized regions. Microstructures caused by higher cooling rates, such as martensite or bainite, were not seen in the heat-affected zone.

4.4 Further Work

It is possible to alloy specific regions of the rail weld by changing the guide tube and filler wire compositions by alloying specific regions of the guide tube. It is possible to produce a 100% lower bainite microstructure at the rail base where cyclic tensile stresses are the greatest from rail bending (31); and in the same weld produce a 100% pearlite microstructure at the rail head, matching the rail steel's microstructure and mechanical properties. The pearlitic rail head microstructure would be advantageous from a wear viewpoint.

Cyclic stresses in the rail foot can reach peaks greater than 25 ksi in traffic conditions, increasing somewhat as train speeds rise (Figure 71) (31). A high fracture toughness material at the

rail base in the weld metal would help reduce the possibility of failures starting from that region. A two-fold increase in fracture toughness relates to a four-fold increase in the size of the defect that can be tolerated before catastrophic failure occurs.

It should also be possible using alloyed filler wires and regionally alloyed guide tubes to match the hardness, if not the microstructure as well, over the height of head-hardened rails and in fully heat-treated rails and alloyed rails.

4.5 Recommendations

Ideally the weld filler metal in a rail weld should match the hardness of the rail head running surface. This is necessary to prevent hollows or bumps from forming at the welded region as the rail head wears and deforms due to the passage of trains.

Two alloys were developed which accomplished this. One used a 2¼Cr-1Mo filler wire with a mild steel guide tube and produced a bainitic weld metal deposit that was only slightly harder than the rail steel. The other used a high carbon (0.65wt.%) filler wire with either a mild steel or a half rail/half mild steel composite guide tube and produced a weld metal deposit which matched the rail steel in hardness with a pearlitic microstructure like that of the rail steel. In both cases the mechanical properties of the rail steel were equivalent to or greater than those of the rail steel. For field applications the use of either would depend on the wear properties of a bainitic microstructure versus those of a pearlitic microstructure in the context of the rail/wheel interactions seen in service.

REFERENCES

1. _____; "Report on Assignment 2-Laying," AREA Bulletin, v. 73: p. 468.
2. _____; "Rail Failure Statistics, Covering (a) All Failures, (b) Transverse Failures, (c) Performance of Control-Cooled Rail," AREA Bulletin, v. 73: p. 740.
3. Schoenberg, K. W.; "Evolution of Rail Steel and Rail Sections and What is Being Done Relative to this Material Today," AREA Bulletin, v. 76: p. 653.
4. Masumoto, H., K. Sugino, and H. Hayashida; "Development of Wear Resistant and Anti-Shelling High Strength Rails in Japan," Heavy Haul Railways Conf. Proc., 18-22 Sept., 1978, Session 212, Paper H.1.
5. Geiger, G. H., D. R. Poirer and J. Myers; Metallurgical Evaluation of Thermit-type Railroad Rail Welds, University of Arizona, 1979: p. 34.
6. Hauser, Daniel; Methods for Joining of Rails: Survey Report, July 1977: p. 23.
7. Oishibashi, H. and S. Hakamata; "Automatic submerged slag welding of rail," Quarterly Reports RTRI, v. 13, no. 4, 1972, p. 235.
8. Svetlopolyanskii, Y. I.; "The Semi-Automatic Electroslag Welding of Rails," Avt. Svarka, no. 3, 1966, p. 53.

9. Oi, I., T. Muramoto and S. Hakamada; "Automatic Submerged-Slag Welding of Rails (Report 1): Study of One-side Submerged Arc Welding of Rail Base," Quarterly Reports RTRI, v. 7, no. 4, 1966: p. 11.

10. Clevers, J. A. N. and J. W. A. Stemerdink; "Enclosed Welding of Vertical Grooves Facilitated by the Development and Use of Extra-low-hydrogen Electrodes," Welding Journal, March 1960: p. 223.

11. Oishibashi, H.; "Rail Welding Methods," Quarterly Reports RTRI, v. 15, no. 2, 1974: p. 69.

12. Farley, P. G.; "Ultrasonic Testing of Alumino-thermic Rail Welds," Metal Construction, December 1980: p. 678.

13. _____; "Rolling-Load and Slow-Bend Test Results of Butt-Welded Rail Joints," AREA Bulletin, v. 68: p. 385.

14. _____; "Welding System Developed for Crane Rails," Iron and Steel Engineer, April 1963: p. 185.

15. Gorozhaninov, N. E., A. L. Garyaev and I. Zvener; "The Bath Welding of Crane Track Rails," Svar. Proizv., no. 9, 1965: p. 35.

16. Koperman, L. N., and Kh. Kh. Mukanaev; "Electroslag Welding of Crane Rails," Svar. Proizv., no. 5, 1967: p. 32.

17. Liby, A. L., and D. L. Olson; "Metallurgical Aspects of Electro-slag Welding: A Review," Colorado School of Mines Quarterly 69, no. 1, 1974: p. 41.

18. Turpin, R., M.S. Thesis, Oregon Graduate Center, 1982.

19. Knupp, G. G., et al.; "A Review of the Manufacture, Processing, and Use of Rail Steels in North America: A Report of AISI Technical Sub-Committee on Rails and Accessories," Rail Steels: Developments, Processing, and Use: STP 644, D. H. Stone and G. G. Knupp, eds., ASTM, 1978: p. 7.

20. _____; "Railroad-Rail and Joint-Bar Production," The Making, Shaping, and Treating of Steel, Ninth ed., Harold E. McGannon, ed., U. S. Steel, 1971: p. 754.

21. Atkins, M.; Atlas of Continuous Cooling Transformation Diagrams for Steel, ASM, 1980: p. 228.

22. Cias, Witold W.; Phase Transformation Kinetics and Hardenability of Medium-Carbon Alloy Steels, Climax Molybdenum, p. 8.

23. Kehl, George L.; The Principles of Metallographic Laboratory Practice, McGraw-Hill Book Co., New York, 1949: p. 186.

24. _____; "Standard Methods of Tension Testing of Metallic Materials, E8-79a," 1980 Annual Book of Standards, Part 10, Metals-Physical, Mechanical, Corrosion Testing, ASTM, 1980: p. 197.

25. _____; "Standard Test Method for Plane-Strain Fracture Toughness of Metallic Materials, E399-78a," 1980 Annual Book of Standards, Part 10, Metals-Physical, Mechanical, Corrosion Testing, ASTM, 1980: p. 580.

26. Fletcher, F. B., and J. W. Morrow; "The Chrome-Moly Rail Steels," Molybdenum Mosaic, v. 4, no. 2: p. 10.

27. Paton, B. E.; Electroslag Welding, 2nd ed., New York, 1962: p. 80.

28. Stone, D.; "An Introduction to the Fracture Mechanics of Railroad Rails," Railroad Track Mechanics and Technology, Arnold D. Kerr, ed., 1978: p. 353.

29. Stone, D. H. and W. J. Harris, Jr.; "High Strength Steels for Rail Transport," Alloys for the 80's, Robert Q. Barr, ed., Climax Molybdenum Co., 1980: p. 85.

30. Stone, D. H. and R. K. Steele; "The Effects of Mechanical Properties Upon the Performance of Railroad Rails," Rail Steels: Developments, Processing, and Use, STP 644, D. H. Stone and G. G. Knupp, eds., ASTM, 1978: p. 38.

31. Eisenmann, Dr. -ing.Josef; "Stress Distribution in the Permanent Way Due to Heavy Axle Loads and High Speeds," AREA Bulletin, v. 71: p. 24.

32. _____; "ASTM Specification for Carbon Steel Tee Rails, A1-76," 1980 Annual Book of ASTM Standards, Part 4, ASTM, 1981, p. 1.

33. _____; "Specifications for Steel Rails," AREA Manual for Railway Engineering, AREA, 1979, p. 4-2-1.

34. Venkataraman, Srivathsan; Effect of Process Variables and Microstructures on the Properties of Electroslag Weldments, Ph.D. dissertation, Oregon Graduate Center, Beaverton, OR., 1981.

35. _____; "Rolling-load and Slow-bend Test Results of Butt-welded Rail Joints," AREA Bulletin, v. 68, p. 383-394.

36. _____; "Results of Rolling-load and Slow-bend Tests of Butt-welded Rail Joings," AREA Bulletin, v. 66, p. 515.

37. _____; "Results of Rolling-load and Slow-bend Tests of Butt-welded Rail Joints," AREA Bulletin, v. 67, p. 427.

38. _____; "Investigation of Rails Made by the Australian Iron and Steel Company," AREA Bulletin, v. 70, p. 310.

39. Schoenberg, K. W.; "Metallurgical Examination and Physical Test Results of Chromium and Manganese-Vanadium Alloy Rail Steel Investigation," AREA Bulletin, v. 76, p. 65.

40. _____; "Investigation of Rails Made from Continuously Cast Blooms by Algoma Steel Corporation," AREA Bulletin, v. 73, p. 1.

41. Cramer, R. E.; "Investigation of Failures of Welded Rails at the University of Illinois," AREA Bulletin, v. 65, p. 611.

42. _____; "An Investigation of Welding Used Rail without Cropping," AREA Bulletin, v. 65, p. 637.

43. _____; "Investigation of Service and Detected Butt-Welded Rail Joint Failures," AREA Bulletin, v. 67, p. 423.

44. _____; "Rolling-load and Slow-bend Test Results of Butt-welded Rail Joints," AREA Bulletin, v. 68, p. 383.

45. Cramer, R. E.; "Investigation of Failures of Welded Rails," AREA Bulletin, v. 64, p. 471.

46. _____; "Results of Rolling-load and Slow-bend Tests of Butt-welded Rail Joints," AREA Bulletin, v. 66, p. 516.

47. _____; "Investigation of Rails Made by the Australian Iron and Steel Company, AREA Bulletin, v. 70, p. 344.

48. Schoenberg, K. W.; "Metallurgical Examination and Physical Test Results of Chromium and Manganese-Vanadium Rail Steel Investigation," AREA Bulletin, v. 76, p. 74.

49. _____; "Investigation of Rails Made from Continuously Cast Blooms by Algoma Steel Corporation," AREA Bulletin, v. 73, p. 7.

50. _____; "Rail Failure Statistics, Covering (a) All Failures, (b) Transverse Fissures, (c) Performance of Control-cooled Rail," AREA Bulletin, v. 73, p. 723.

51. _____; "Fabrication," AREA Bulletin, v. 71, p. 646.

52. _____; "Fabrication," AREA Bulletin, v. 70, p. 417.

53. _____; "Butt-weld Failure Statistics," AREA Bulletin, v. 67, p. 436.

54. _____; "Butt-weld Failures," AREA Bulletin, v. 68, p. 397.

55. Marder, A. R. and B. L. Bramfitt; "The Effect of Morphology on the Strength of Pearlite," Metallurgical Transactions A, v. 7a, no. 3, 1976, p. 365.

56. Guest, P. J.; The Micromechanics of Fracture of Pearlitic Structural Steels, Ph.D. dissertation, University of California at Berkeley, Berkeley, CA., December 1969.

Table I. THERMIT REACTIONS*

Reaction	Reaction Temperature °F/°C	Energy Released kcal
$3\ FeO_4 + 8\ Al \rightarrow 9\ Fe + 4\ Al_2O_3$	5590/3088	719.3
$3\ FeO + 2\ Al \rightarrow 3\ Fe + Al_2O_3$	4532/2500	187.1
$Fe_2O_3 + 2\ Al \rightarrow 2\ Fe + Al_2O_3$	5360/2960	181.5
$3\ CuO + 2\ Al \rightarrow 3\ Cu + Al_2O_3$	8790/4865	275.3
$3\ Cu_2O + 2\ Al \rightarrow 6\ Cu + Al_2O_3$	5680/3138	260.3
$3\ NiO + 2\ Al \rightarrow 3\ Ni + Al_2O_3$	5740/3171	206.6
$Cr_2O_3 + 2\ Al \rightarrow 2\ Cr + Al_2O_3$	5390/2977	546.5
$3\ MnO + 2\ Al \rightarrow 3\ Mn + Al_2O_3$	4400/2427	403.0
$3\ MnO_2 + 4\ Al \rightarrow 3\ Mn + 2\ Al_2O_3$	5020/2771	104.1

*See Ref. 5.

Table II. WELD FILLER WIRE CHEMISTRIES (wt.%) BY MANUFACTURER AND BY WIRE BUTTONS*

Wires	C	Mn	Si	S	P	Cr	Ni	Mo	Cu	V
2¼Cr-1Mo (manufacturer's analysis)	0.07-0.12	0.40-0.70	0.45-0.60	0.025	0.025	2.25-2.75	--	0.90-1.10	--	--
2¼Cr-1Mo (button analysis)	0.058	0.484	0.259	0.029	0.010	2.515	0.100	0.913	0.370	0.006
2Mn-½Mo (manufacturer's analysis)	0.07-0.12	1.60-2.10	0.50-0.80	0.035	0.025	0.15	0.40-0.60	--	--	--
0.65C (manufacturer's analysis)	0.55-0.65	0.90-1.25	0.10-0.20	0.035	0.025	--	--	--	0.15	--
0.65C (button analysis)	0.628	0.723	0.384	0.015	0.013	0.027	0.021	<0.001	0.185	0.002
Mild steel (manufacturer's analysis)	0.06-0.15	0.90-1.40	0.45-0.70	0.035	0.025	--	--	--	--	--
Mild steel (button analysis)	0.060	1.019	0.703	0.023	0.006	0.014	0.029	<0.001	0.291	0.003

*Some elements may have been lost in the smelting of the wire button.

Table III. CHEMICAL ANALYSIS OF RAIL STEELS (wt.%)

Rail	C	Mn	Si	S	P	Cr	Ni	Mo	Cu	V	Al	B
45400	0.73	0.93	0.225	0.043	0.033	0.09	0.09	<0.005	0.23	0.005	0.006	0.0005
20304	0.72	0.85	0.196	0.022	0.033	0.04	0.08	<0.005	0.06	0.004	0.009	0.0004
14192	0.732	0.893	0.213	0.040	0.025	0.046	0.068	<0.001	0.085	0.005	0.007	0.0003
001	0.696	0.838	0.717	0.030	0.016	0.024	0.076	<0.001	0.070	0.005	0.004	0.0003
002	0.705	0.867	0.729	0.034	0.017	0.024	0.079	<0.001	0.071	0.005	0.005	0.0004
003	0.708	0.608	0.322	0.025	0.011	0.598	0.057	0.172	0.075	0.006	0.017	0.0003
004	0.694	0.597	0.320	0.031	0.010	0.580	0.054	0.166	0.073	0.006	0.017	0.0003
AREA* spec.	0.70/ 0.82	0.75/ 1.05	0.10/ 0.35	0.04 max	0.034 max	--	--	--	--	--	--	--
ASTM** spec.	0.69/ 0.82	0.70/ 1.00	0.10/ 0.25	0.05 max	0.04 max	--	--	--	--	--	--	--

*See Ref. 32.

**See Ref. 33.

Table IV. CHEMICAL ANALYSIS OF RAIL WELDS (wt.%)

Weld Metals	C	S	P	Mn	Si	Cr	Ni	Mo	Cu	V	Al	B
Thermit Weld	0.496	0.021	0.033	1.093	0.366	0.031	0.063	0.091	0.033	0.006	0.369	0.0004
2¼Cr-1Mo ESRW #51	0.203	0.029	0.019	0.562	0.164	1.454	0.088	0.647	0.308	0.005	0.004	0.0004
2¼Cr-1Mo ESRW #53	0.142	0.028	0.016	0.587	0.175	1.827	0.086	0.785	0.322	0.005	0.006	0.0004
2Mn-½Mo ESRW #92	0.112	0.019	0.007	0.902	0.384	0.006	0.025	0.019	0.264	0.005	0.001	0.0005
0.65C ESRW #93	0.514	0.014	0.009	0.627	0.197	0.032	0.029	<0.001	0.248	0.004	0.007	0.0004
0.65C + ½ rail qt ESRW #97	0.599	0.014	0.011	0.774	0.207	0.023	0.055	<0.001	0.177	0.003	0.014	0.0004

Table V. MECHANICAL PROPERTY TEST RESULTS

	Hardness (HRC)	UTS (ksi)	YS (ksi)	R.A. (%)	Elong. (%)	CVN Toughness	K_{ID} ksi $\sqrt{in}$
Rail Steel	24 min	135	68	7	12% in 2 inches	2 ft lbs (ave)	26[1]
Thermit Weld[2]	31	115	N.A.	none detected	1% in 5 inches	2.5 ft lbs (ave)	N.A.
2½Cr-1Mo Electroslag Weld	29	135	90	11	16% in 2 inches	3.5 ft lbs (ave)	31.7 (ave)
2Mn-½Mo Electroslag Weld	8	85.2	57.2	15	28% in 2 inches	N.A.	56.5 (ave)
0.65C Electroslag Weld	22	118	75	1.6[3]	2.5% in 2 inches	2 ft lbs (ave)	38.4 (ave)
0.65C wire + ½ rail Guide Tube Electroslag Weld	25	[4]	[4]	[4]	[4]	2 ft lbs (ave)	40.95 (ave)

[1]See Ref. 6.
[2]See Ref. 5,6.
[3]Small defect in tensile bar.
[4]Large defect in tensile bar.

Table VI. ANALYSIS OF HOBART PF-201 NEUTRAL RUNNING FLUX*

Compound	Amount (wt.%)
CaO	12.20
MgO	2.34
MnO	22.46
CaF_2	8.62
SiO_2	32.95
Al_2O_3	8.32
TiO_2	8.02
K_2O	0.88
Na_2O	0.57
FeO	1.81
P_2O_5	<0.05

*See Ref. 34.

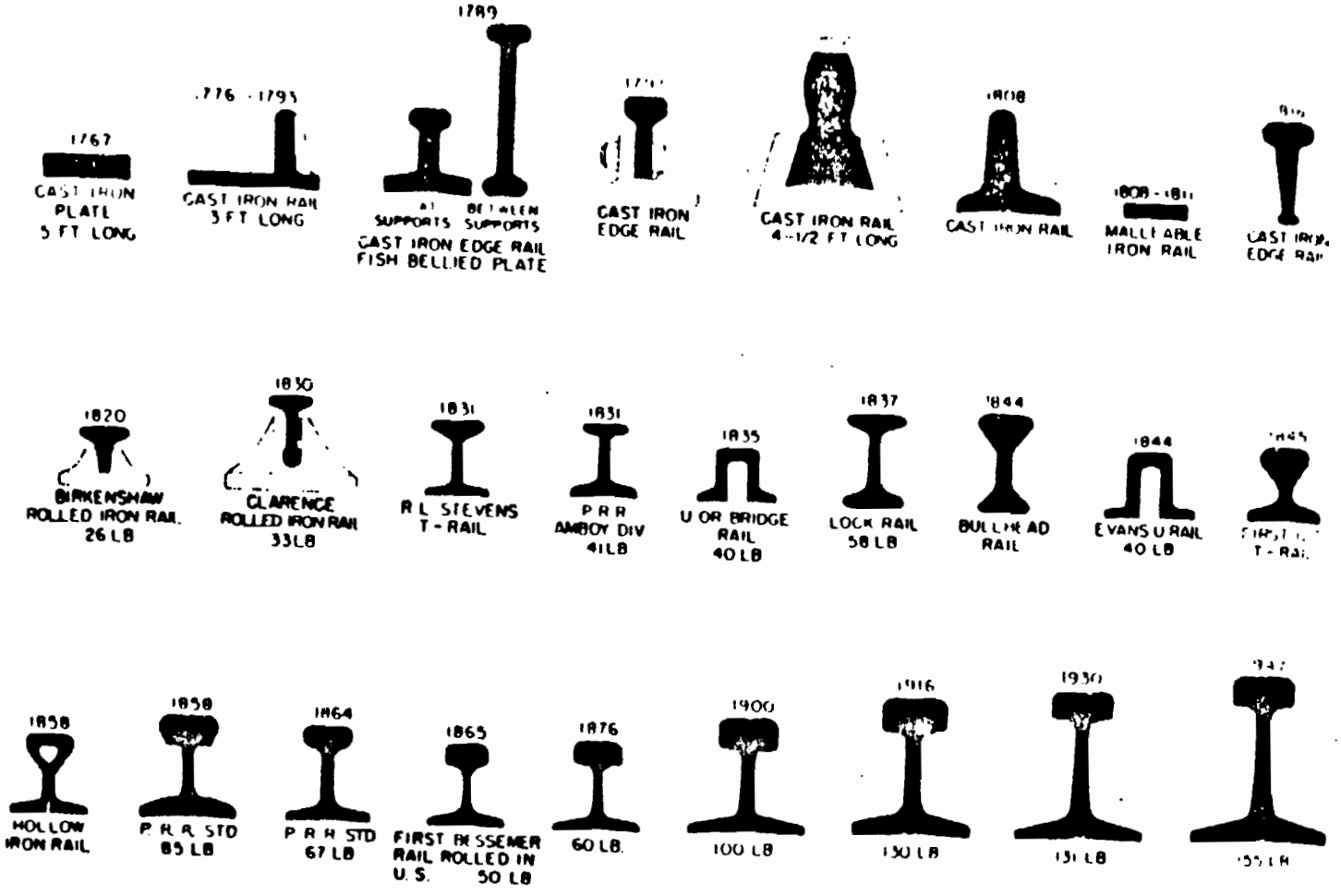

Figure 1. RAIL SECTION SHAPES.

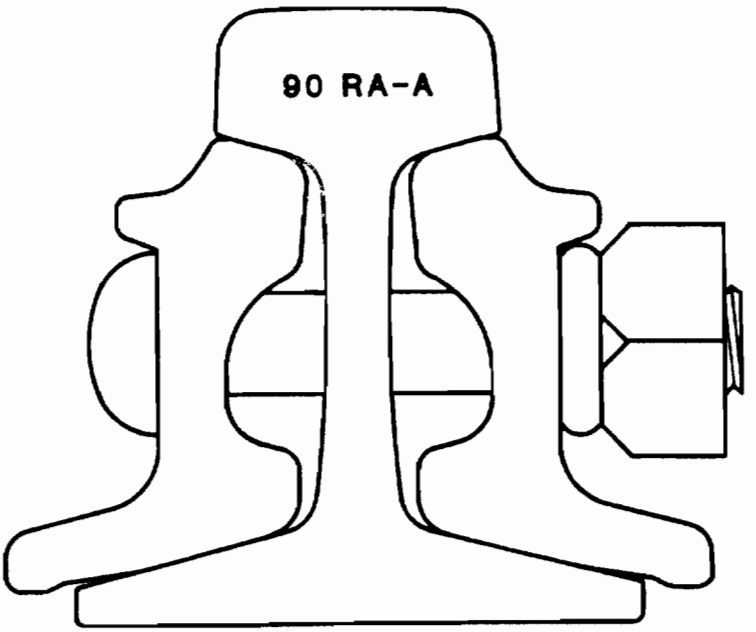

Figure 2. BOLTED JOINT CROSS SECTION.

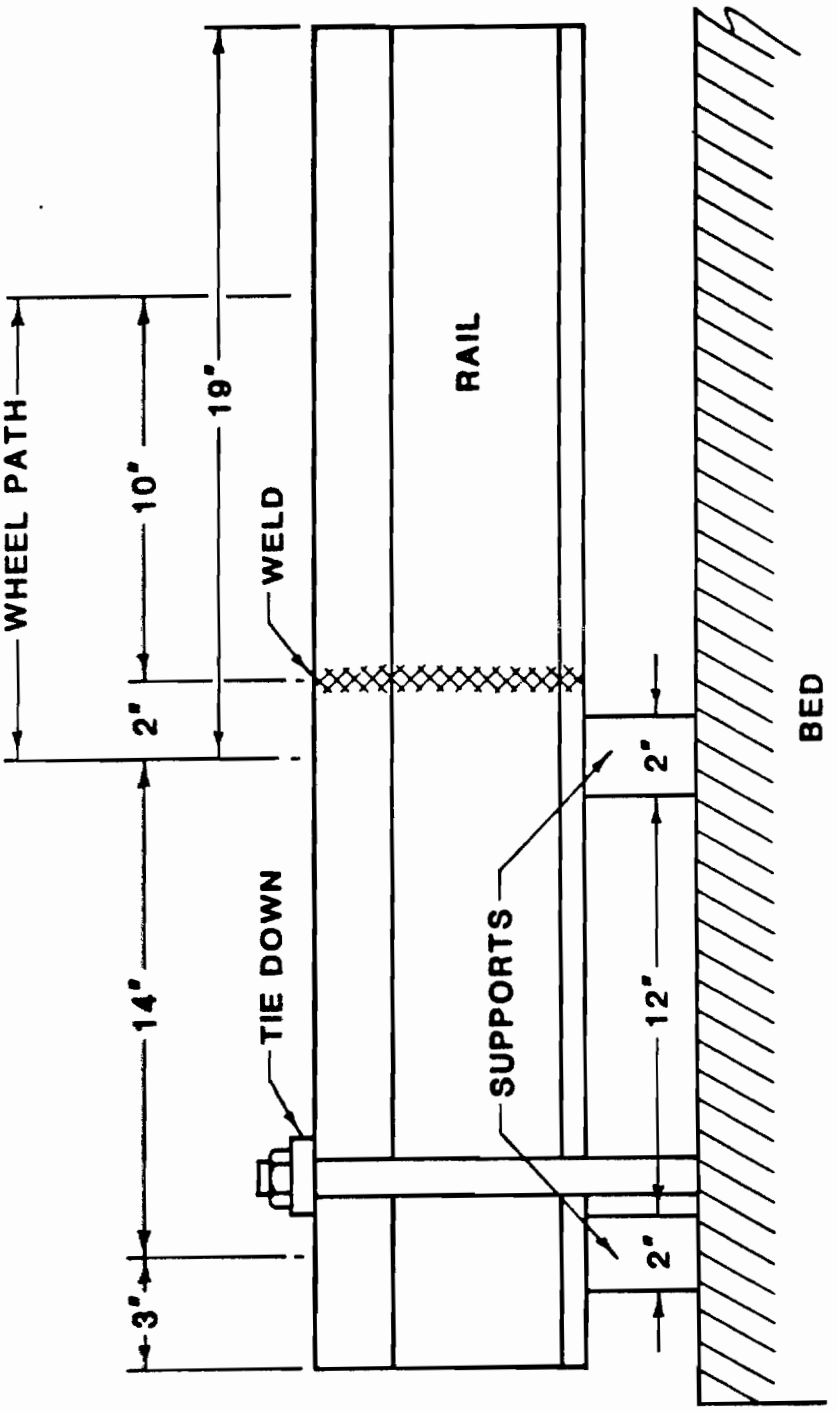

Figure 3. DIAGRAM OF ROLLING LOAD TEST.

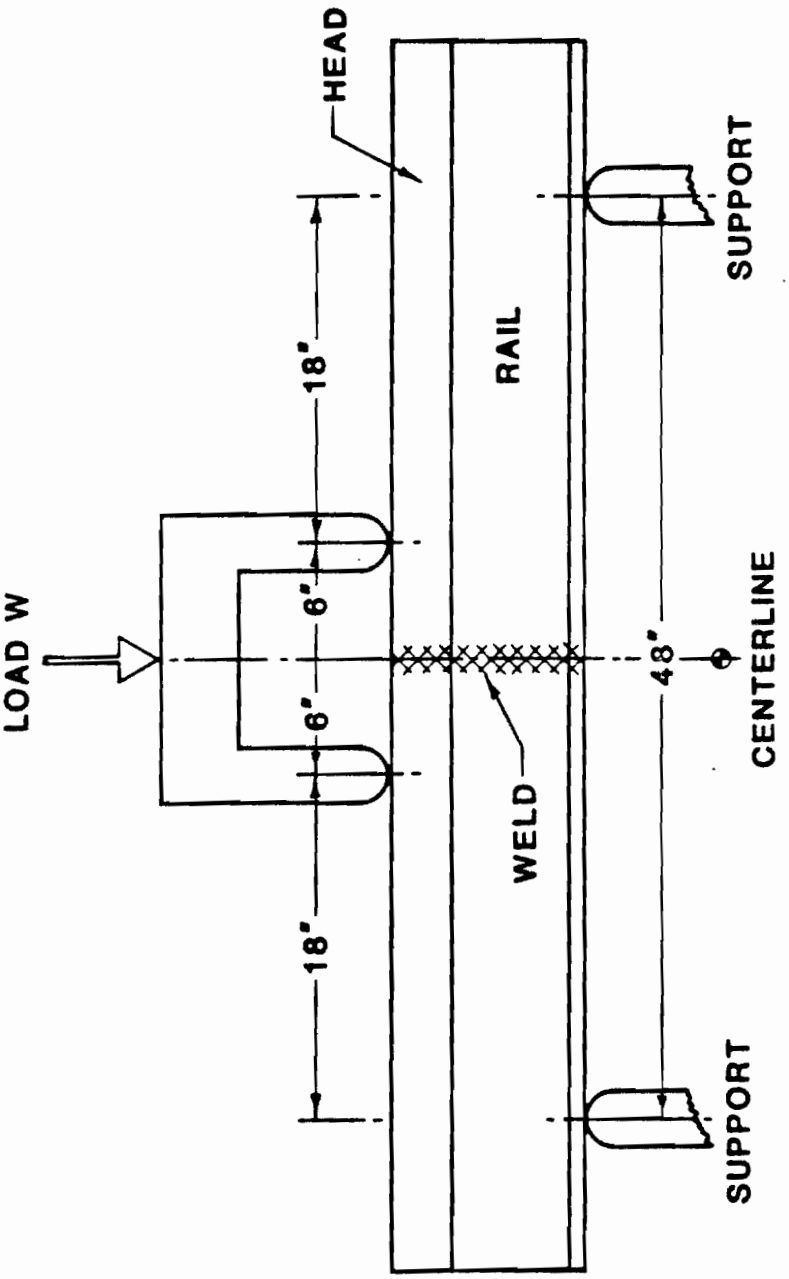

Figure 4. DIAGRAM OF SLOW BEND TEST.

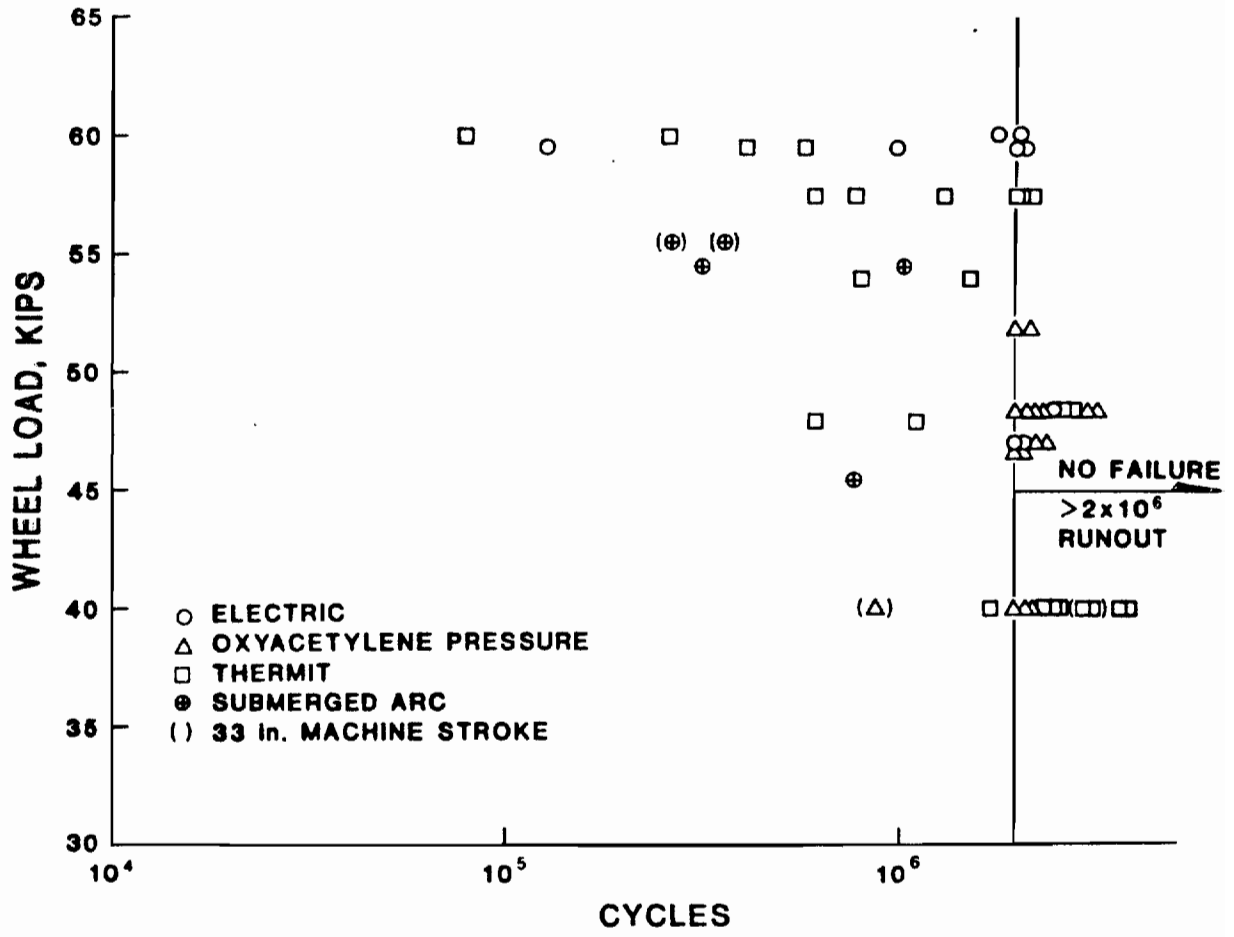

Figure 5. ROLLING LOAD TEST RESULTS.

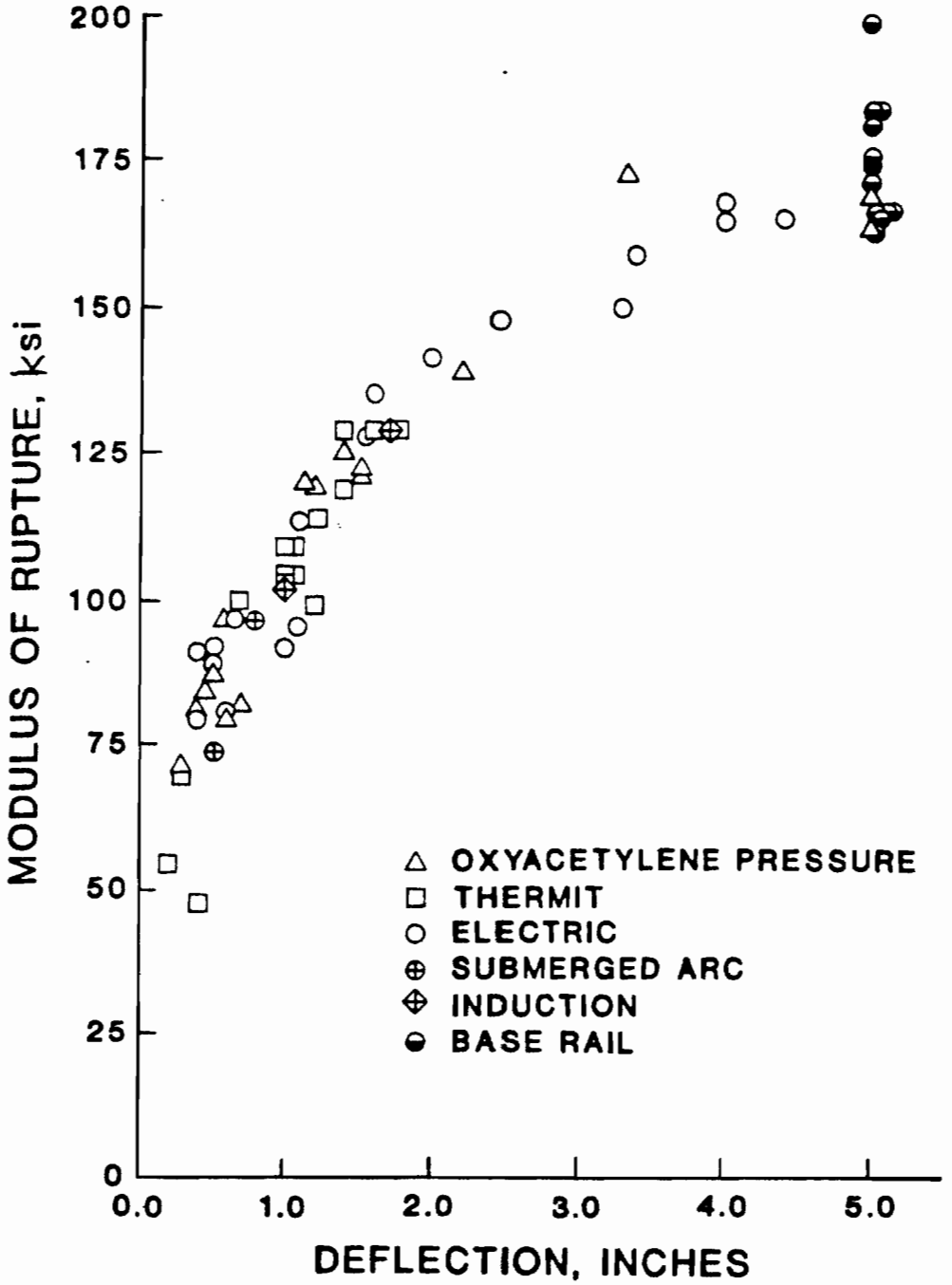

Figure 6. SLOW BEND TEST RESULTS.

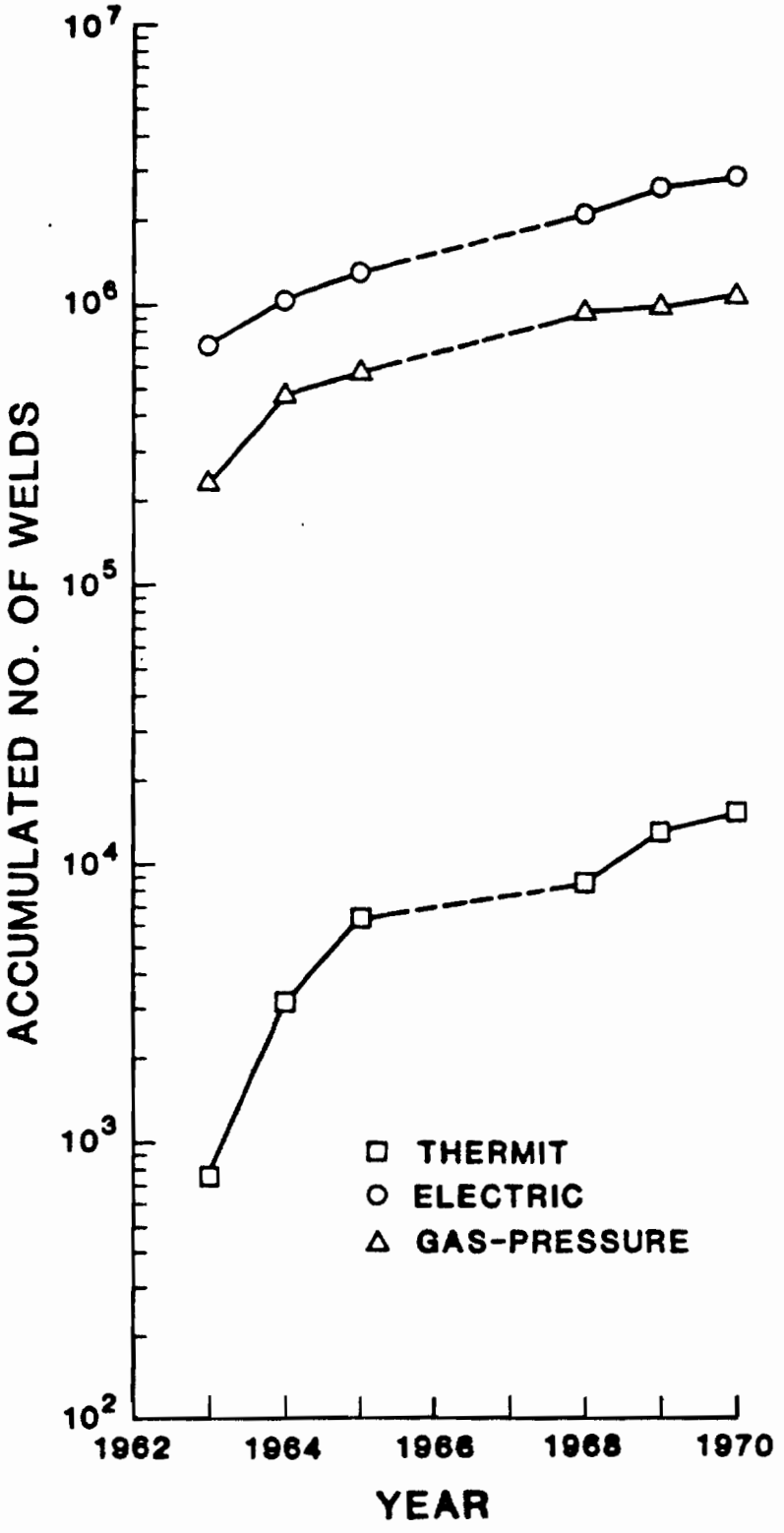

Figure 7. ACCUMULATED NUMBER OF WELDS.

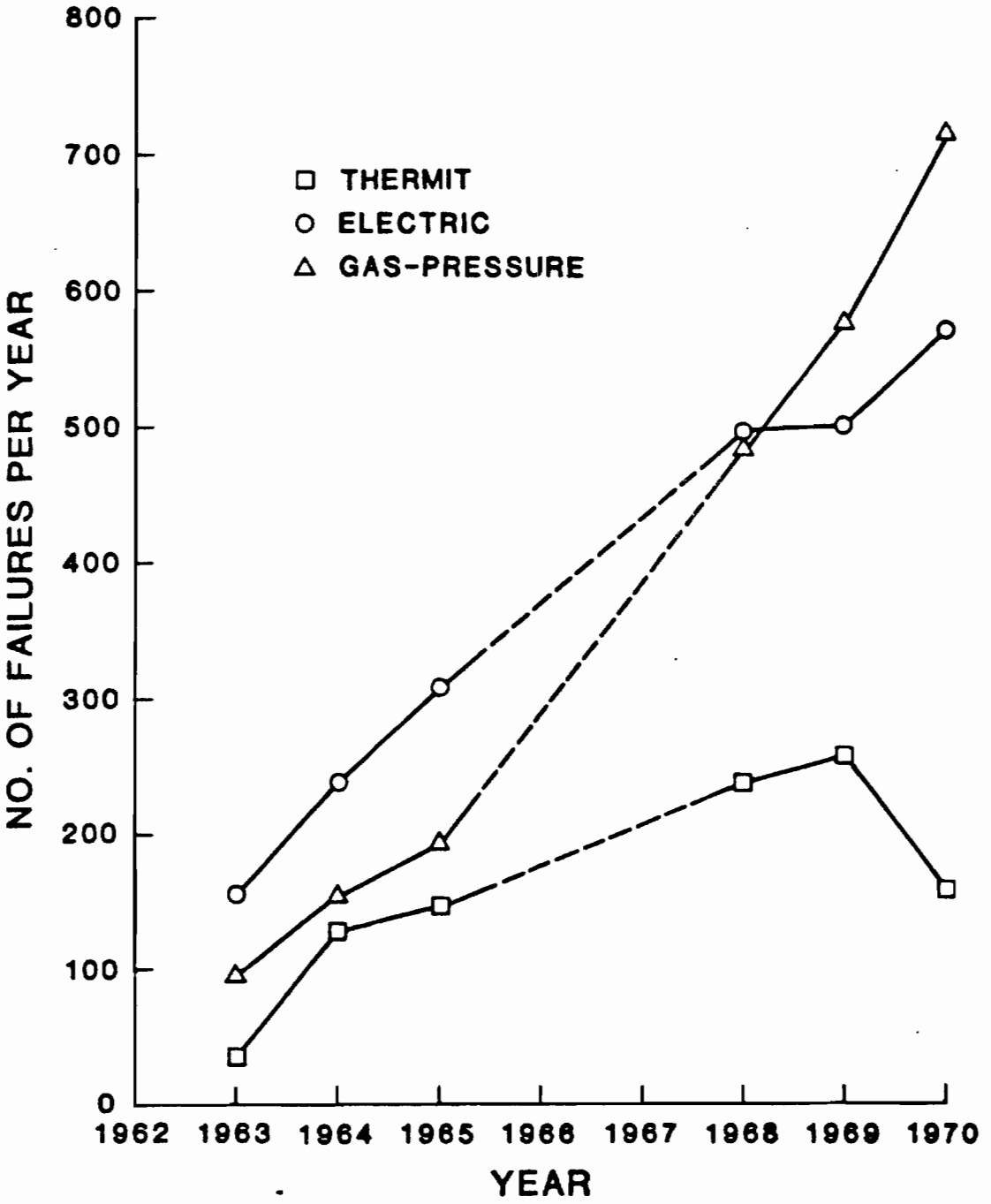

Figure 8. NUMBER OF WELD FAILURES PER YEAR.

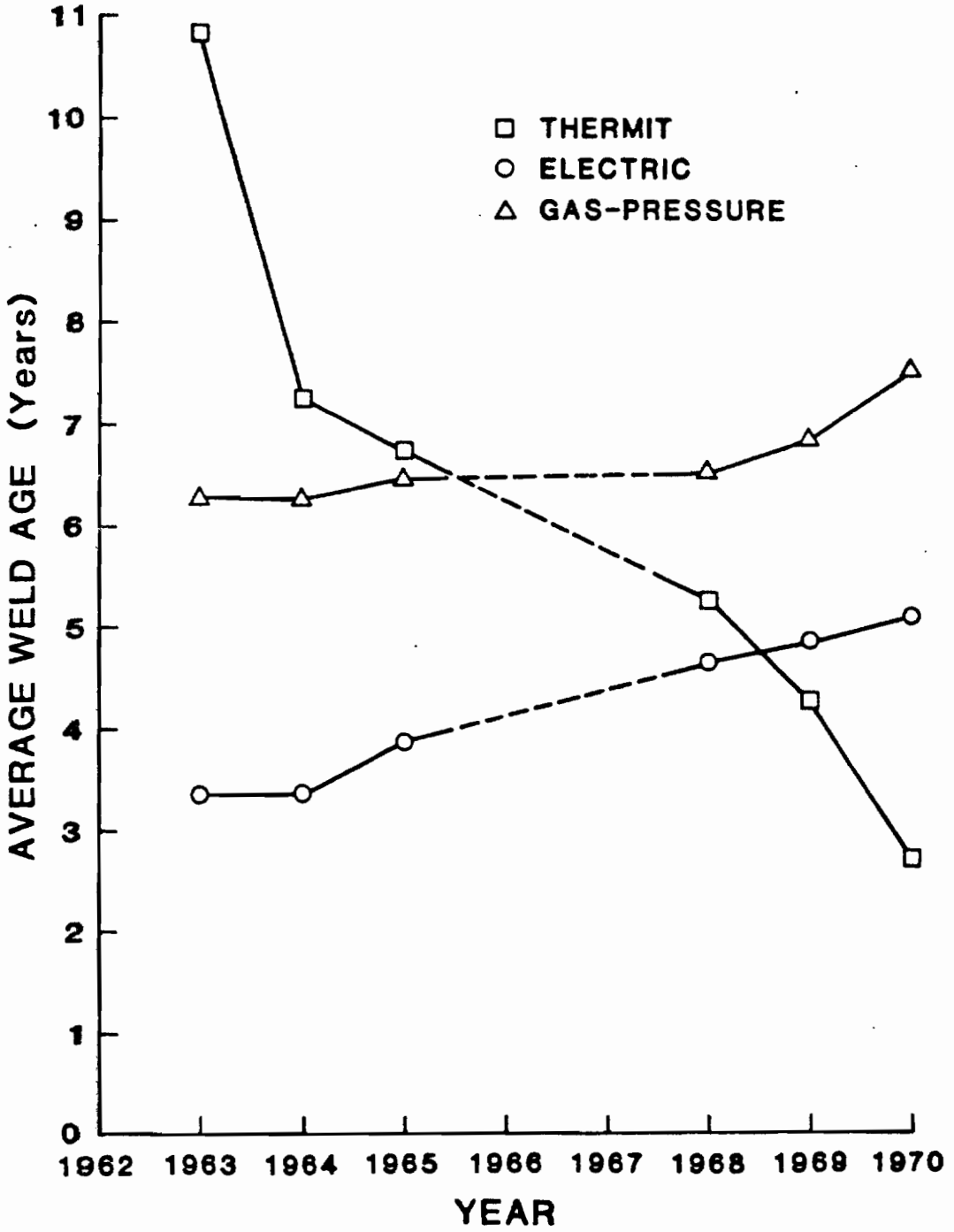

Figure 9. AVERAGE AGE OF WELDS.

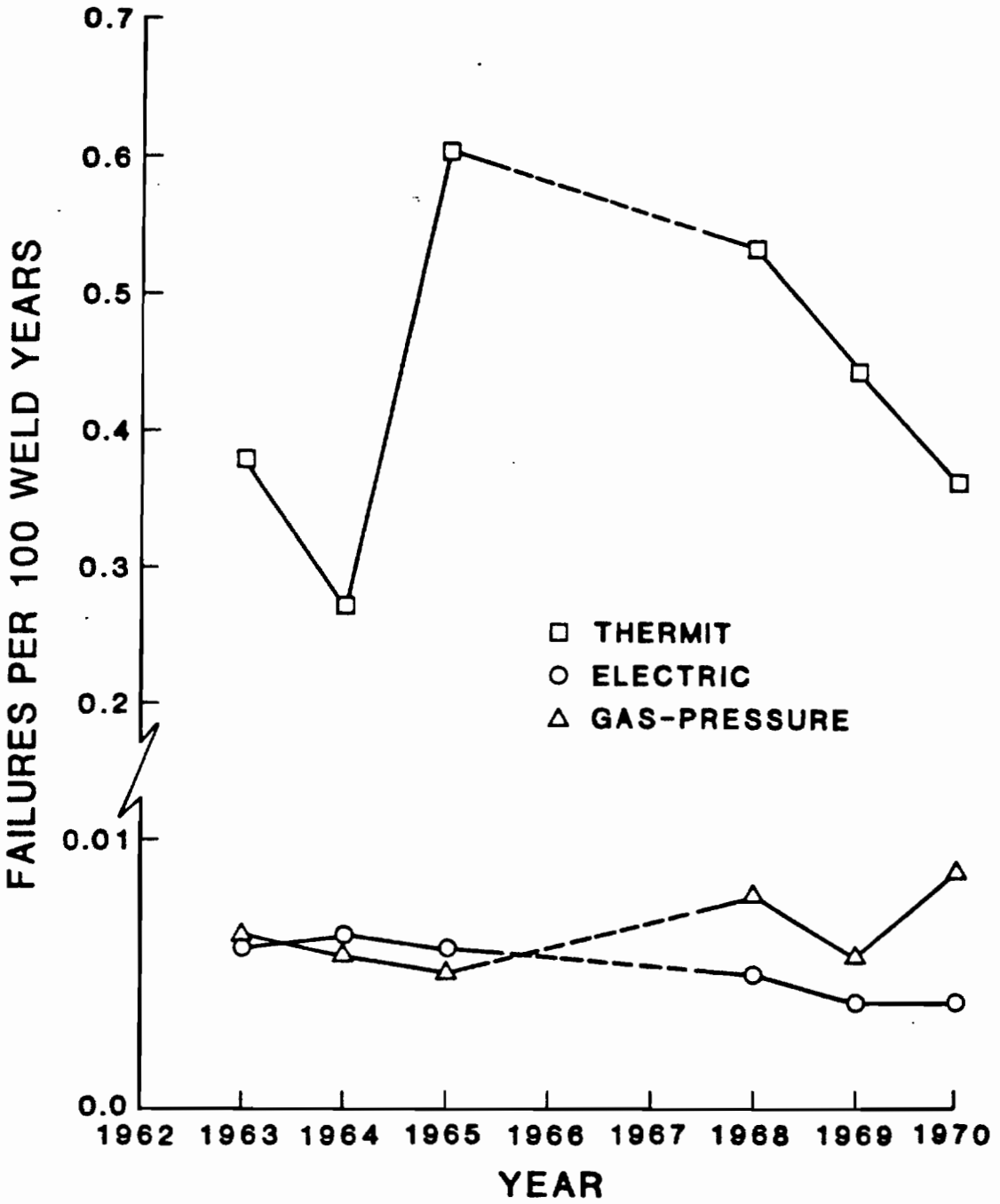

Figure 10. NUMBER OF WELD FAILURES PER 100 WELD YEARS.

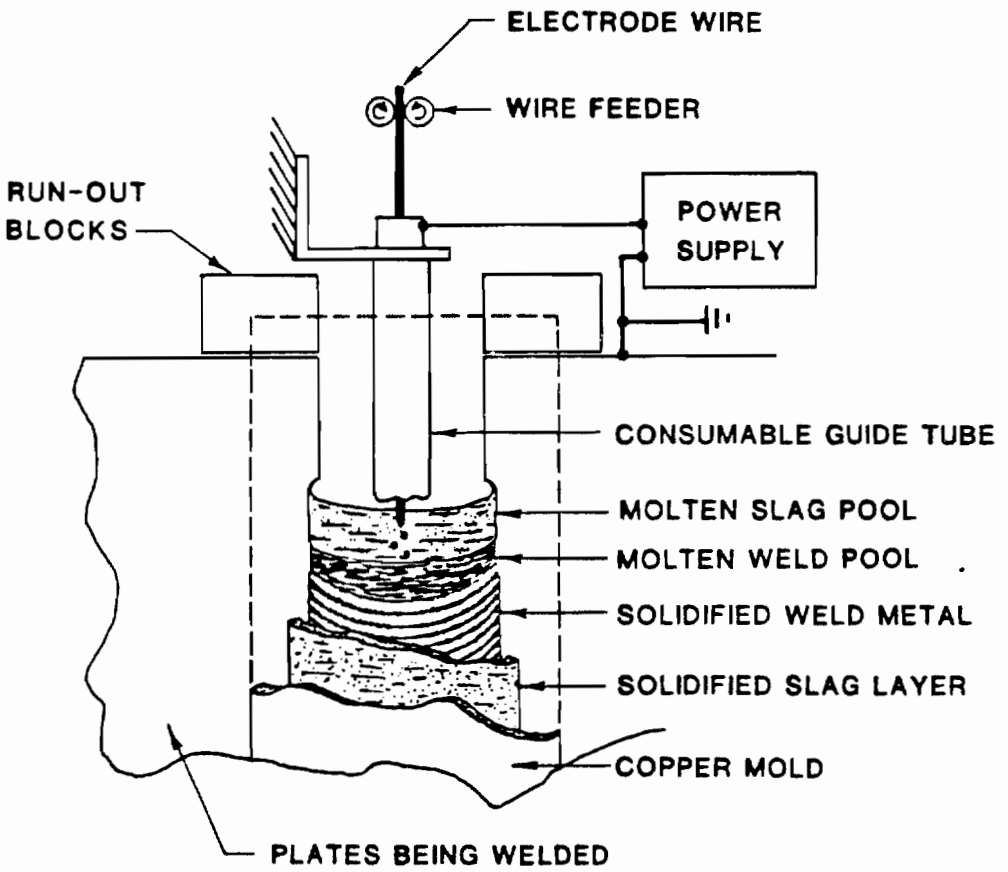

Figure 11. DIAGRAM OF ELECTROSLAG WELDING WITH A CONSUMABLE GUIDE TUBE.

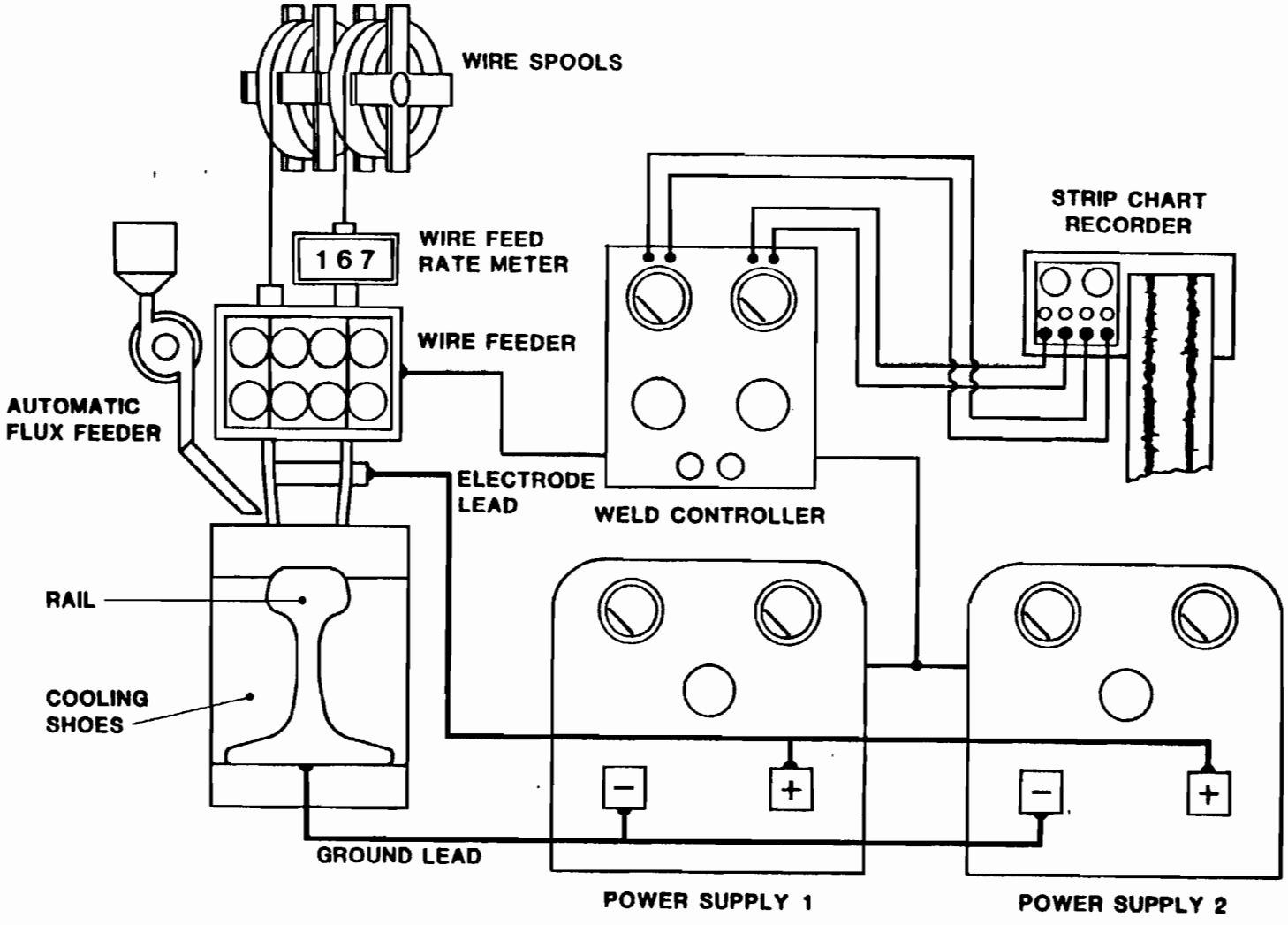

Figure 12. SCHEMATIC OF CONSUMABLE GUIDE TUBE ELECTROSLAG WELDING PROCESS.

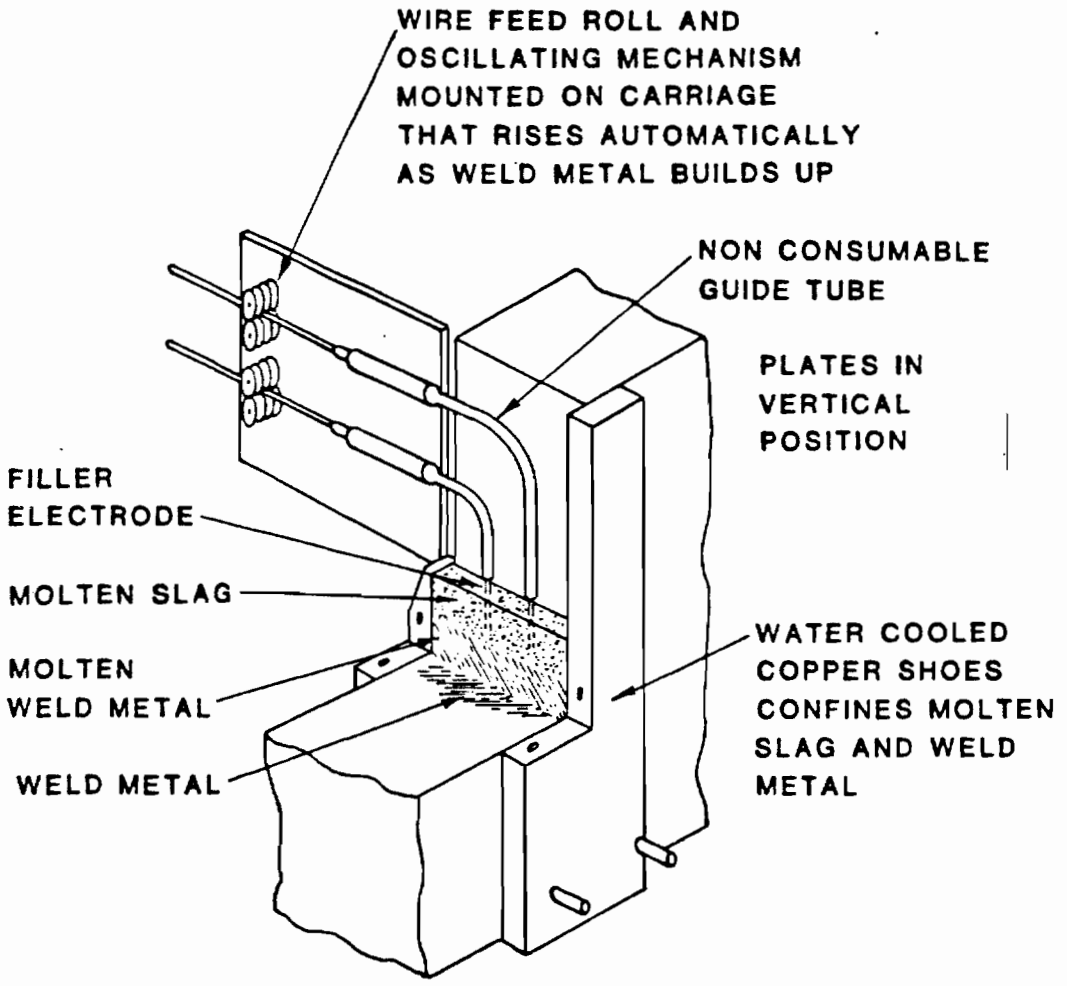

Figure 13. DIAGRAM OF ELECTROSLAG WELDING WITH NON-CONSUMABLE GUIDE TUBE.

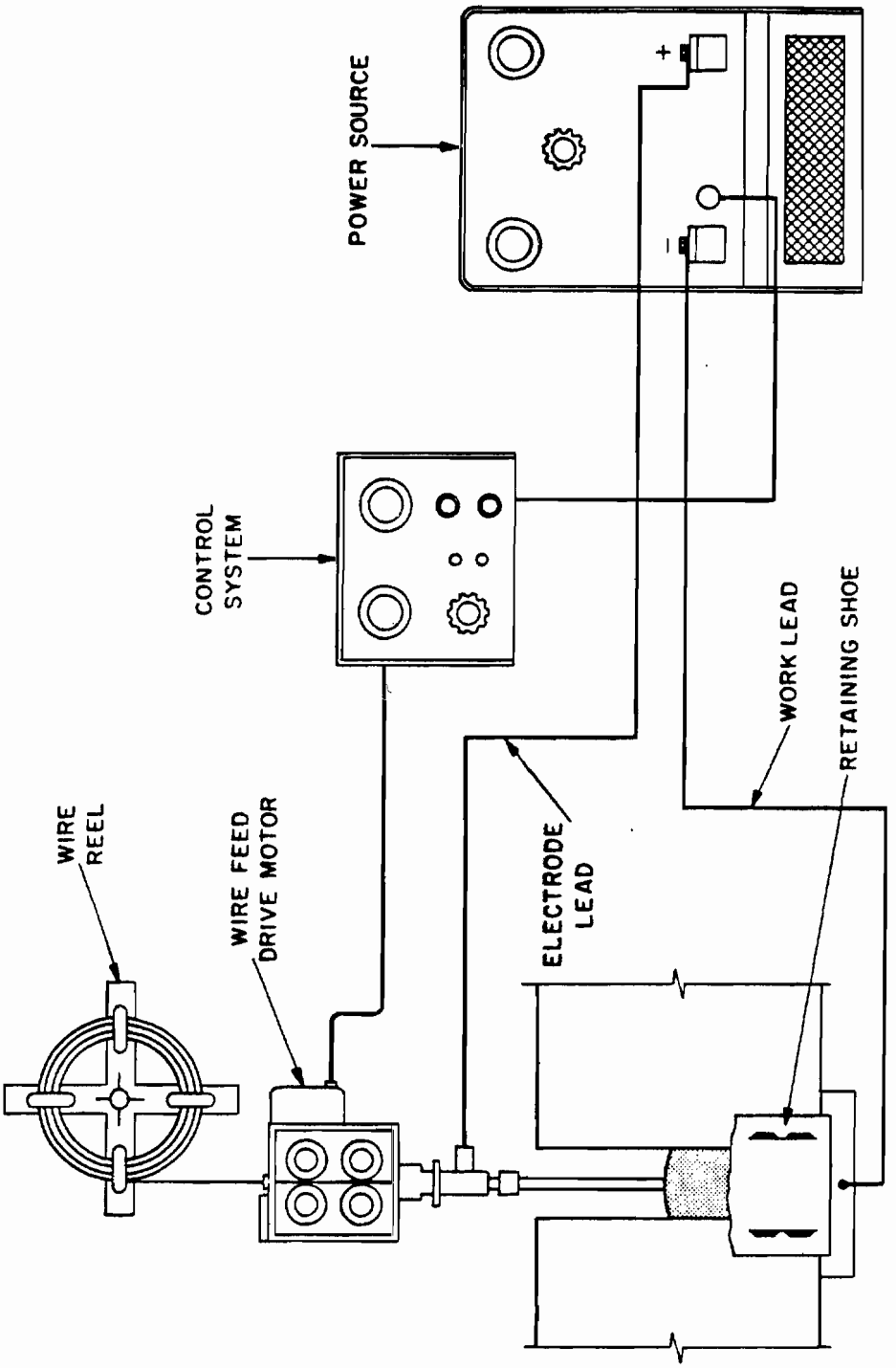

Figure 14. SCHEMATIC OF ELECTROSLAG RAIL WELDING.

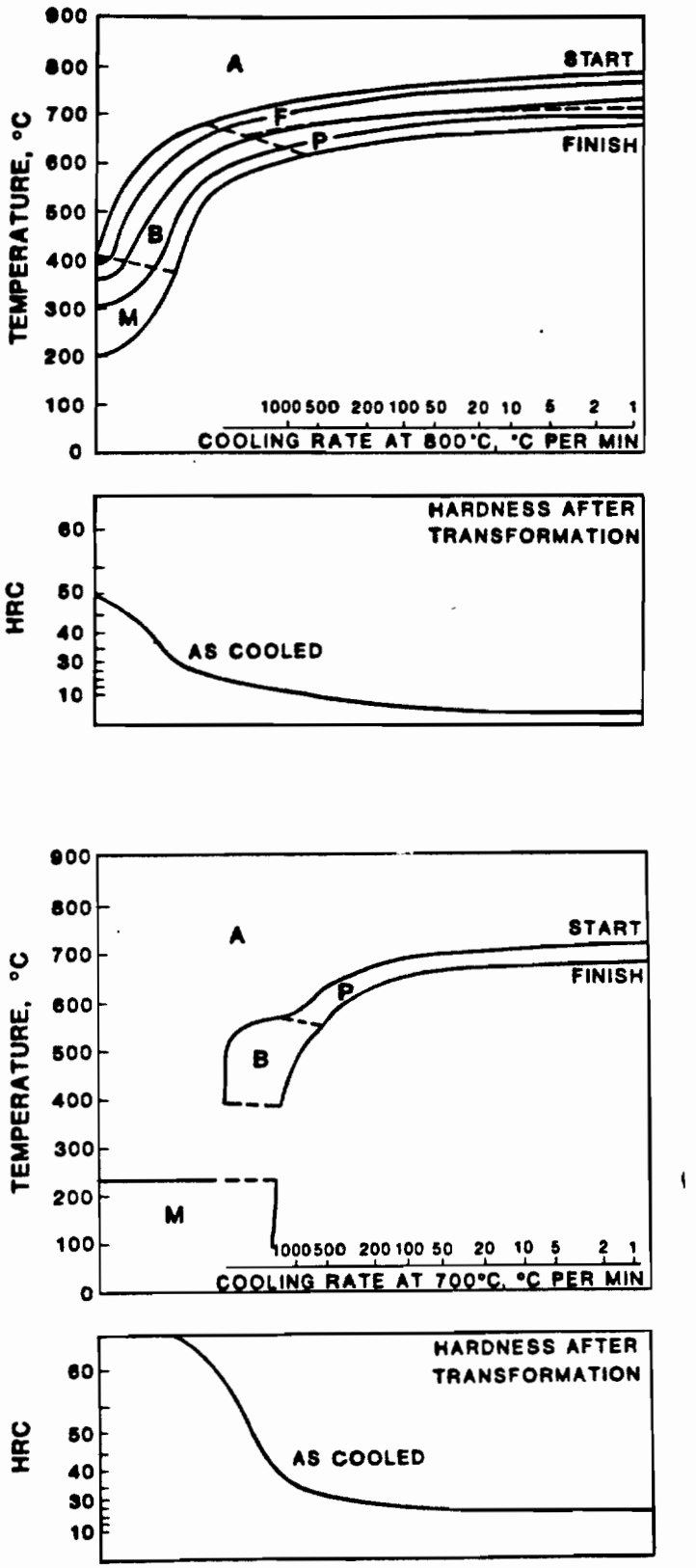

Figure 15. CONTINUOUS COOLING TRANSFORMATION DIAGRAMS.

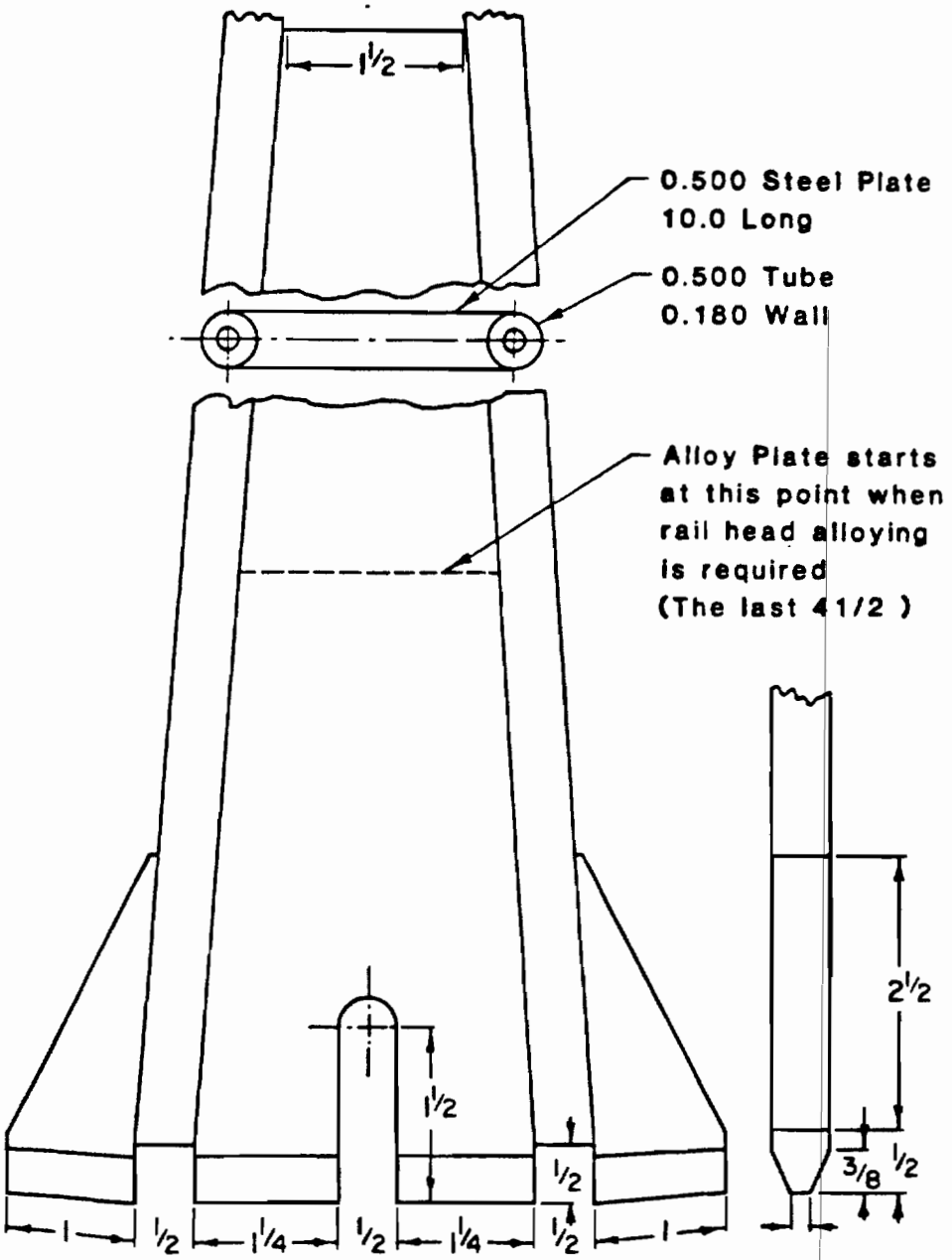

Figure 16. ELECTROSLAG RAIL WELD PLATE GUIDE TUBE DESIGN.

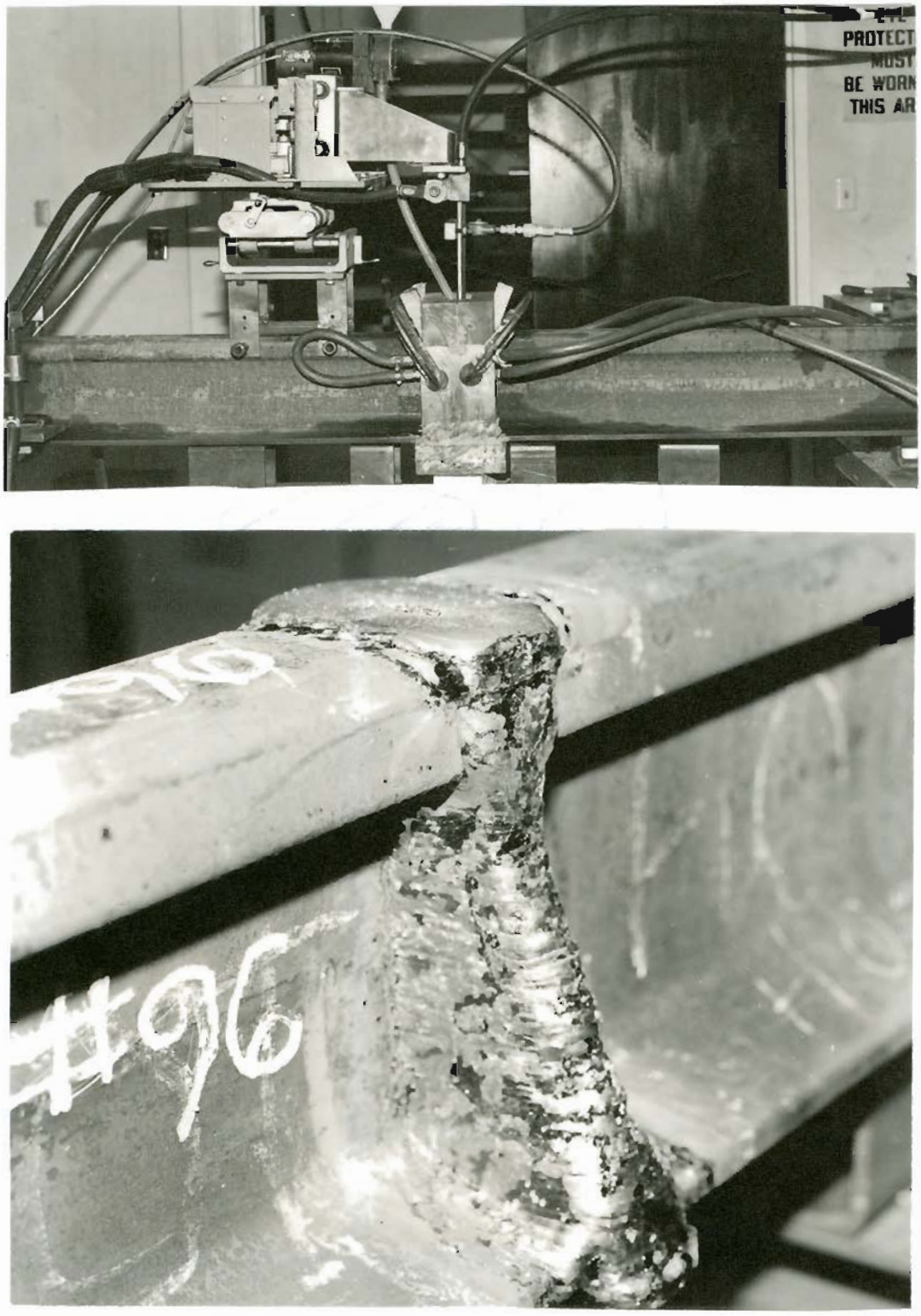

Figure 17. ELECTROSLAG RAIL WELDING SETUP AND COMPLETED WELD.

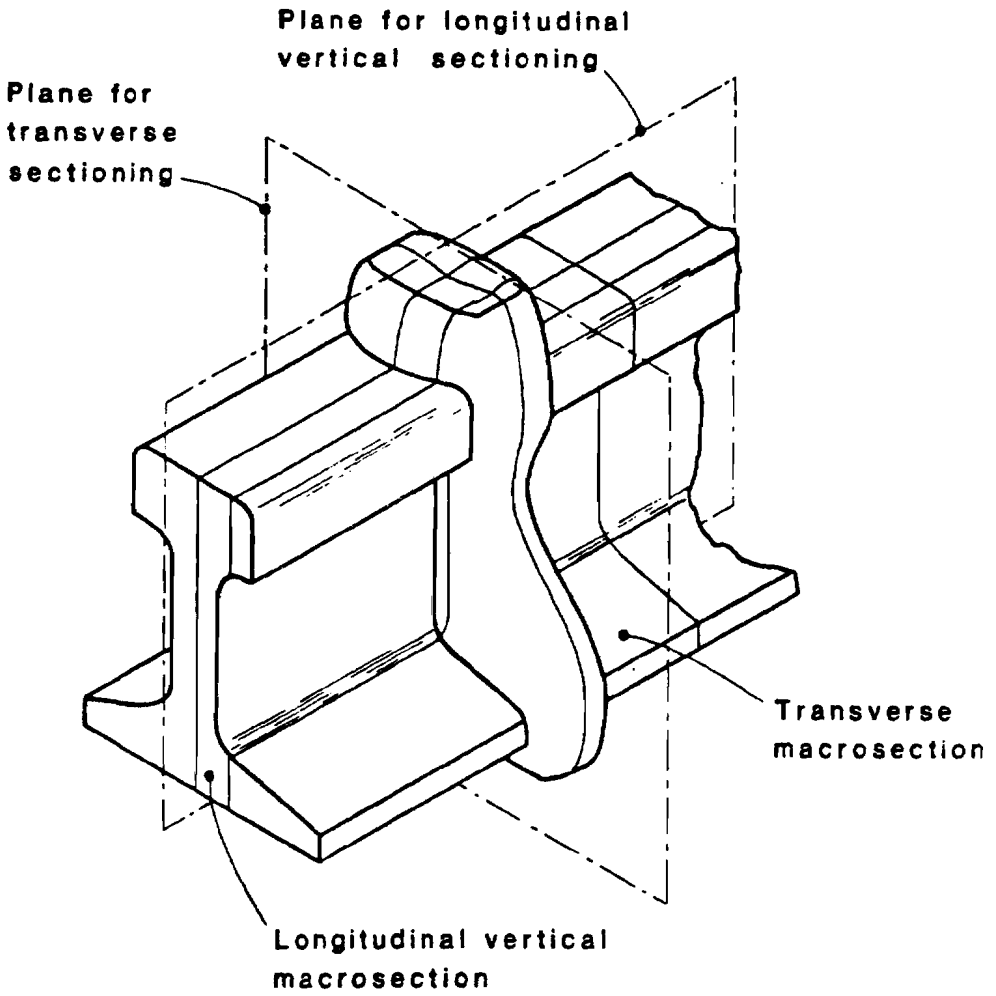

Figure 18. MACROSECTIONING DIAGRAM.

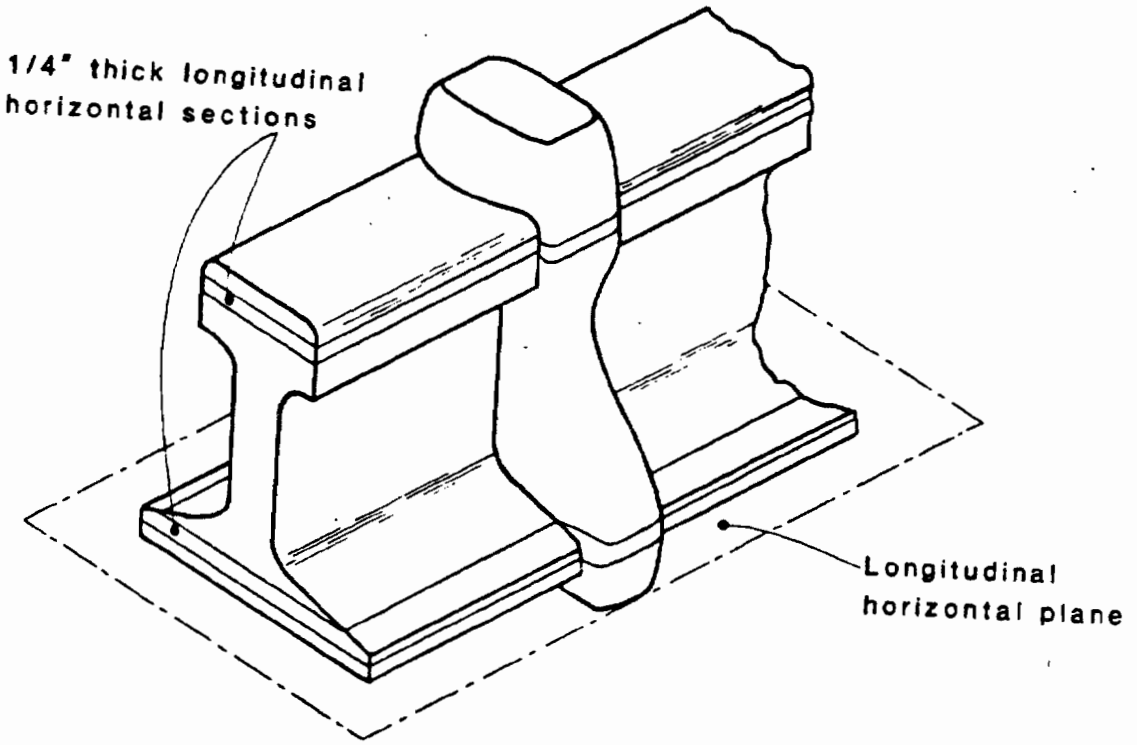

Figure 19. SECTIONING DIAGRAM FOR DILUTION MEASUREMENTS.

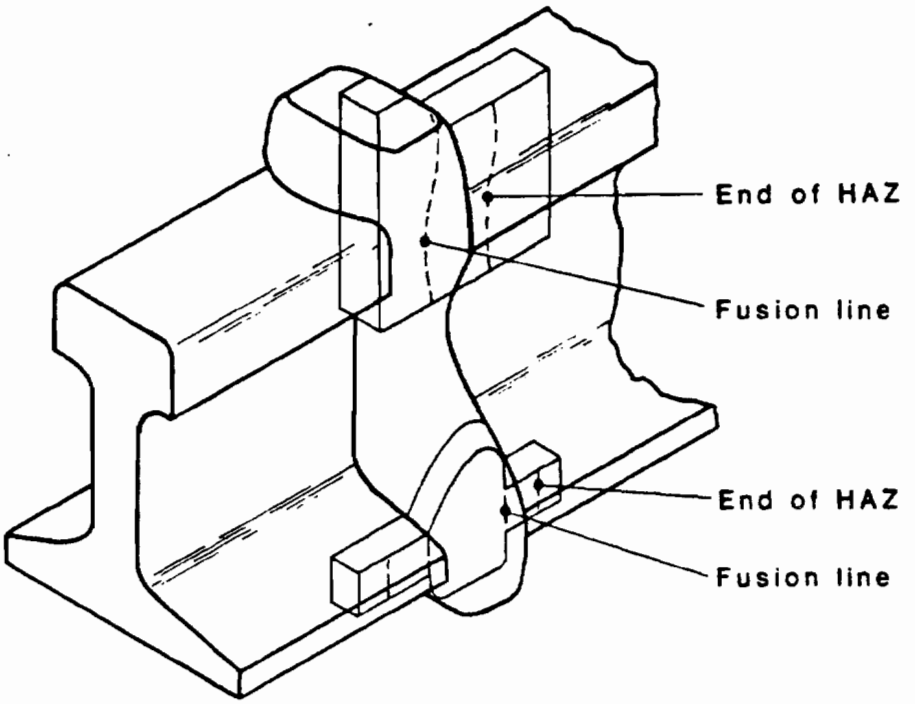

Figure 20. SECTIONING DIAGRAM FOR MICROSCOPIC EXAMINATION SPECIMENS.

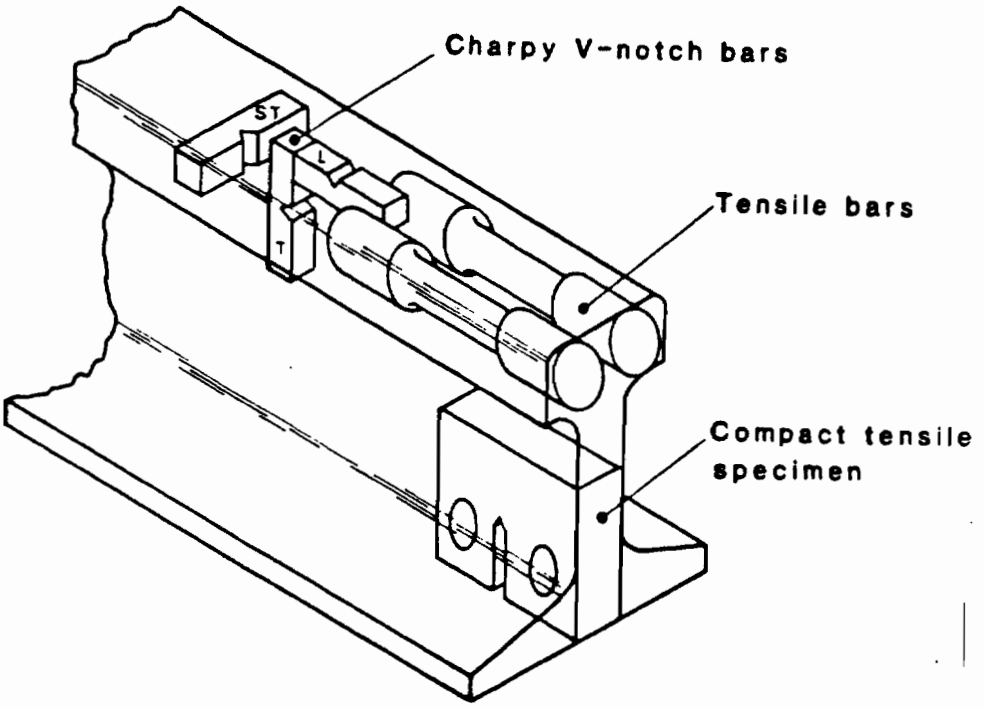

Figure 21. LOCATION OF RAIL MECHANICAL PROPERTY SPECIMENS.

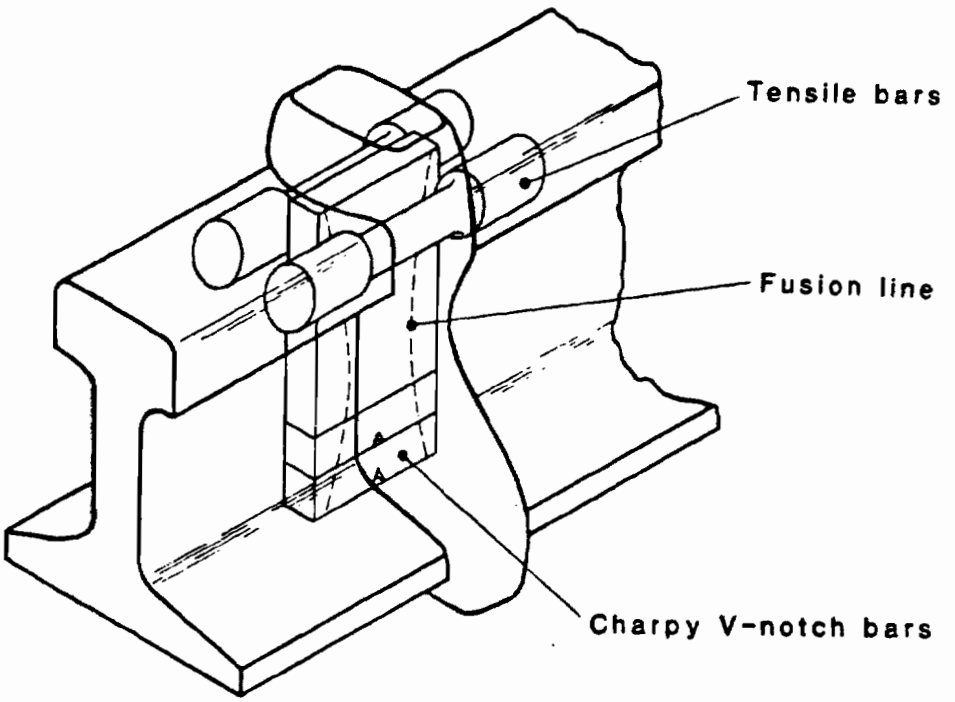

Figure 22. LOCATION OF ELECTROSLAG RAIL WELD MECHANICAL PROPERTY SPECIMENS.

Figure 23. HALF-RAIL/HALF-MILD STEEL GUIDE PHOTOGRAPH.

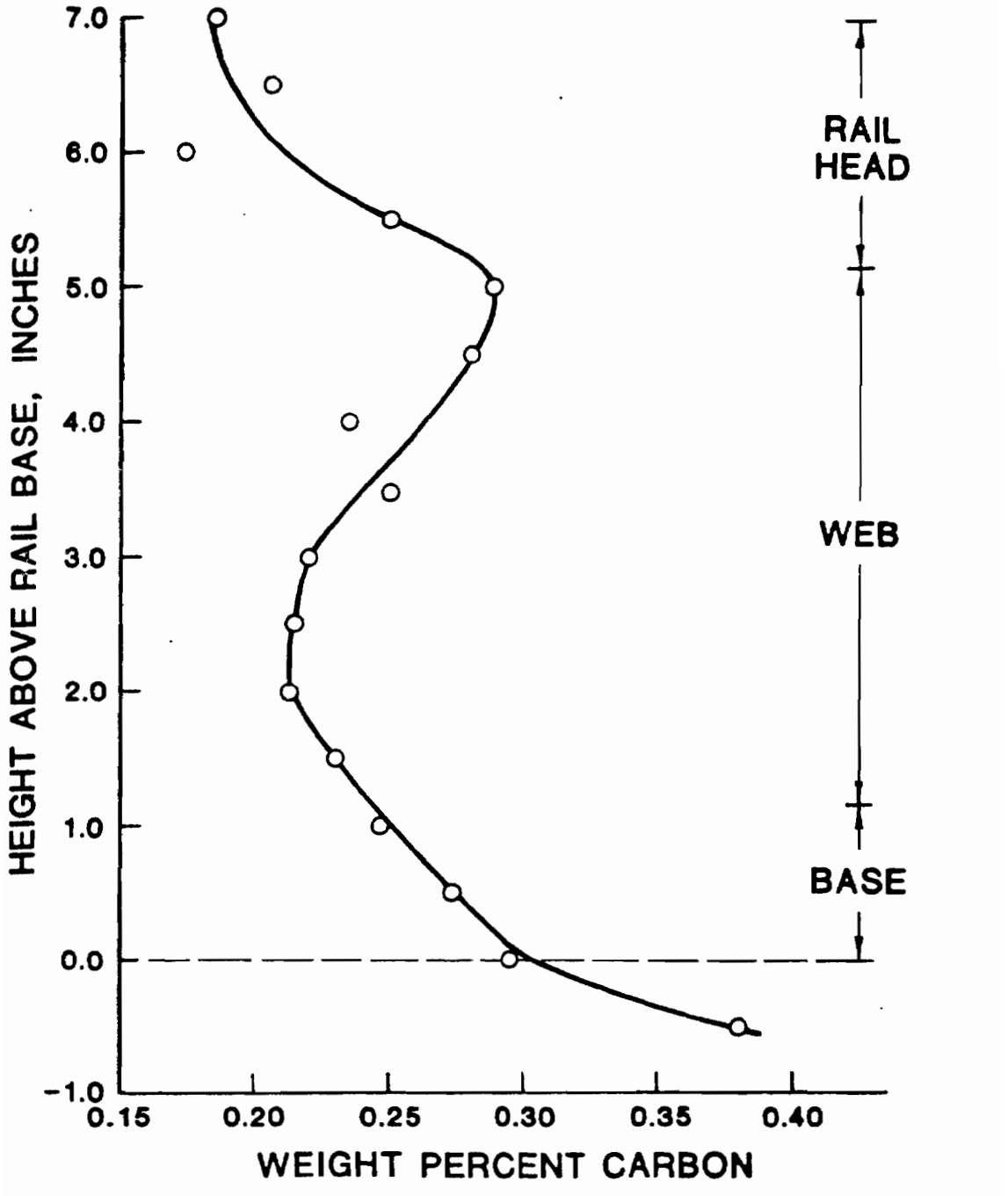

Figure 24. VARIATION IN CARBON CONTENT IN A WELD USING MILD STEEL FILLER WIRE AND MILD STEEL GUIDE TUBE.

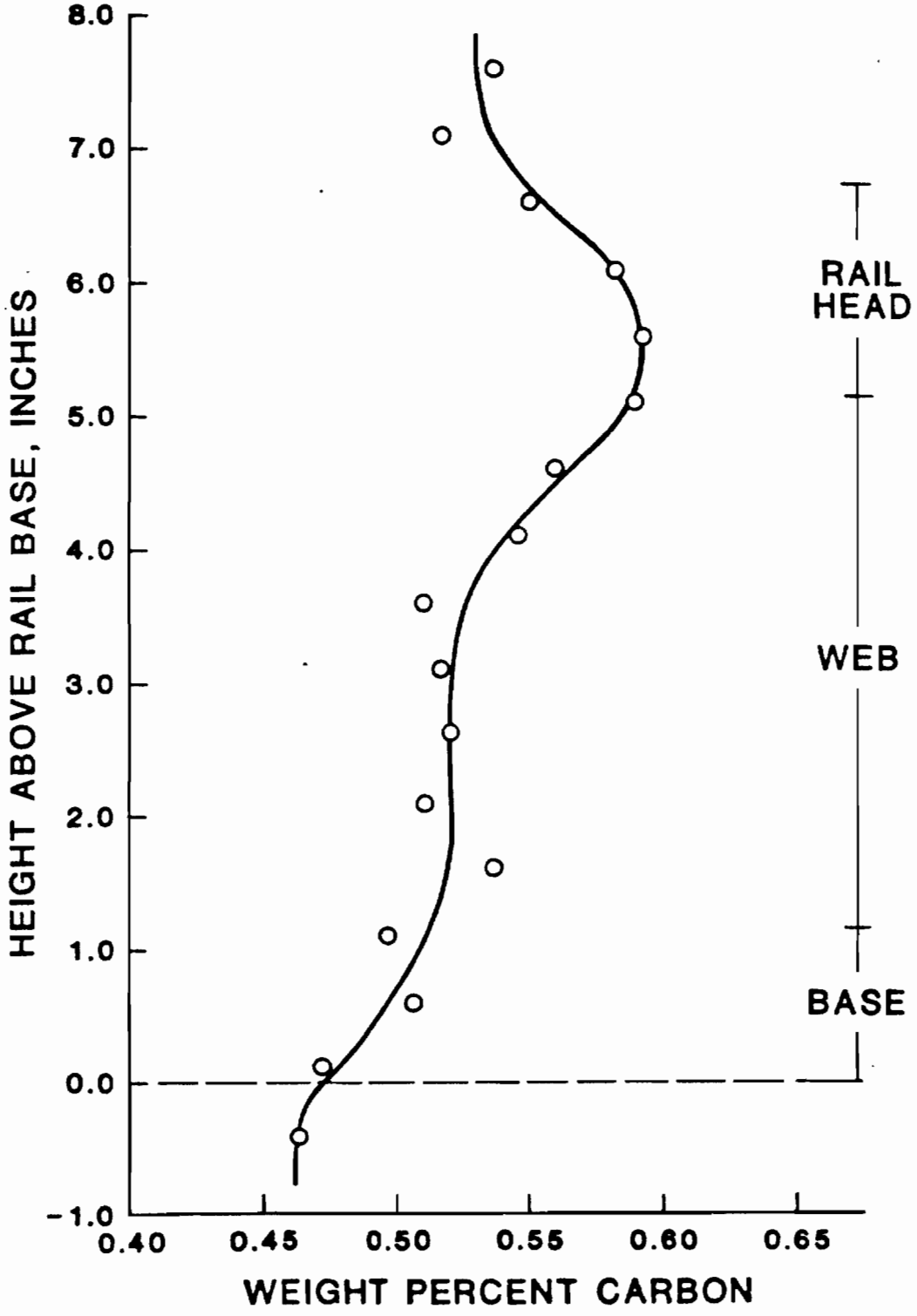

Figure 25. VARIATION IN CARBON CONTENT IN A WELD USING HIGH CARBON (0.65 wt.%C) WIRE AND MILD STEEL GUIDE TUBE.

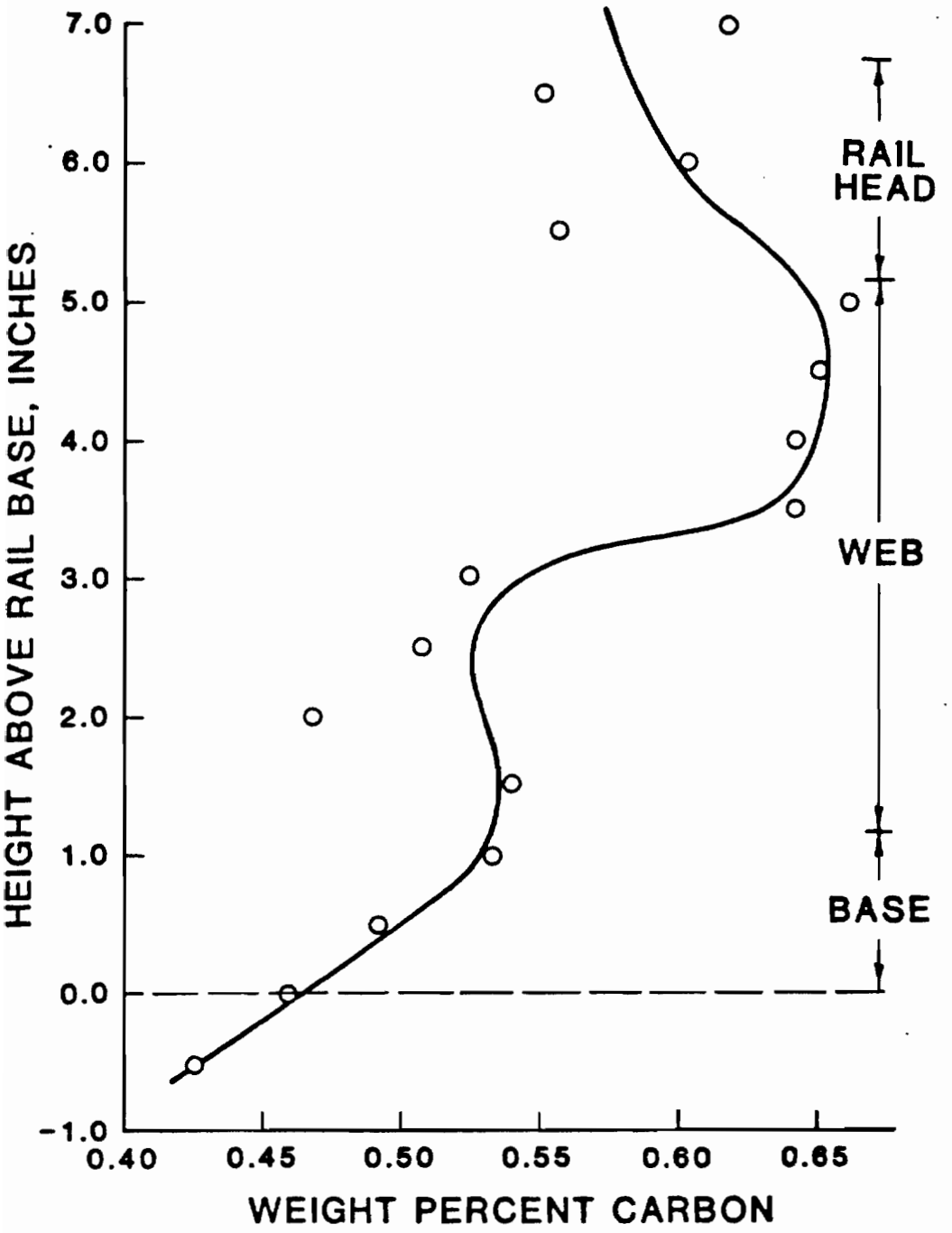

Figure 26. VARIATION IN CARBON CONTENT IN A WELD USING HIGH CARBON (0.65 wt.%C) FILLER WIRE AND HALF-RAIL/HALF-MILD STEEL GUIDE TUBE.

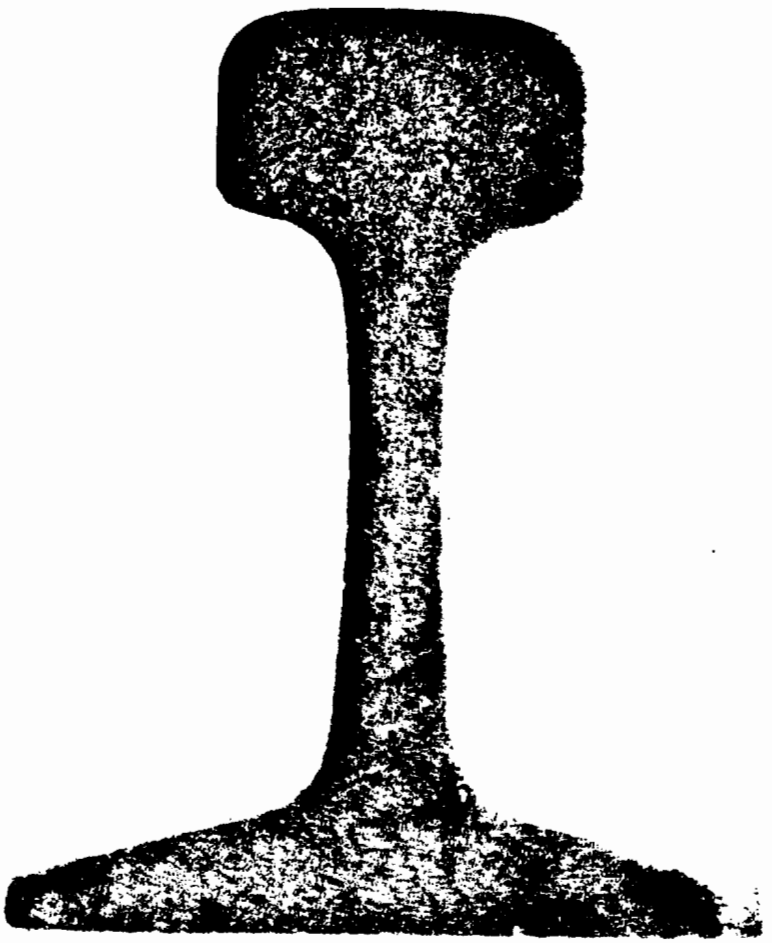

Figure 27. SULFUR PRINTS OF RAIL STEEL.

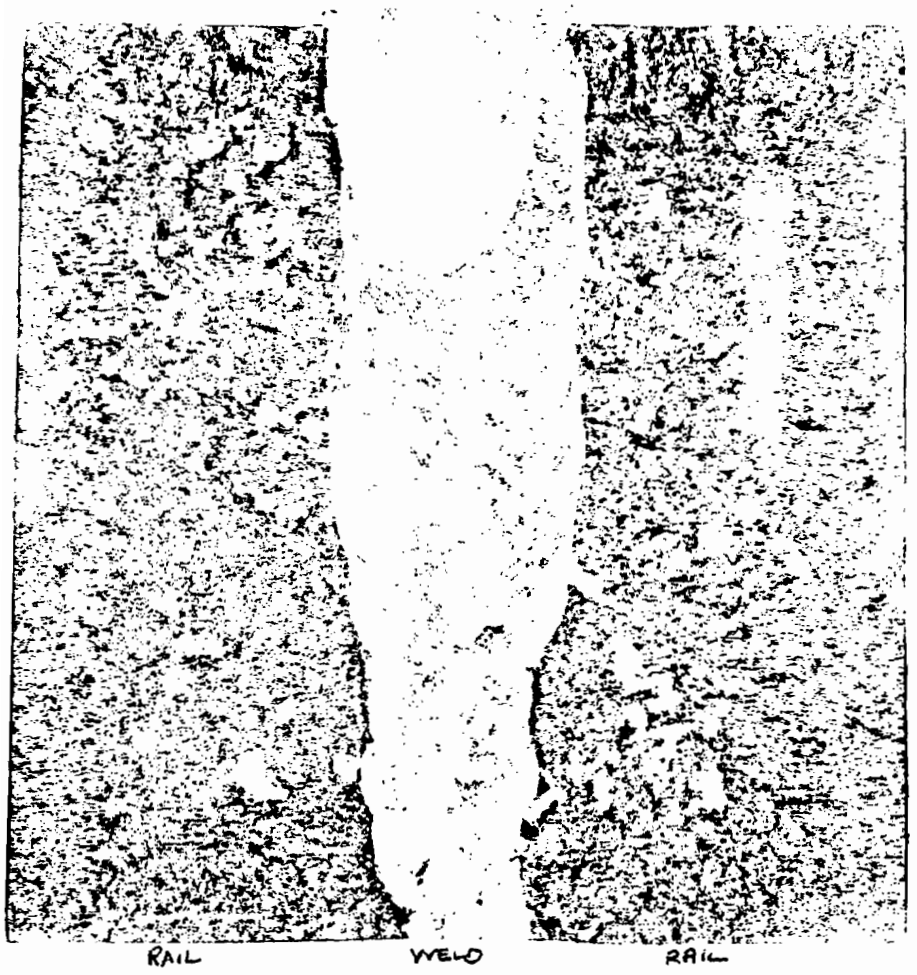

Figure 28. SULFUR PRINT OF ELECTROSLAG RAIL WELD.

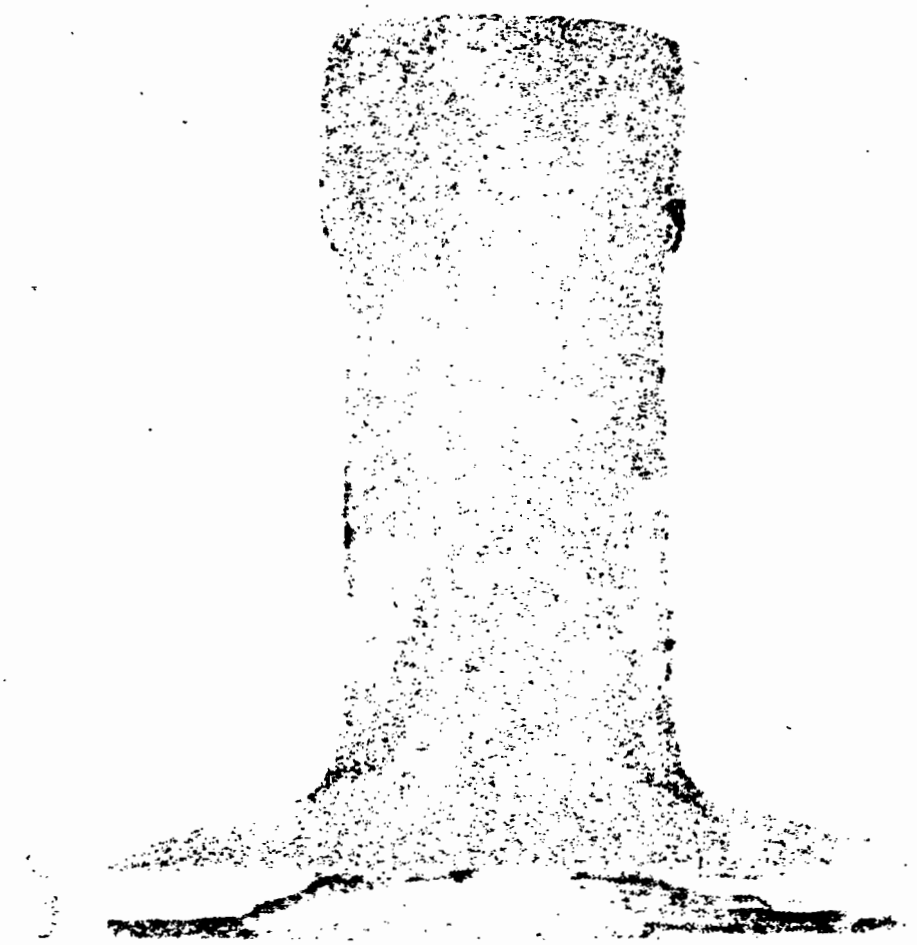

Figure 29. SULFUR PRINT OF THERMIT WELD.

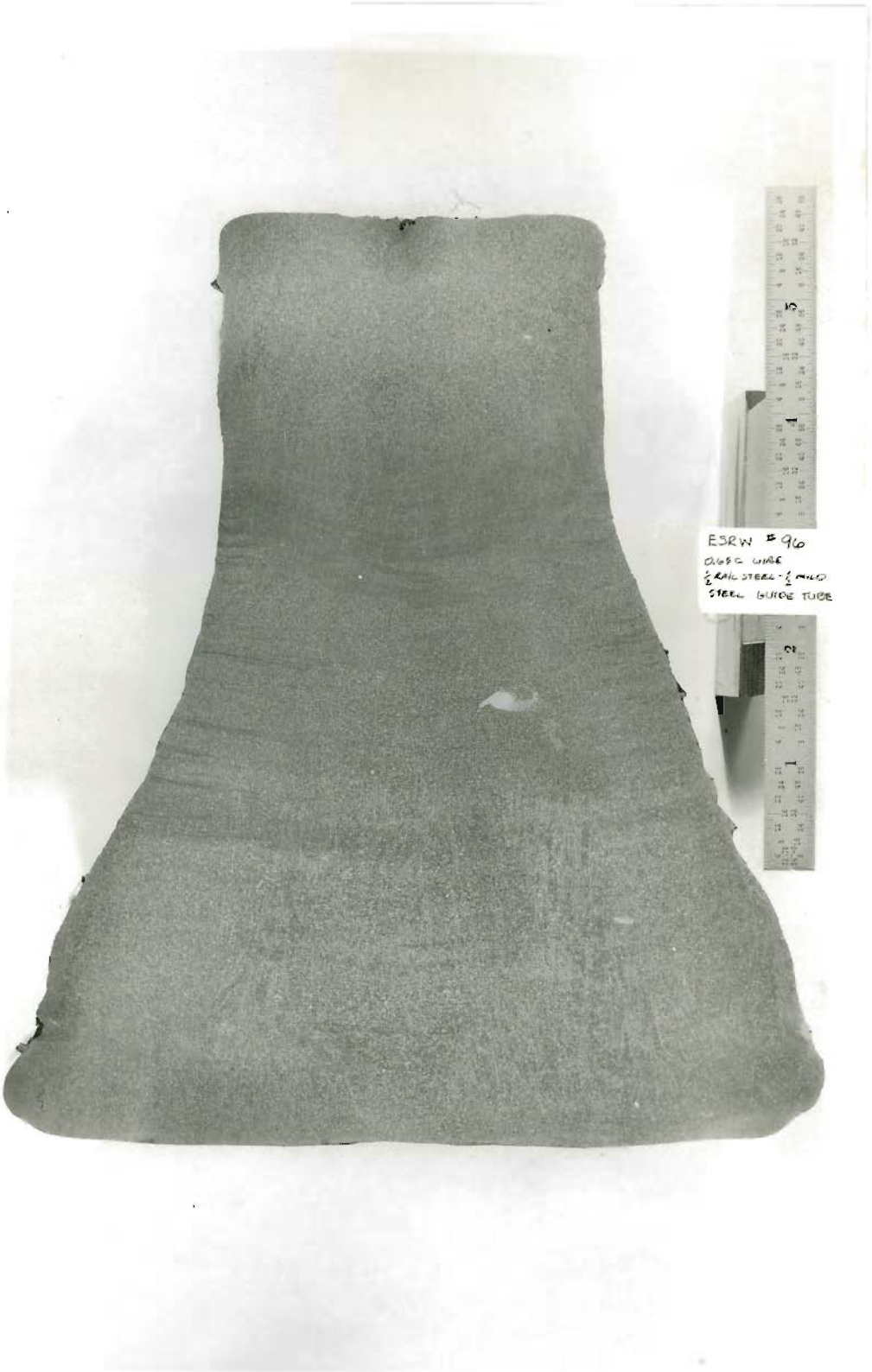

Figure 30. TRANSVERSE MACROSECTIONS OF RAIL WELDS.

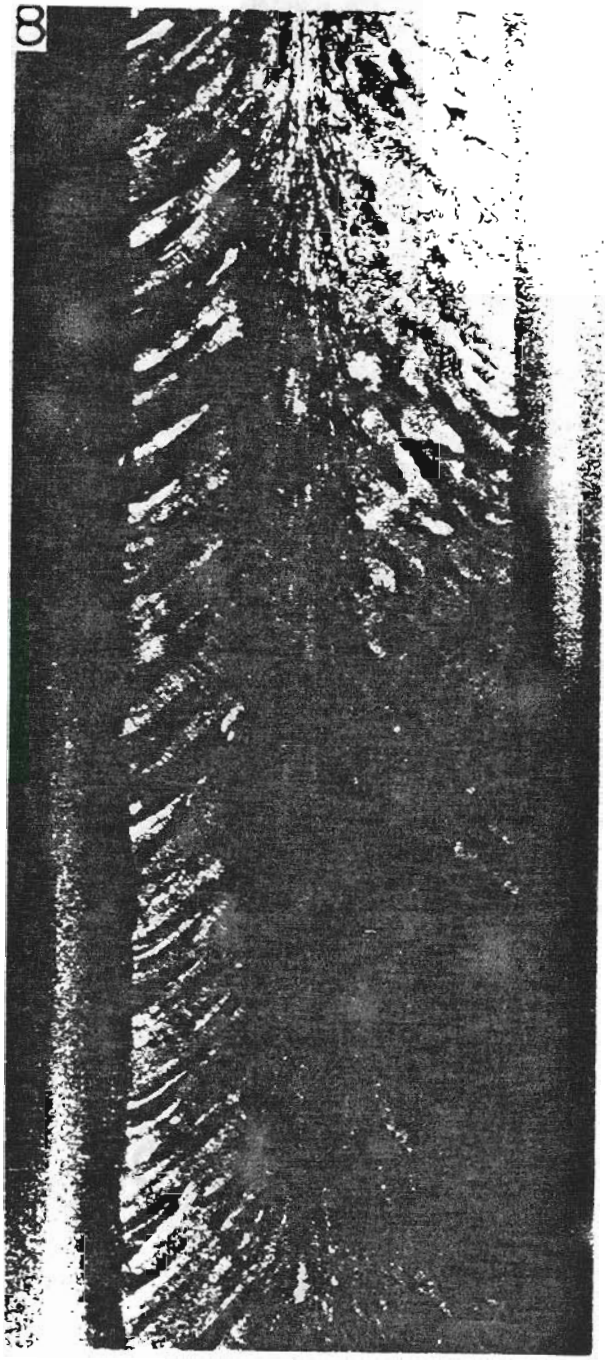

Figure 31. MACROSTRUCTURE OF ELECTROSLAG PLATE WELD.

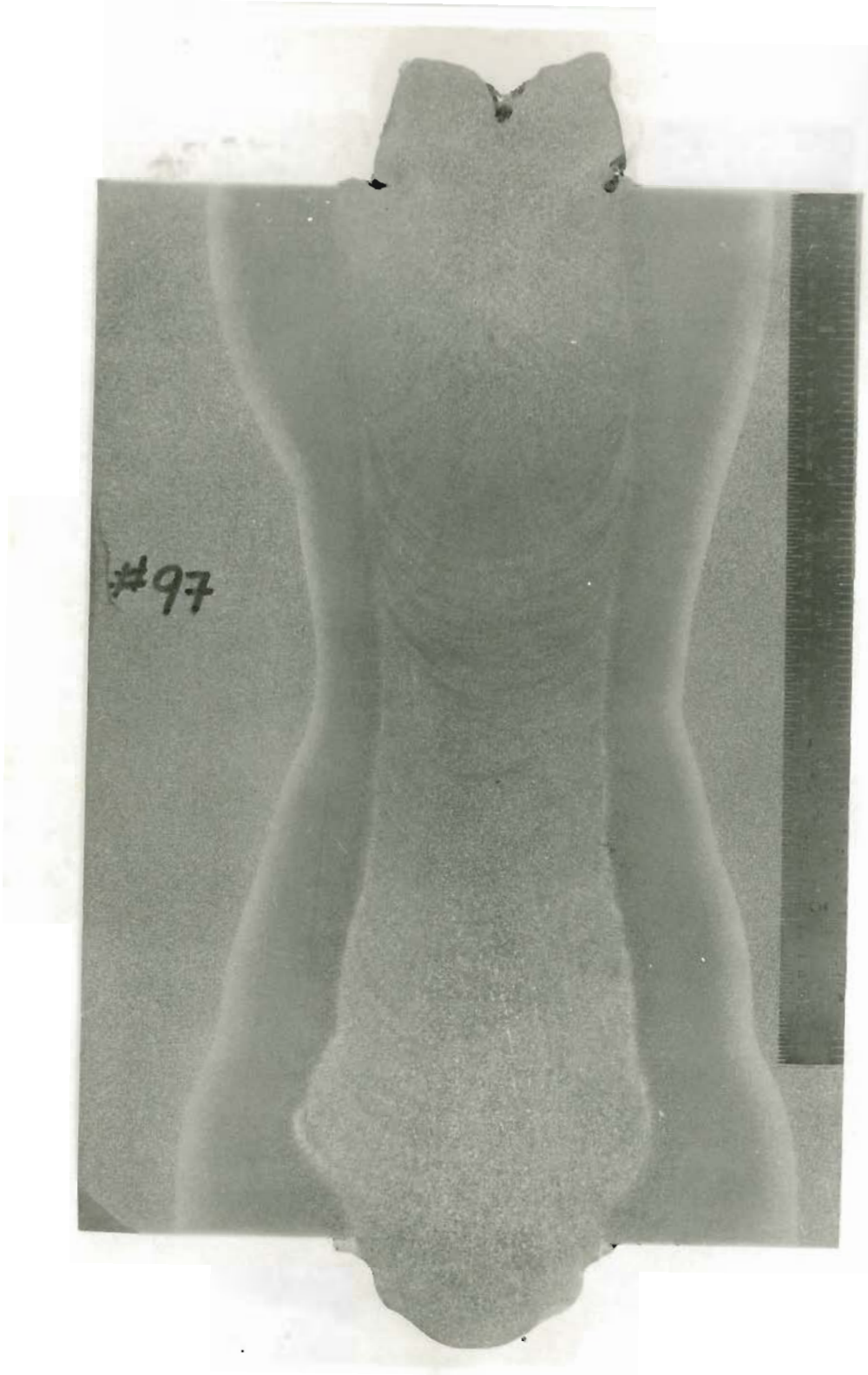

Figure 32. LONGITUDINAL VERTICAL MACROSECTIONS OF RAIL WELDS.

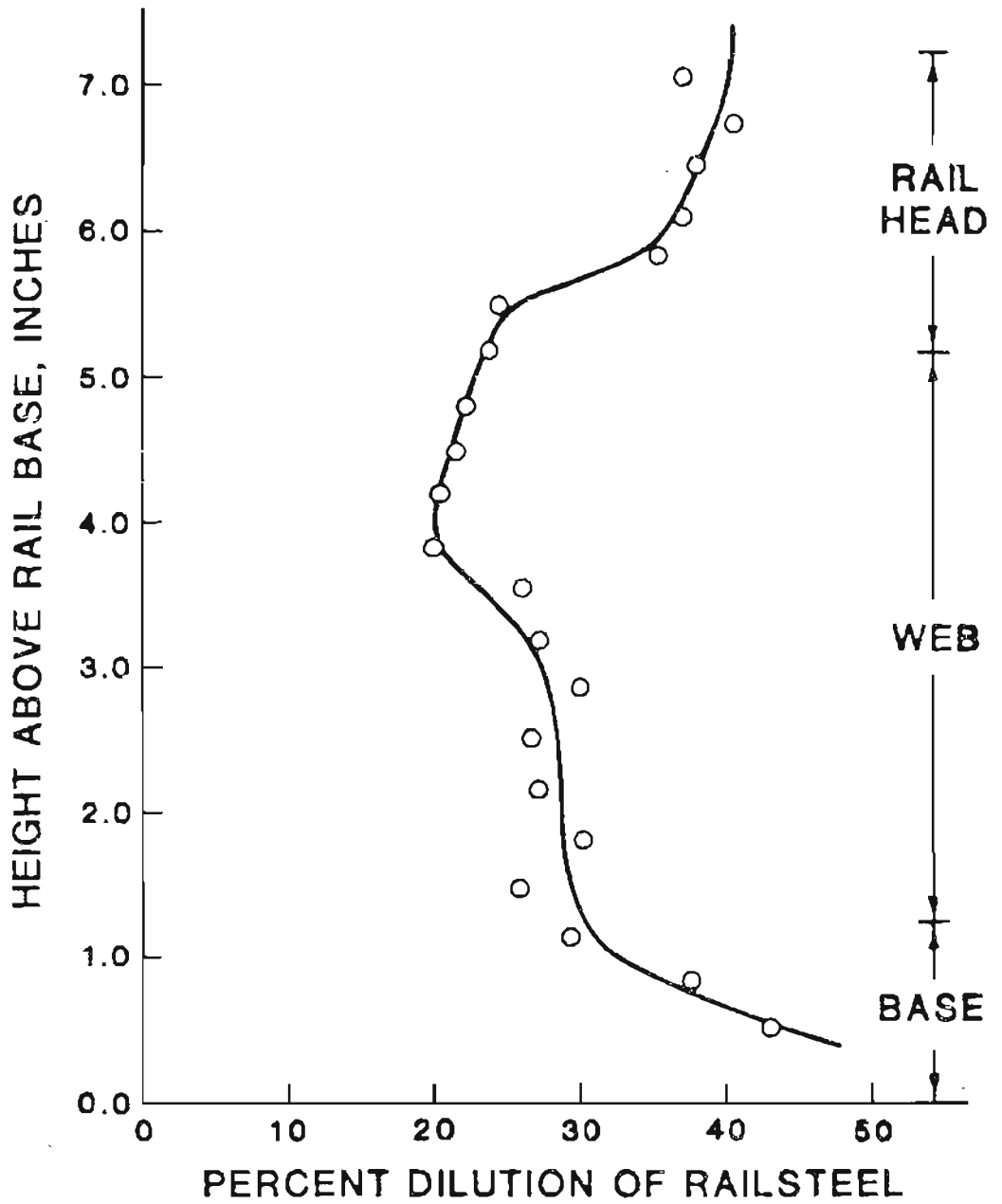

Figure 33. PERCENT DILUTION OF WELD METAL BY RAIL STEEL FOR A 1 INCH GAP.

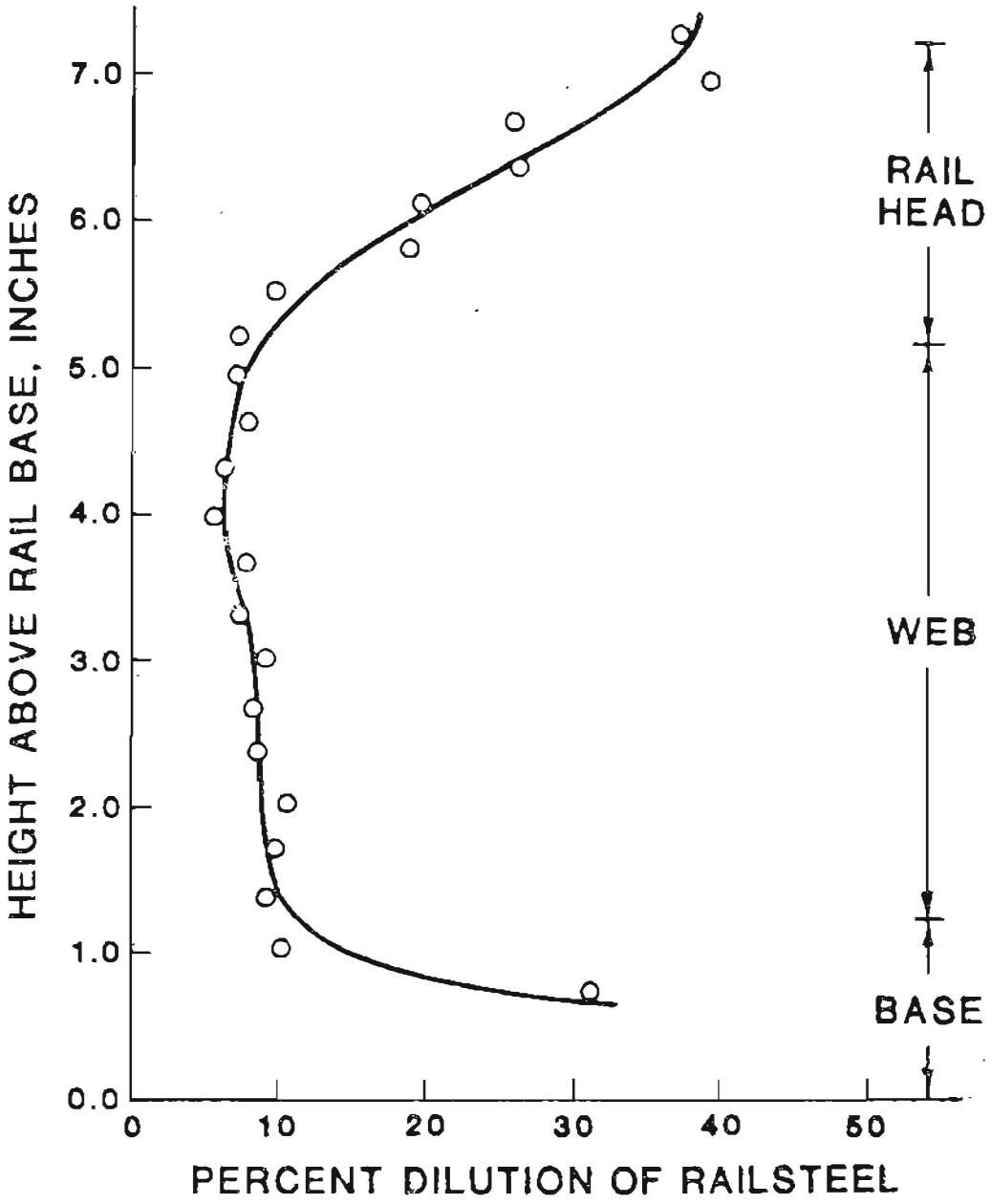

Figure 34. PERCENT DILUTION OF WELD METAL BY RAIL STEEL FOR A 1-¼ INCH GAP.

100X

1000X

Figure 35. PHOTOMICROGRAPHS OF RAIL STEEL.

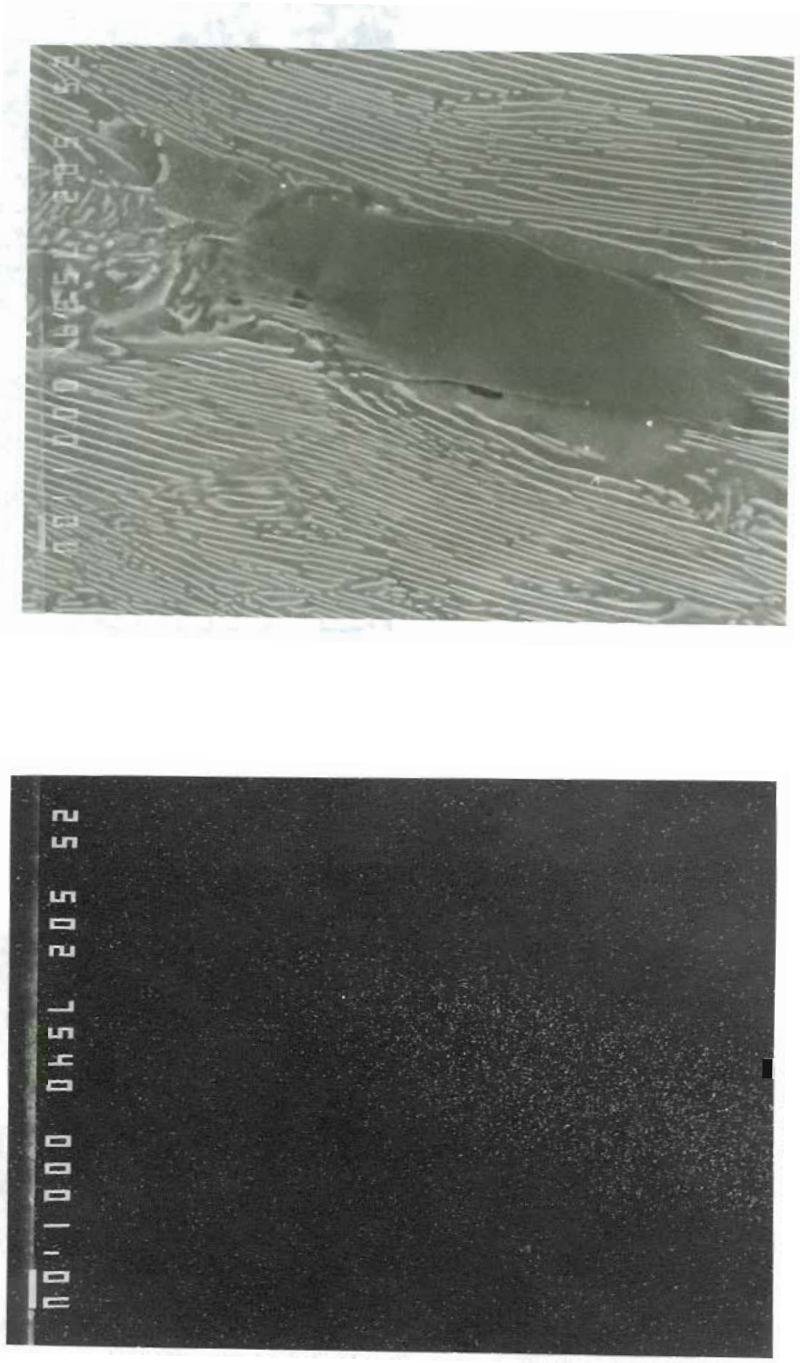

Figure 36. X-RAY MAPS OF RAIL INCLUSIONS.

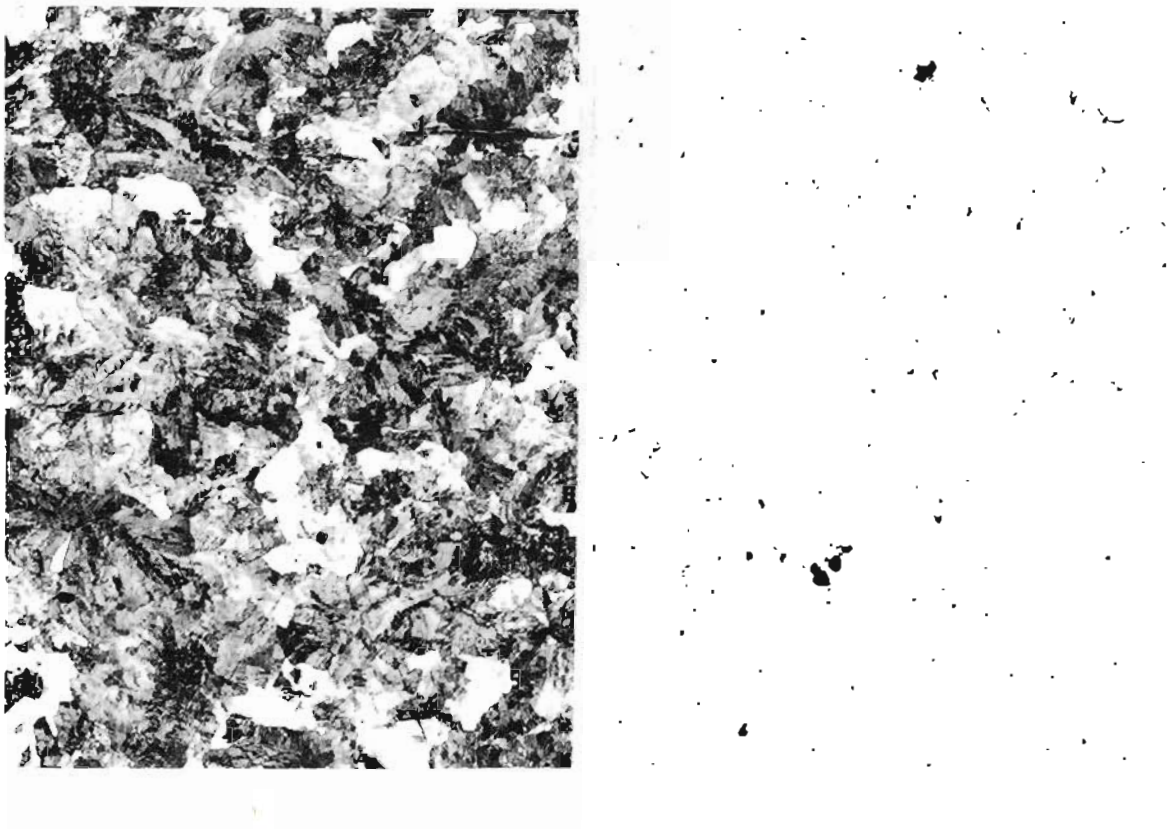

Figure 37. PHOTOMICROGRAPHS OF THERMIT WELD METAL.

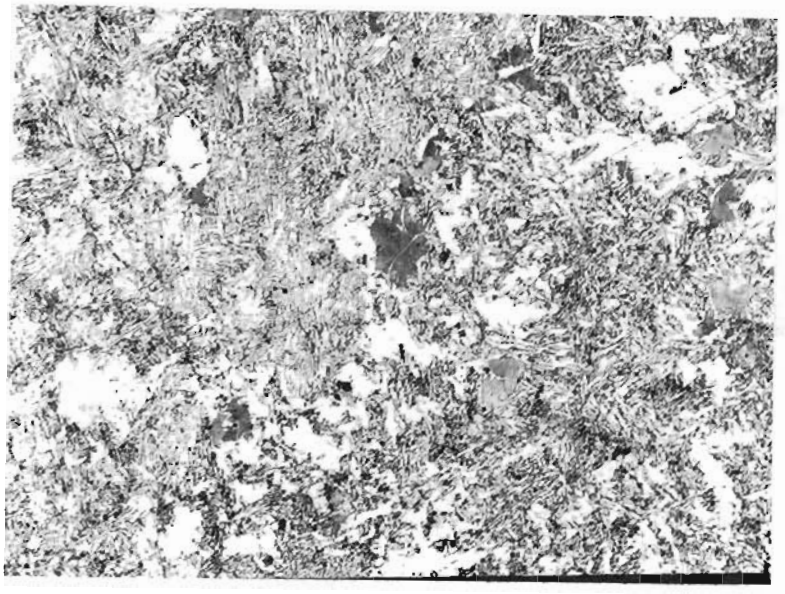

Figure 38. PHOTOMICROGRAPHS OF THERMIT WELD BASE.

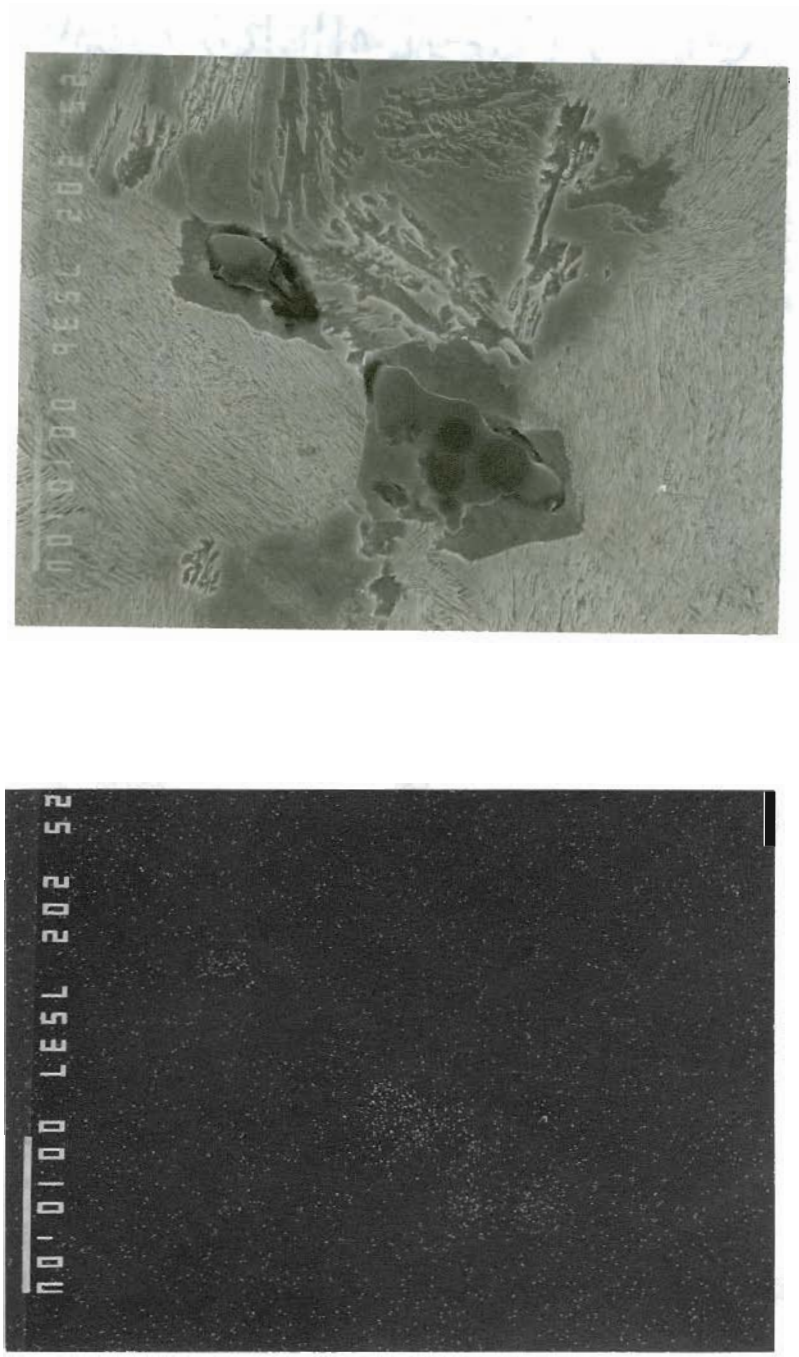

Figure 39. X-RAY MAP OF THERMIT WELD INCLUSIONS.

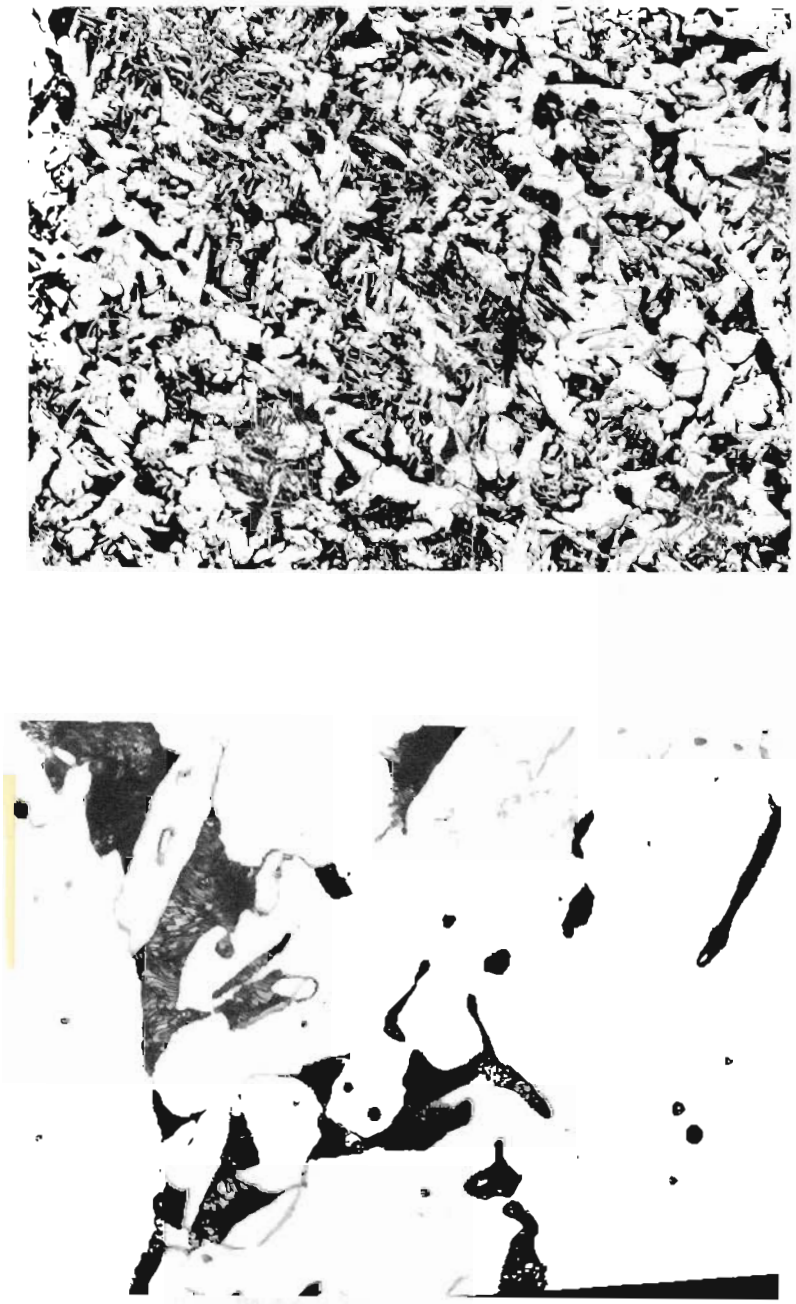

Figure 40. PHOTOMICROGRAPHS OF RAIL WELD USING MILD STEEL FILLER WIRE AND MILD STEEL GUIDE TUBE.

100x

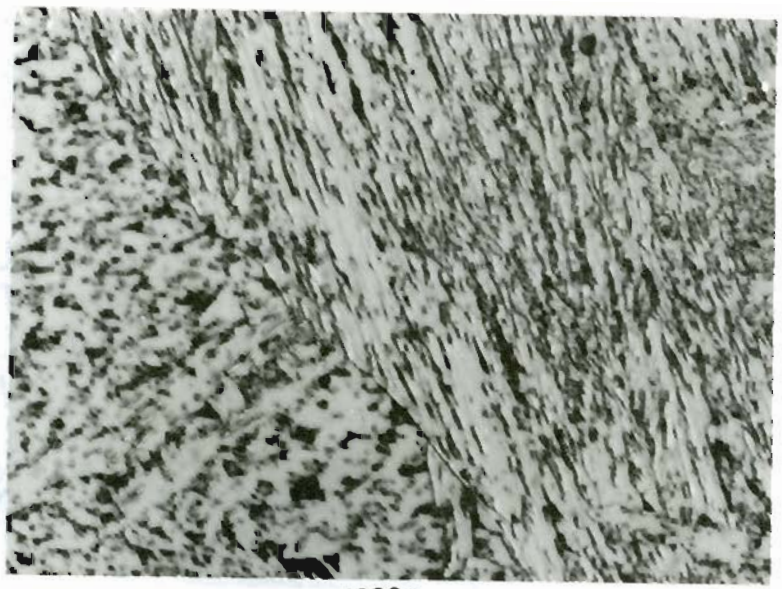

1000x

Figure 41. PHOTOMICROGRAPHS OF RAIL WELD USING 2¼Cr-1Mo FILLER WIRE AND MILD STEEL GUIDE TUBE.

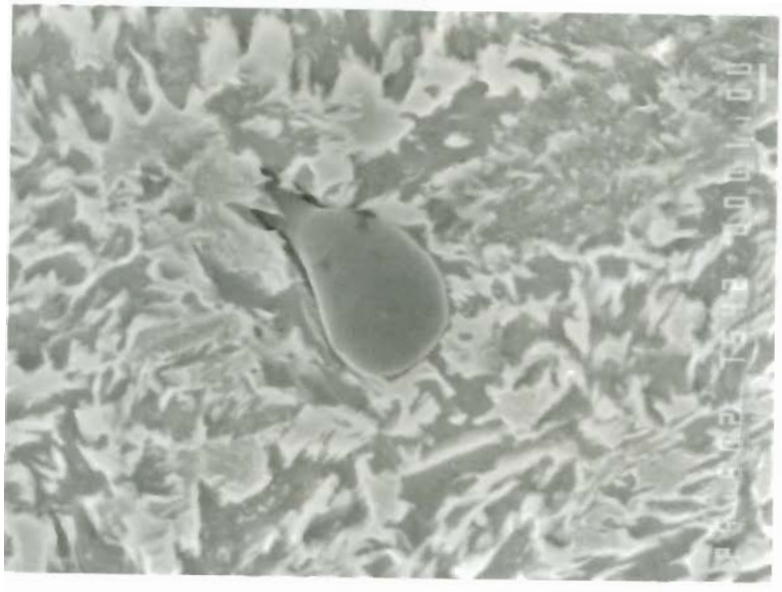

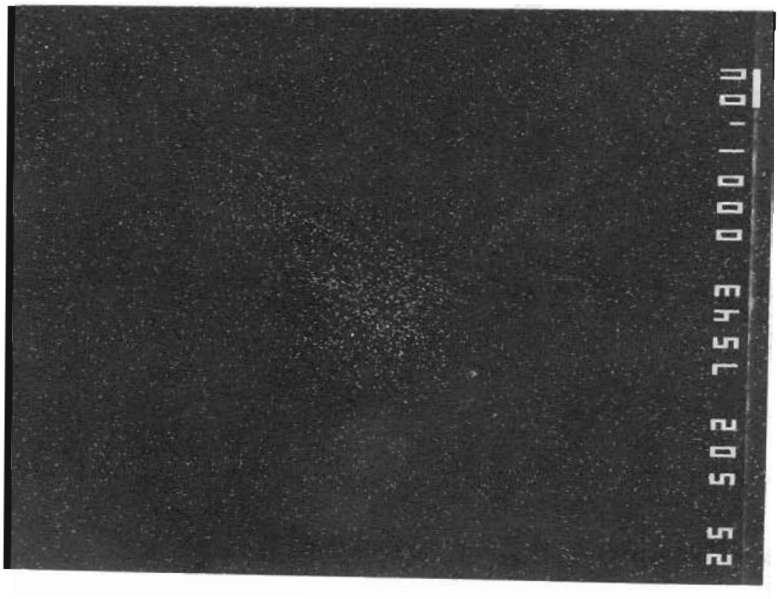

Figure 42. X-RAY MAP OF ELECTROSLAG WELD INCLUSIONS.

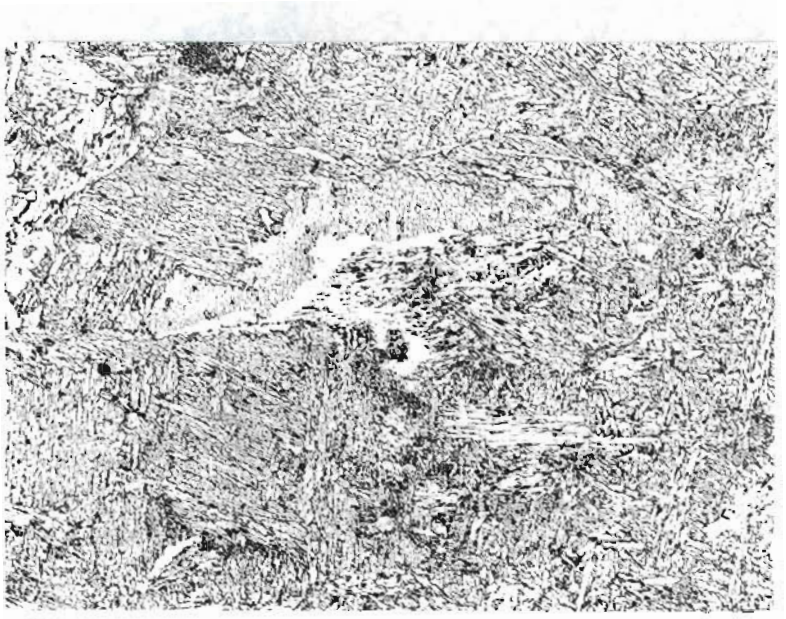

100×

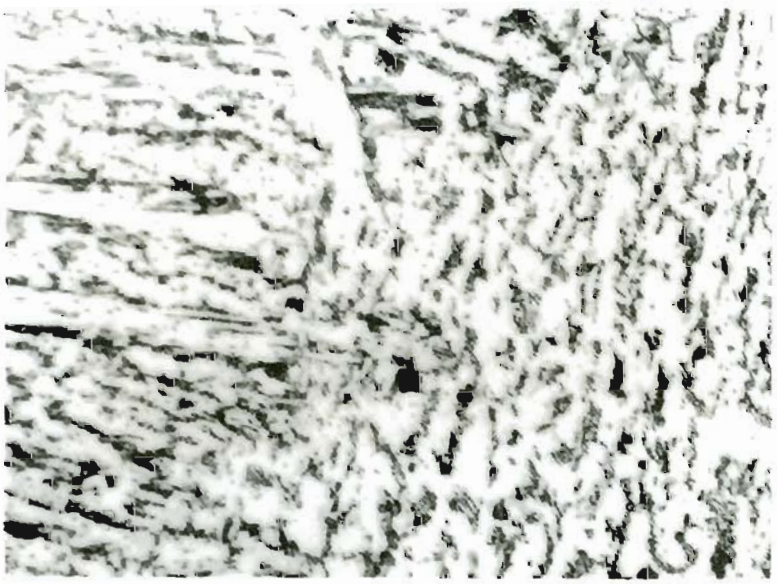

1000×

Figure 43. PHOTOMICROGRAPHS OF THE BASE OF THE 2¼Cr-1Mo RAIL WELD.

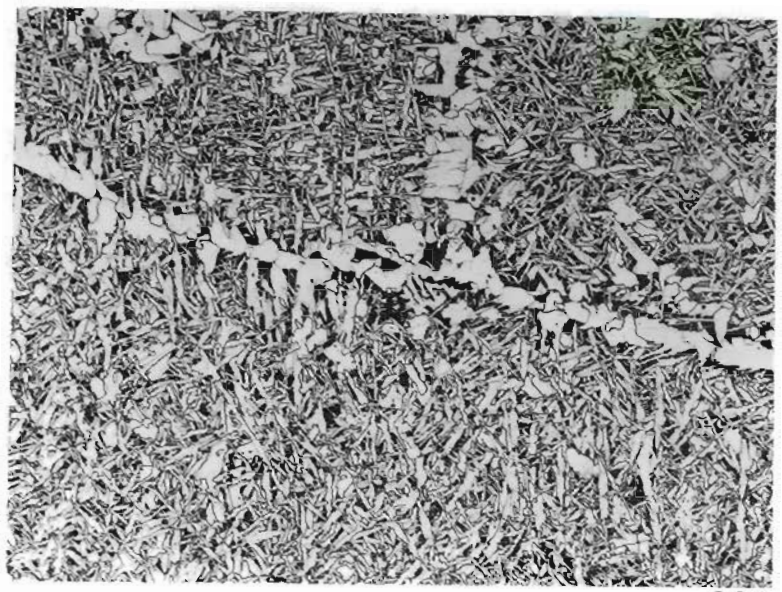

100x

1000x

Figure 44. PHOTOMICROGRAPHS OF RAIL WELD USING 2Mn-½Mo FILLER WIRE AND MILD STEEL GUIDE TUBE.

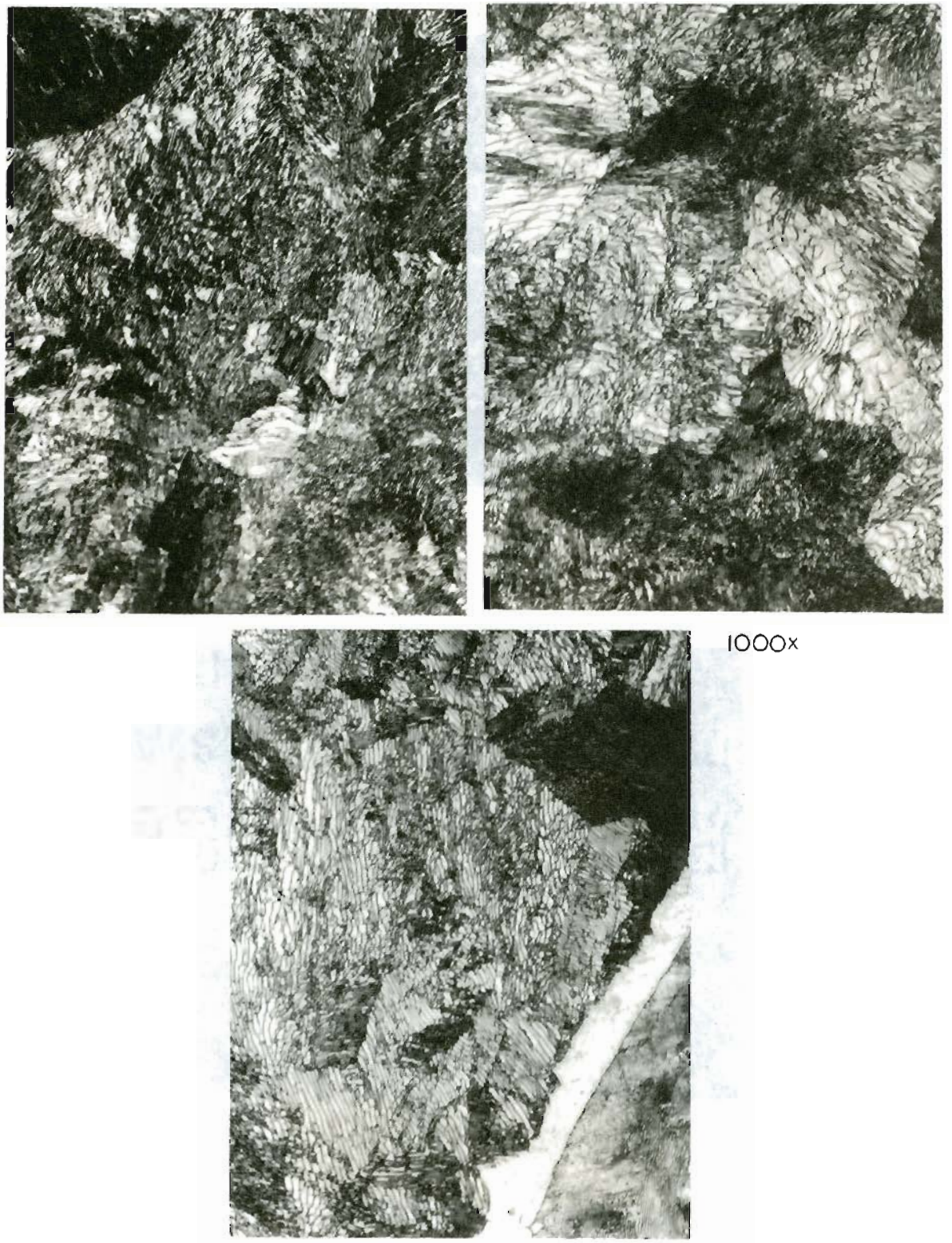

Figure 46. PEARLITIC MICROSTRUCTURES.

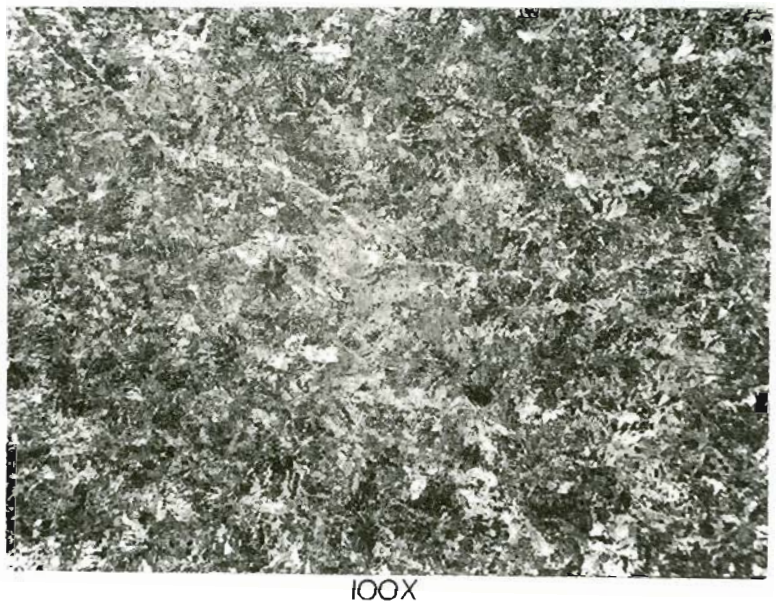

100X

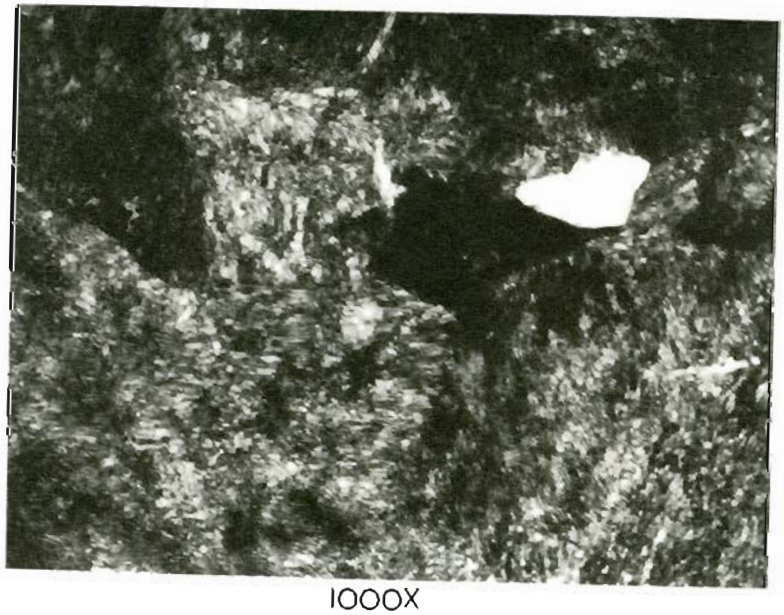

1000X

Figure 47. PHOTOMICROGRAPHS OF RAIL WELD USING 0.65 wt.% C FILLER WIRE AND HALF-RAIL/HALF-MILD STEEL GUIDE TUBE.

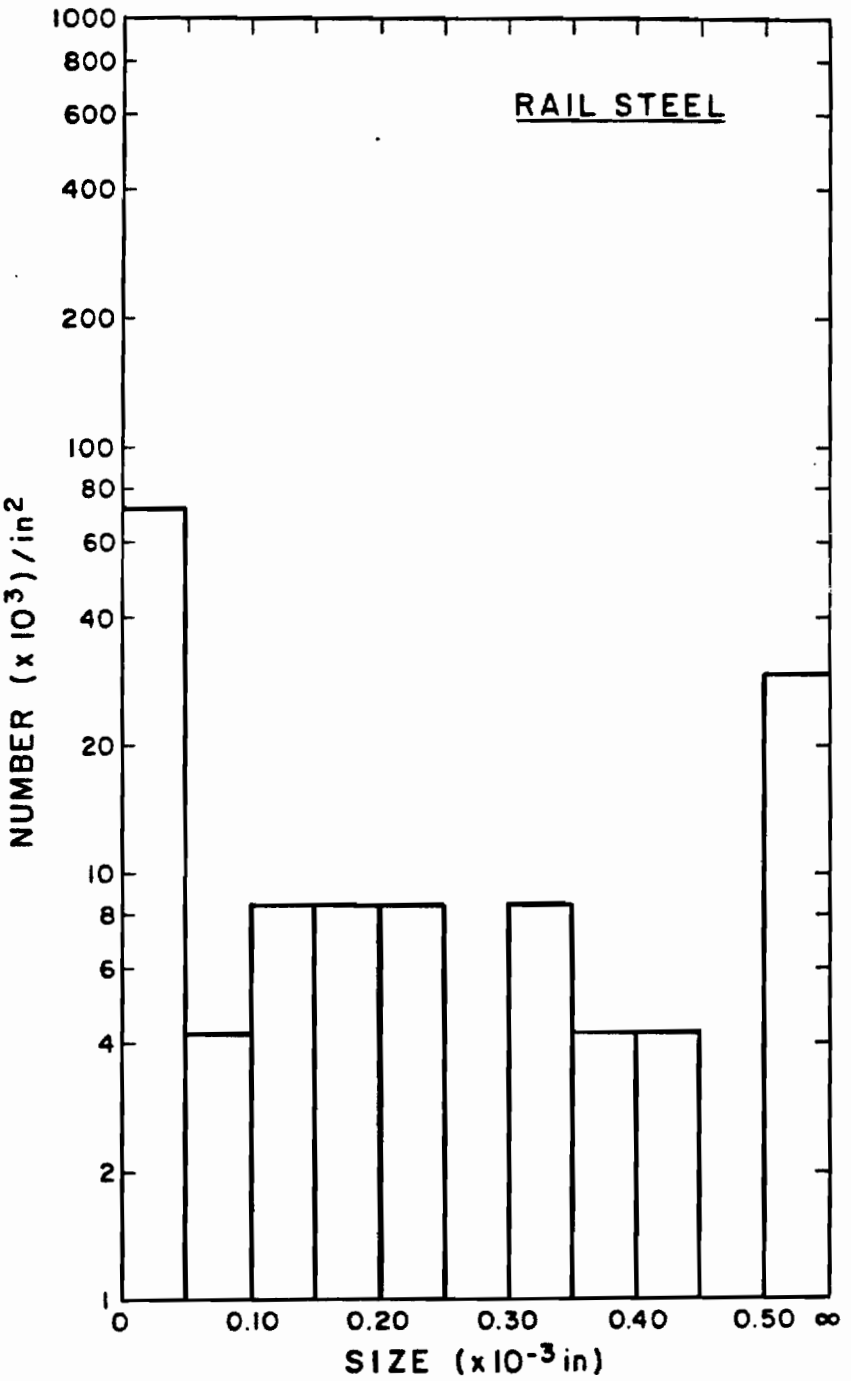

Figure 48. DISTRIBUTION OF INCLUSIONS IN RAIL STEEL.

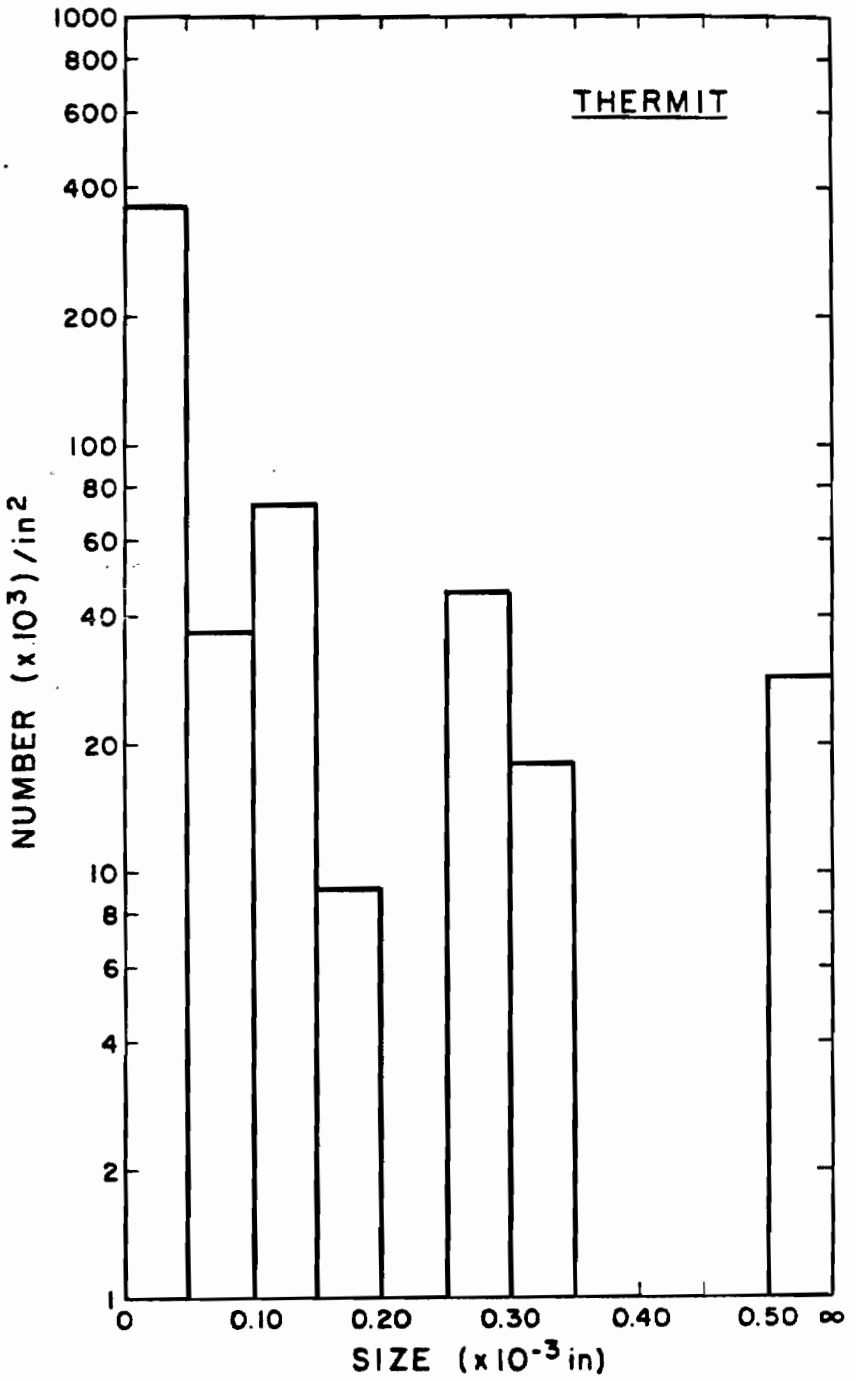

Figure 49. DISTRIBUTIONS OF INCLUSIONS IN THERMIT WELD METAL.

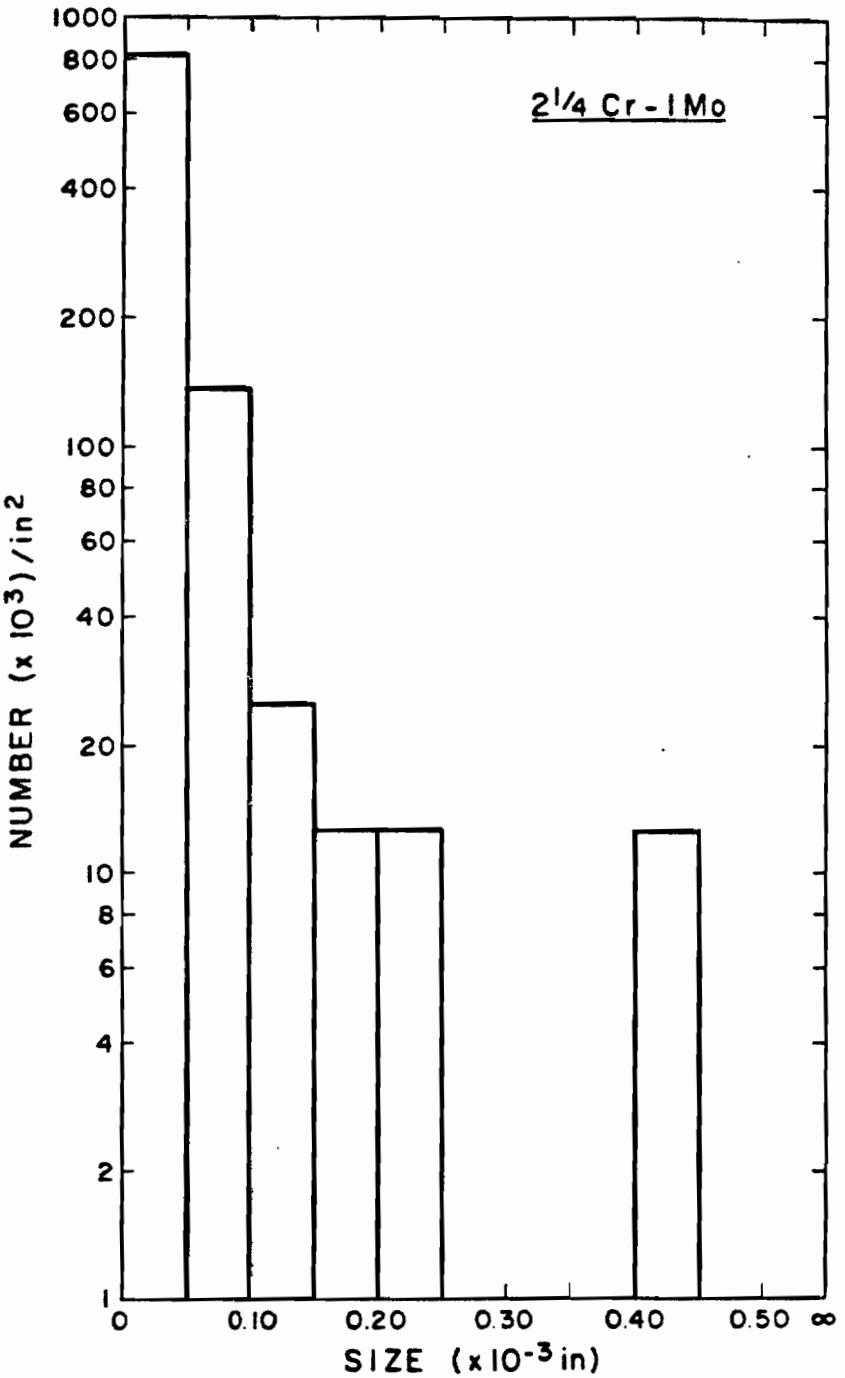

Figure 50. DISTRIBUTION OF INCLUSIONS IN 2¼Cr-1Mo ELECTROSLAG RAIL WELD METAL.

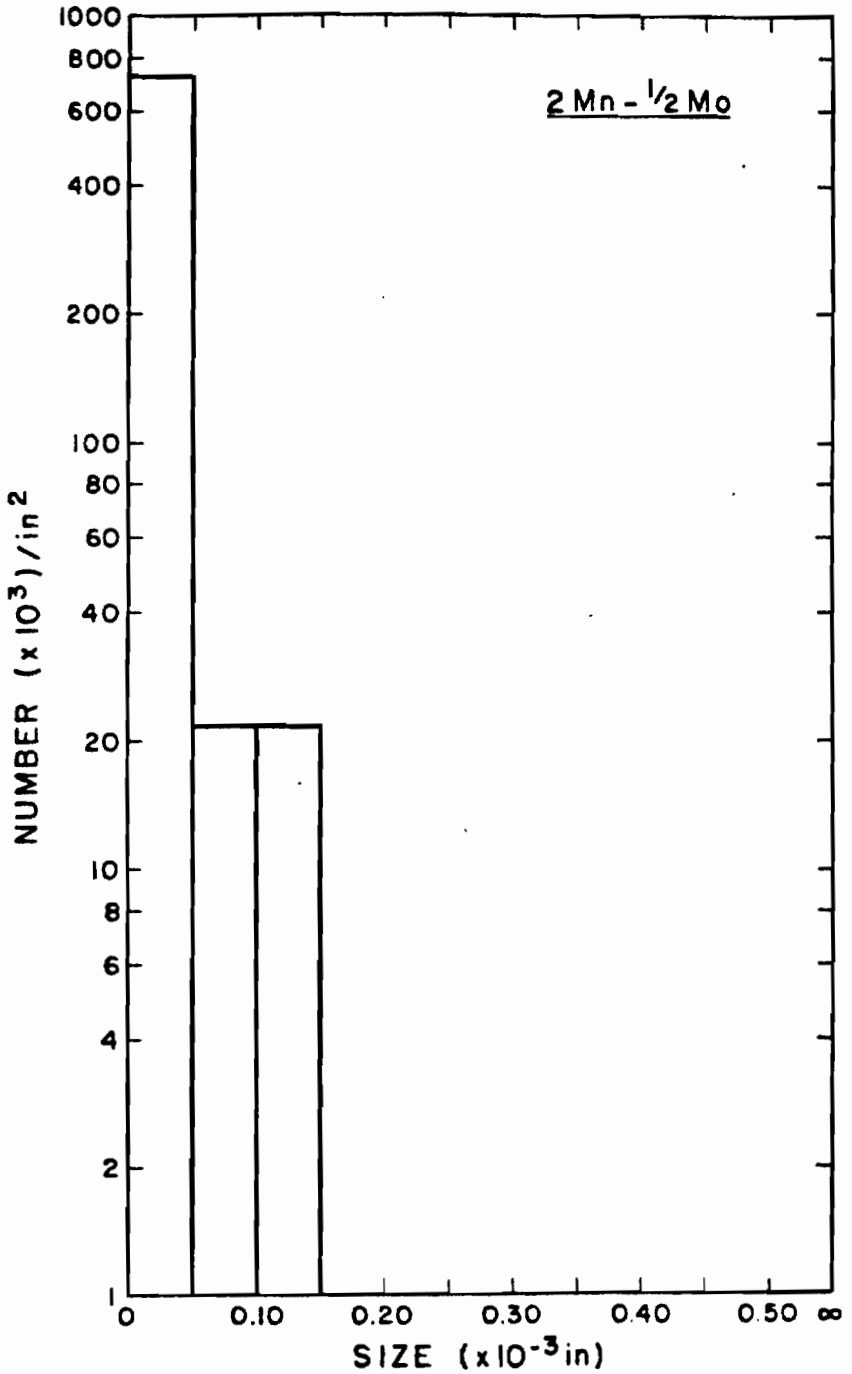

Figure 51. DISTRIBUTION OF INCLUSIONS IN 2Mn-½Mo ELECTROSLAG RAIL WELD METAL.

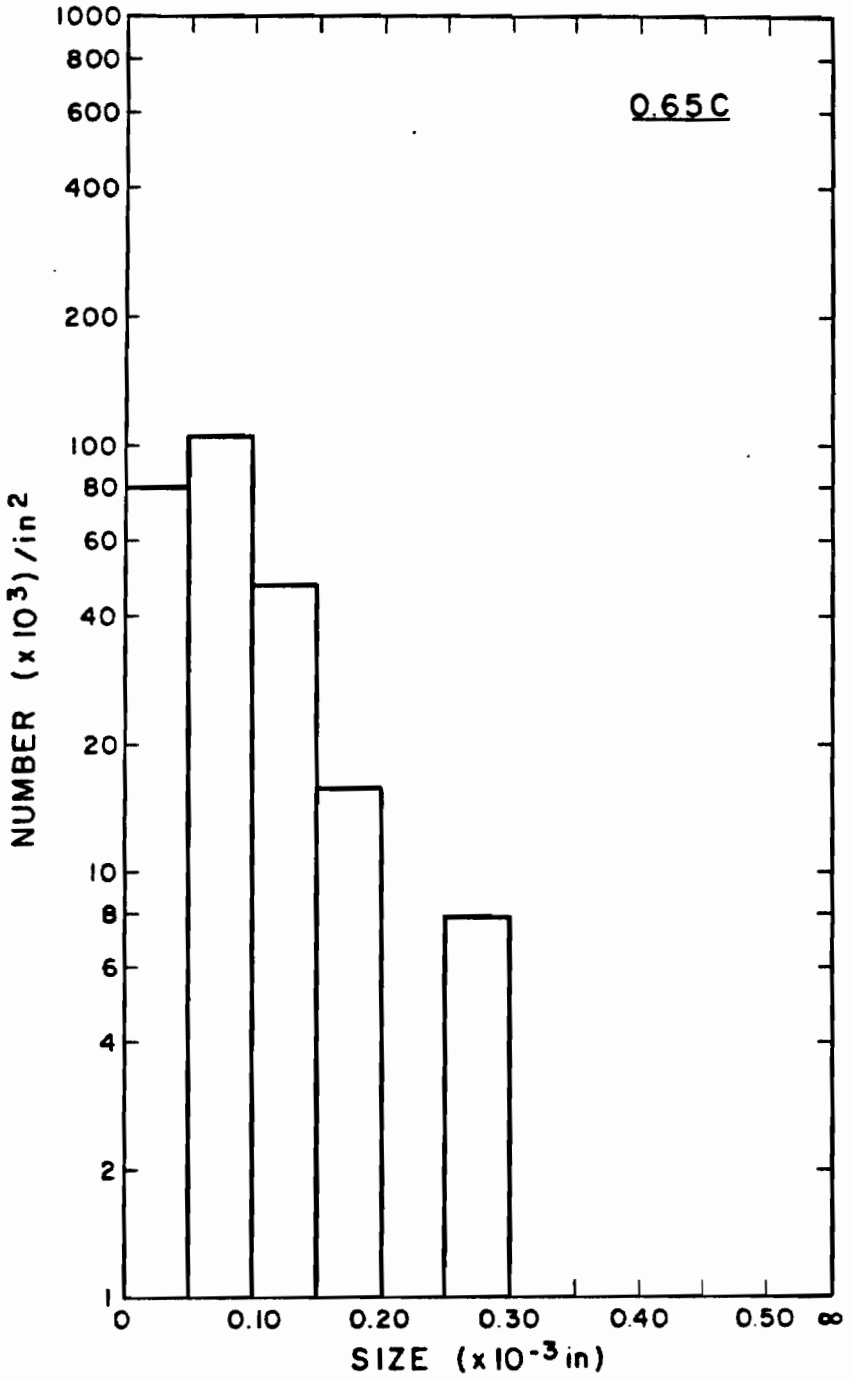

Figure 52. DISTRIBUTION OF INCLUSIONS IN HIGH CARBON ELECTROSLAG RAIL WELD METAL.

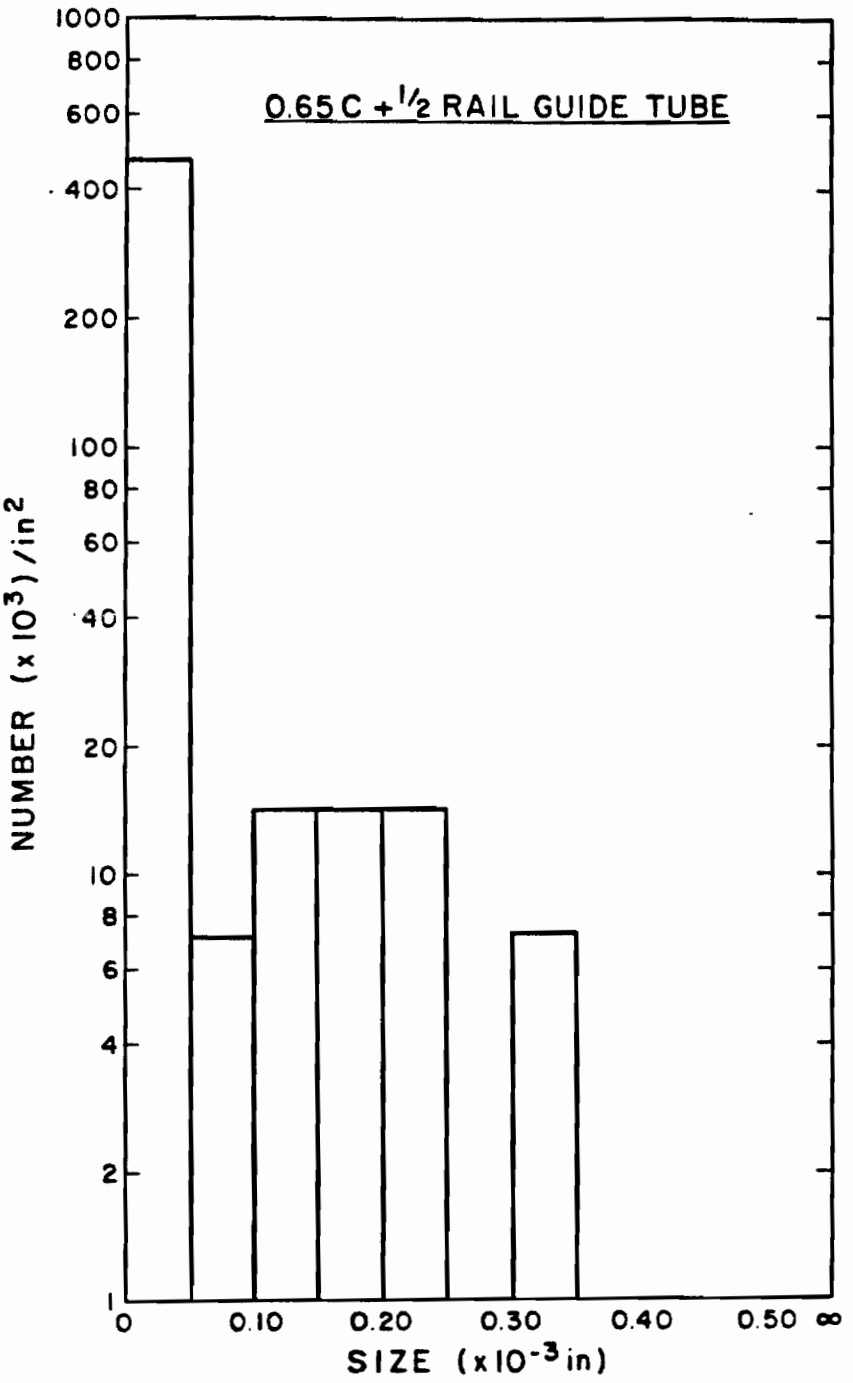

Figure 53. DISTRIBUTION OF INCLUSIONS IN ELECTROSLAG RAIL WELD USING 0.65 wt.% C FILLER WIRE AND HALF-RAIL/HALF-MILD STEEL GUIDE TUBE.

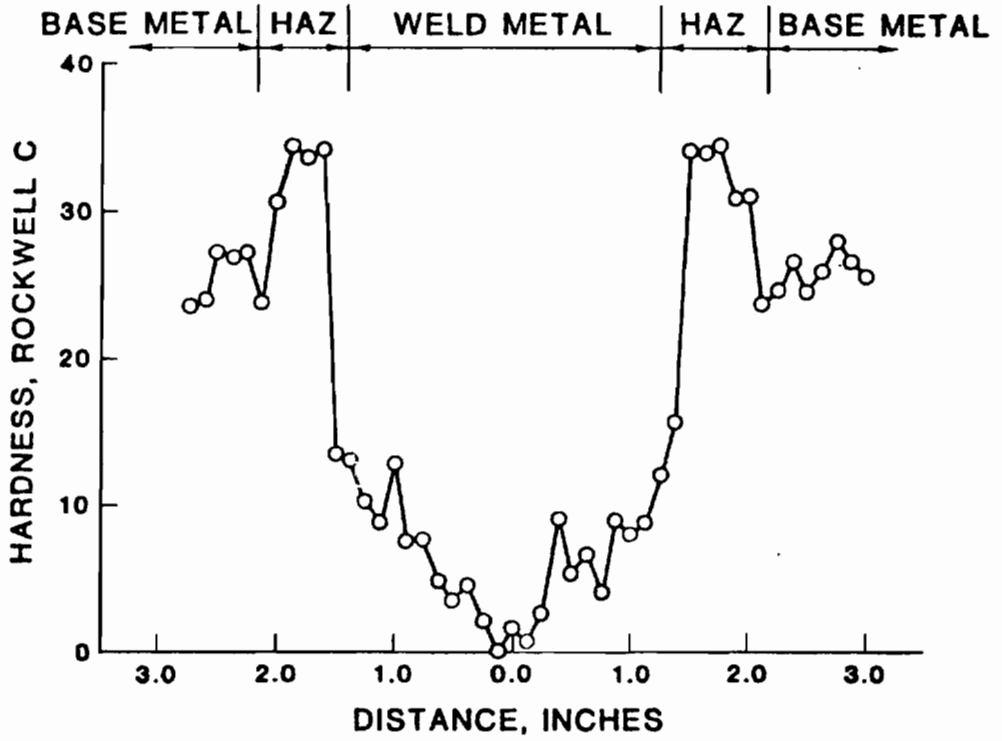

Figure 54. HARDNESS TRAVERSE OF RAIL WELD USING MILD STEEL FILLER WIRE AND MILD STEEL GUIDE TUBE.

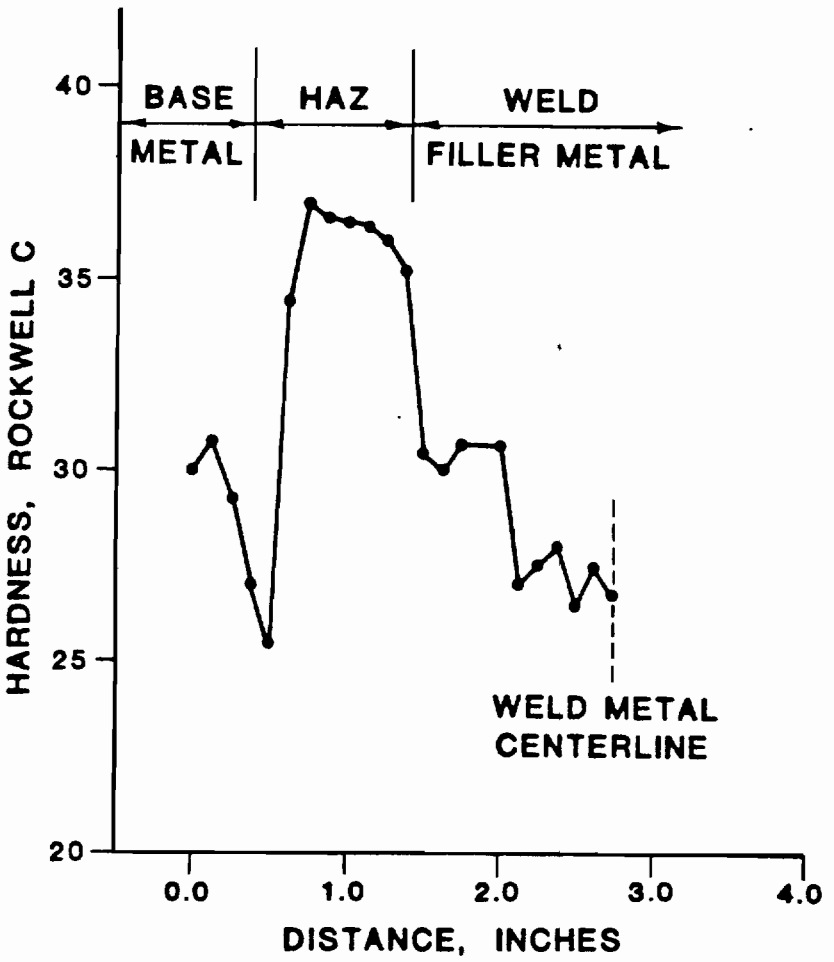

Figure 55. HARDNESS TRAVERSE OF RAIL WELD USING 2¼Cr-1Mo FILLER WIRE AND MILD STEEL GUIDE TUBE.

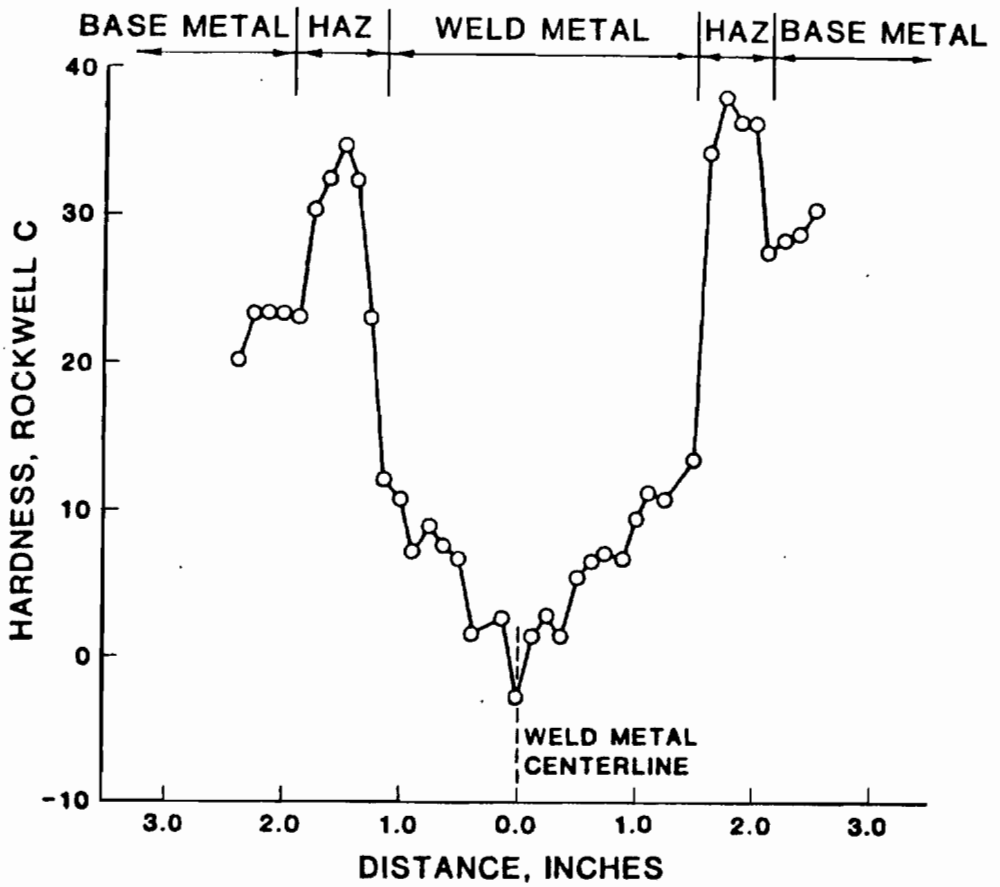

Figure 56. HARDNESS TRAVERSE OF RAIL WELD USING 2Mn-½Mo FILLER WIRE AND MILD STEEL GUIDE TUBE.

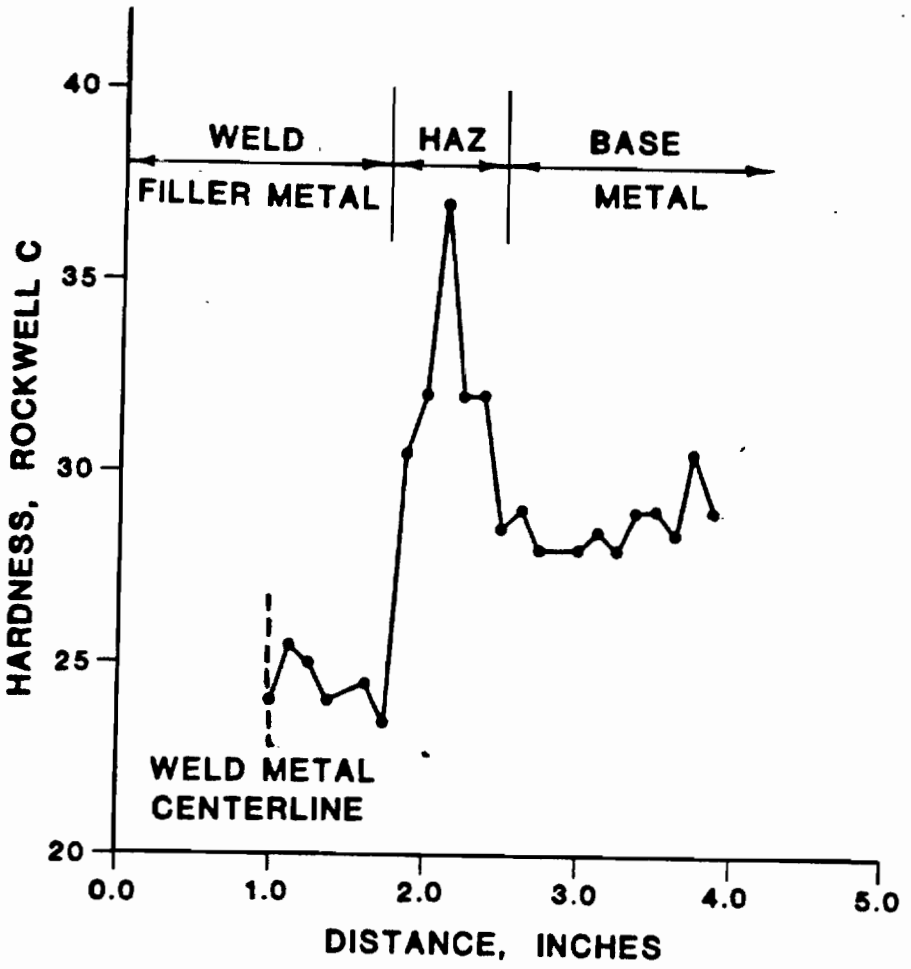

Figure 57. HARDNESS TRAVERSE OF RAIL WELD USING 0.65 wt.% C FILLER WIRE AND MILD STEEL GUIDE TUBE.

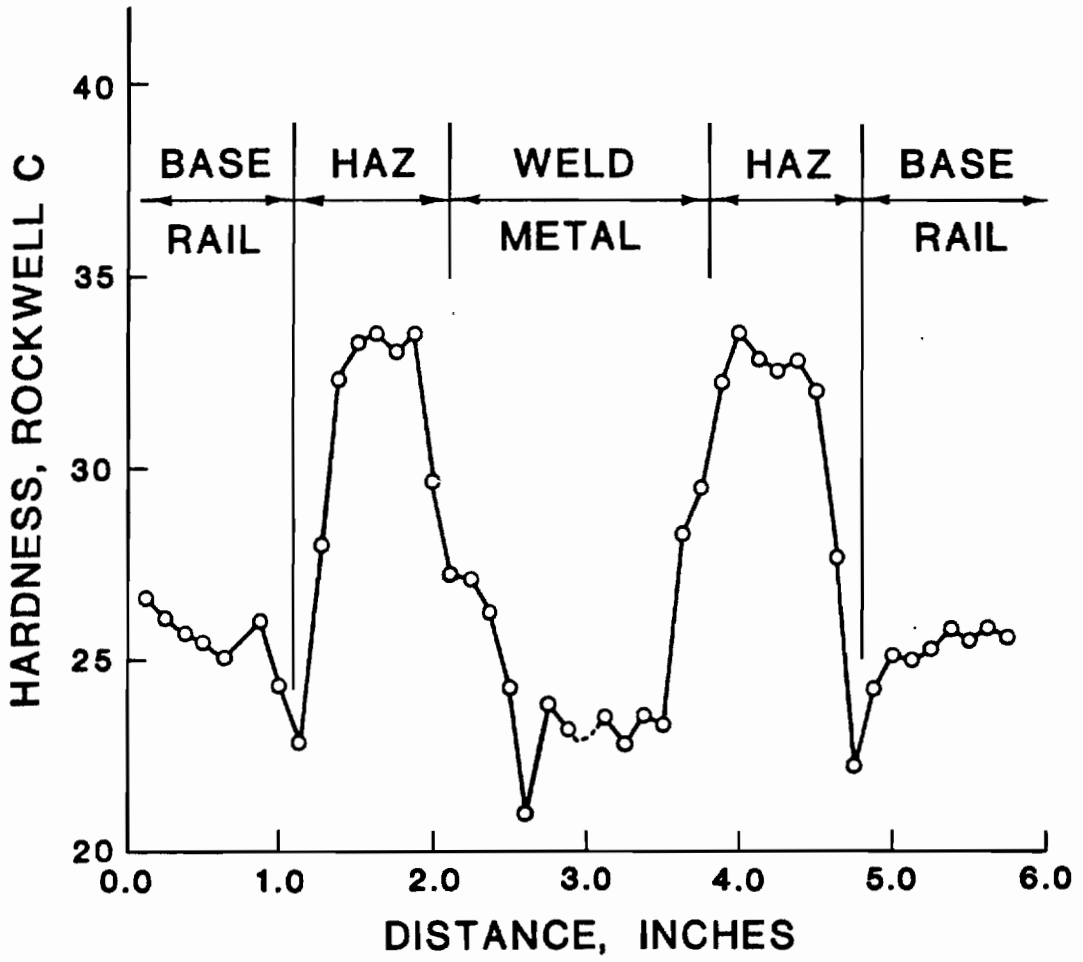

Figure 58. HARDNESS TRAVERSE OF RAIL WELD USING 0.65 wt.% C FILLER WIRE AND A HALF-RAIL/HALF-MILD STEEL GUIDE TUBE.

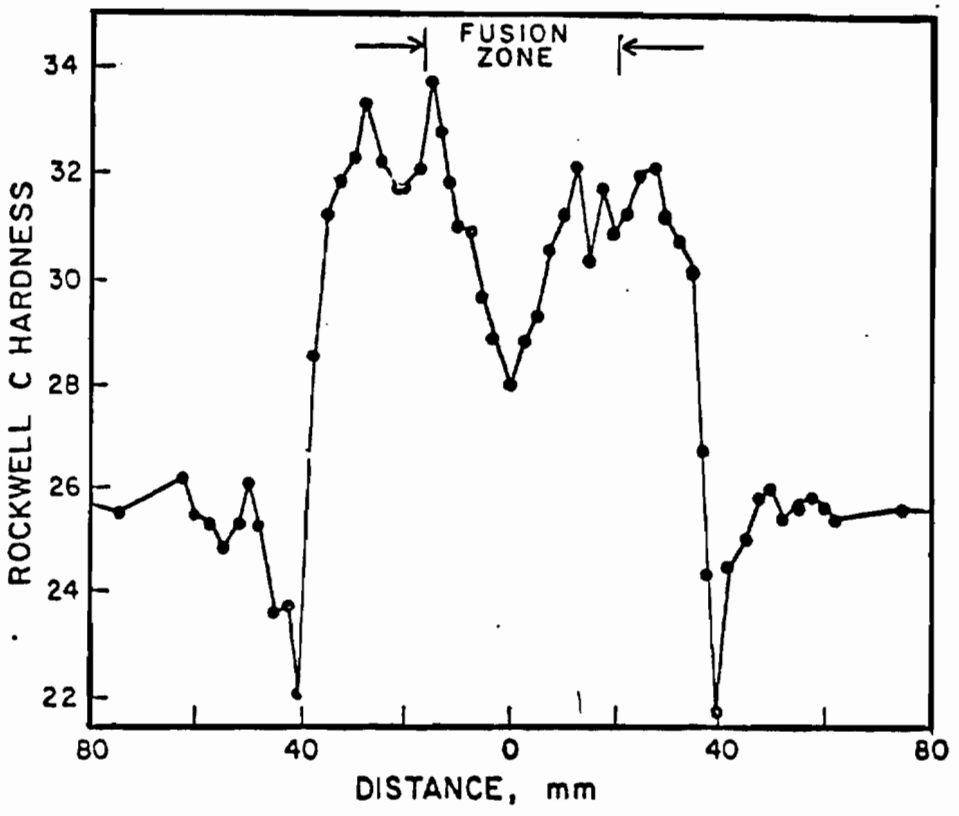

Figure 59. HARDNESS TRAVERSE OF THERMIT WELD.

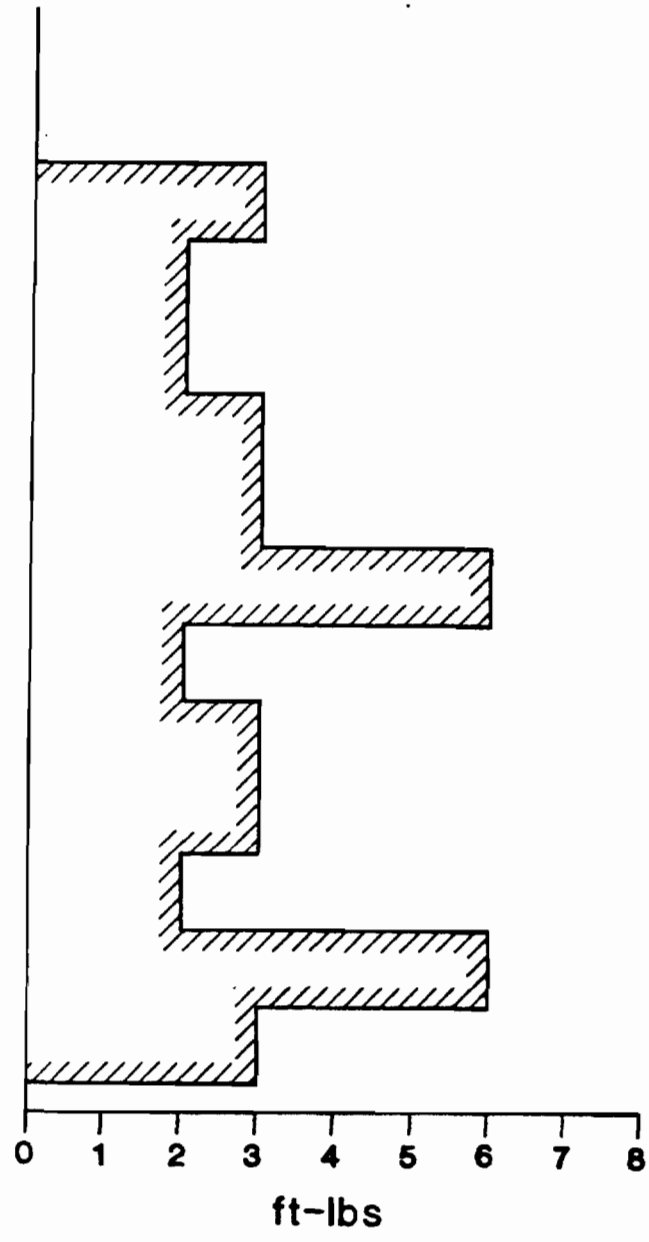

Figure 60. VARIATION IN CVN IMPACT TOUGHNESS OF 2¼Cr-1Mo ELECTRO-SLAG RAIL WELD AT ROOM TEMPERATURE.

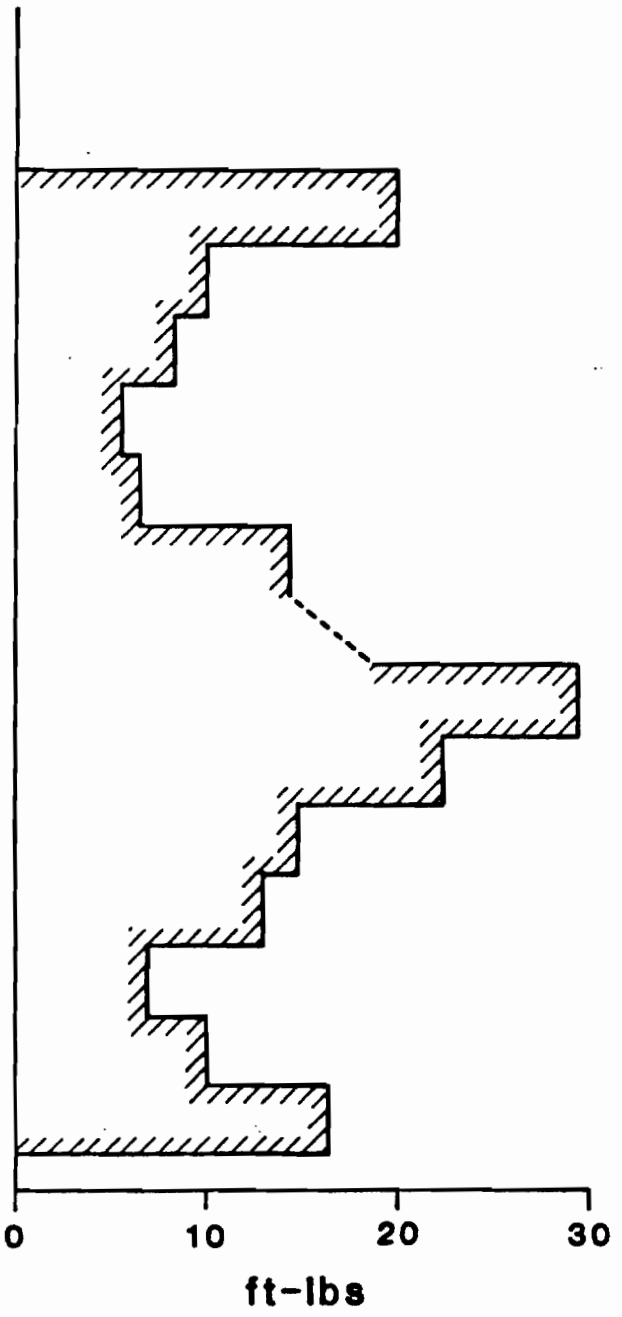

Figure 61. VARIATION IN CVN IMPACT TOUGHNESS OF 2¼Cr-1Mo ELECTRO-SLAG RAIL WELD AT 300°F.

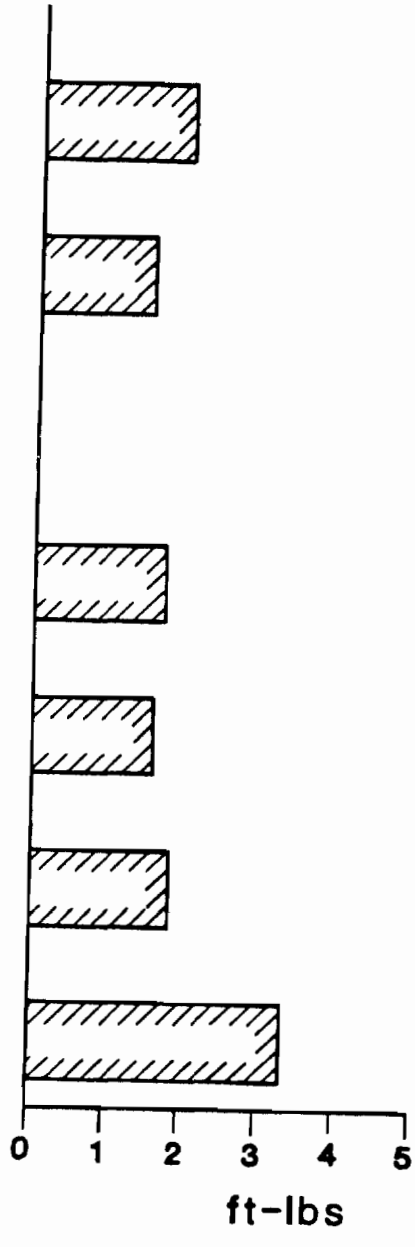

Figure 62. VARIATION IN ROOM TEMPERATURE CVN IMPACT TOUGHNESS OF WELD USING 0.65 wt.% C FILLER WIRE AND MILD STEEL GUIDE TUBE.

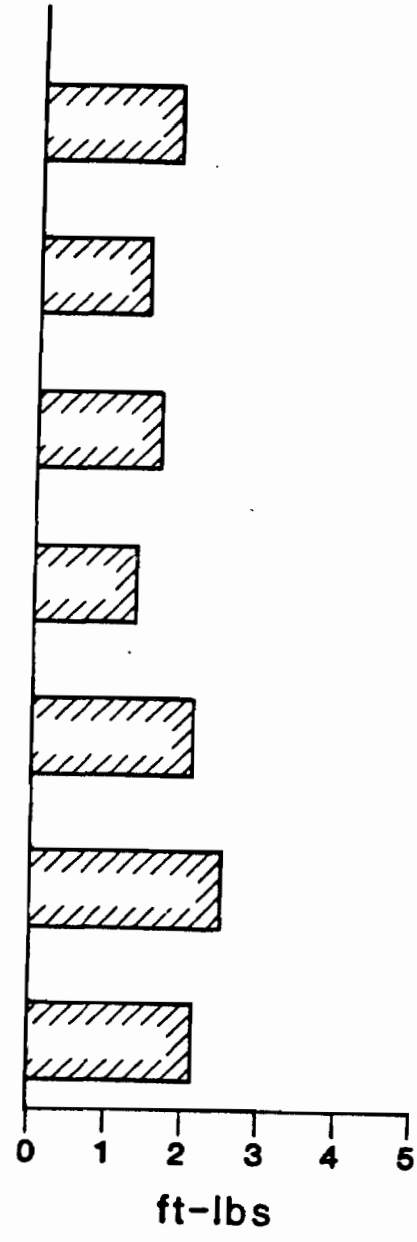

Figure 63. VARIATION IN ROOM TEMPERATURE CVN IMPACT TOUGHNESS OF WELD USING 0.65 wt.% C FILLER WIRE AND HALF-RAIL/ HALF-MILD STEEL GUIDE TUBE.

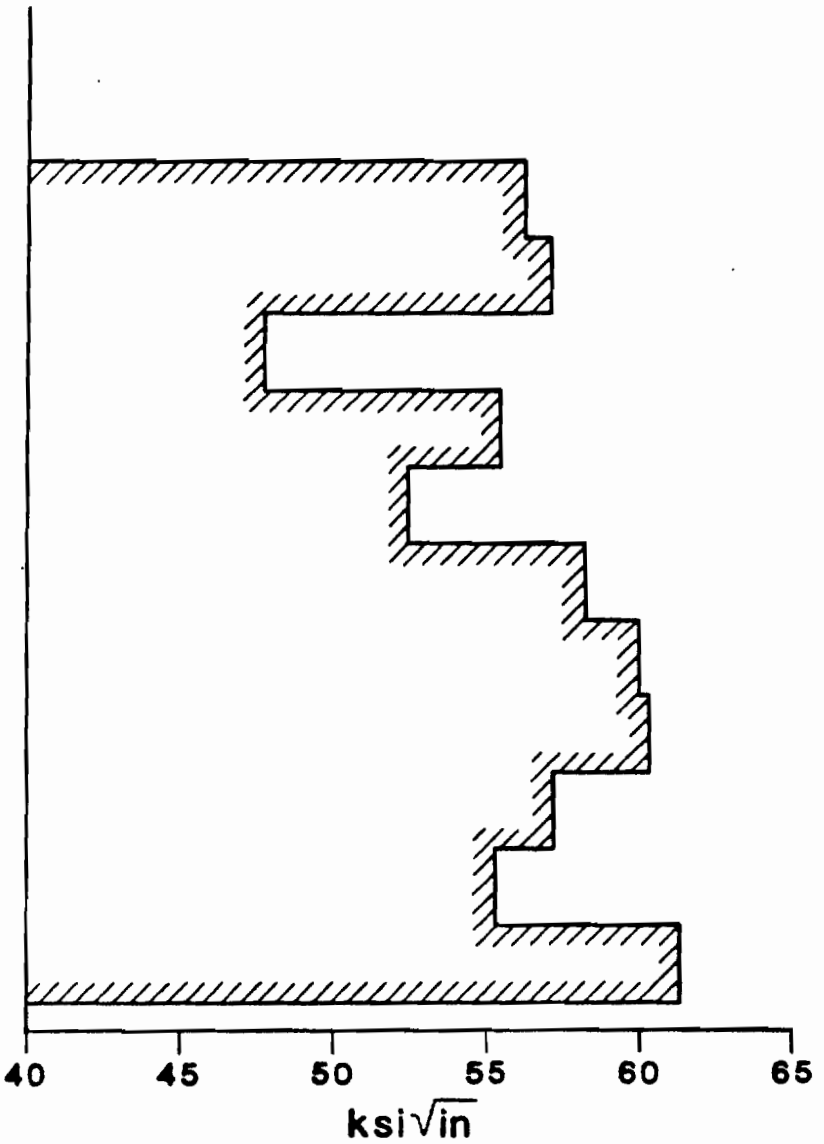

Figure 64. VARIATION IN ROOM TEMPERATURE DYNAMIC FRACTURE TOUGHNESS OF 2Mn-½Mo RAIL WELD METAL.

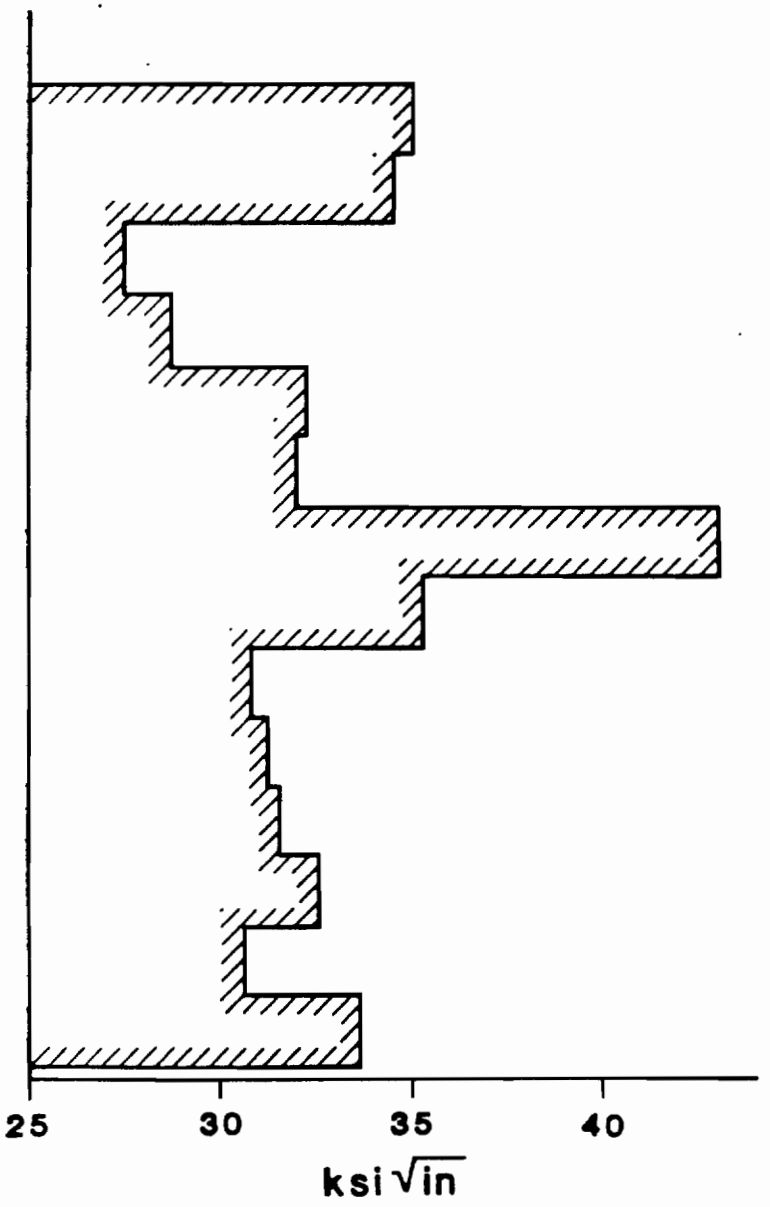

Figure 65. VARIATION IN ROOM TEMPERATURE DYNAMIC FRACTURE TOUGHNESS OF 2¼Cr-1Mo RAIL WELD METAL.

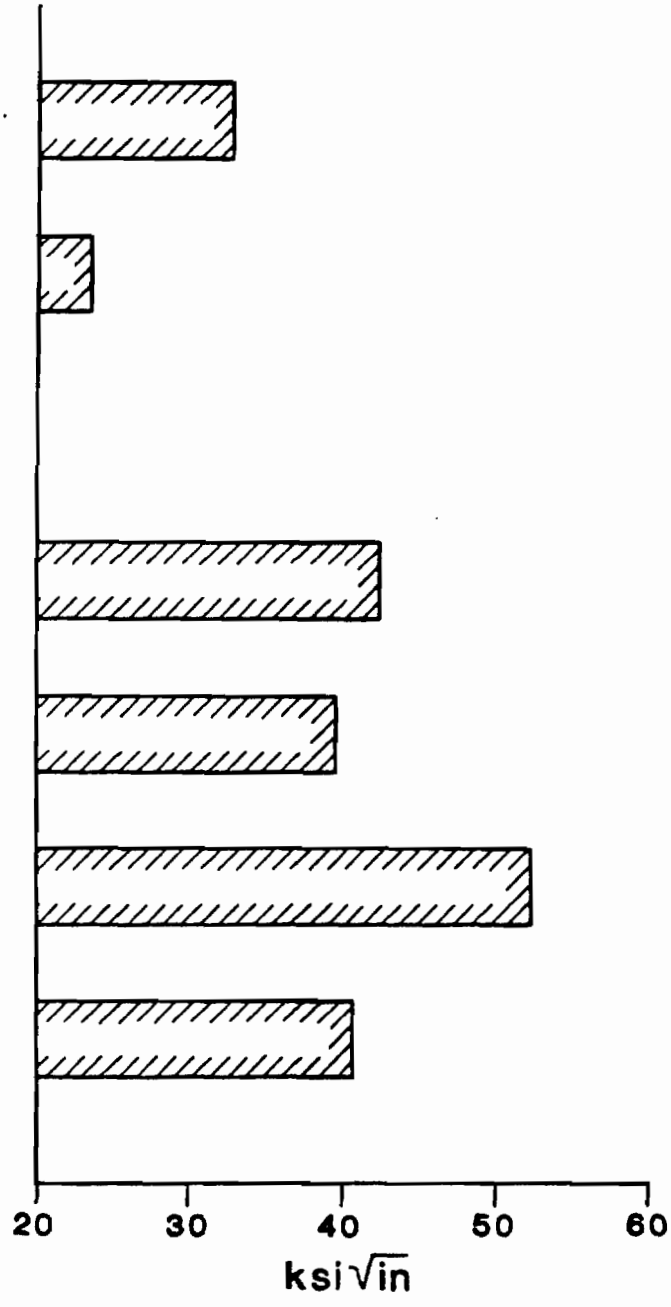

Figure 66. VARIATION IN ROOM TEMPERATURE DYNAMIC FRACTURE TOUGHNESS OF RAIL WELD USING 0.65 wt.% C FILLER WIRE AND MILD STEEL GUIDE TUBE.

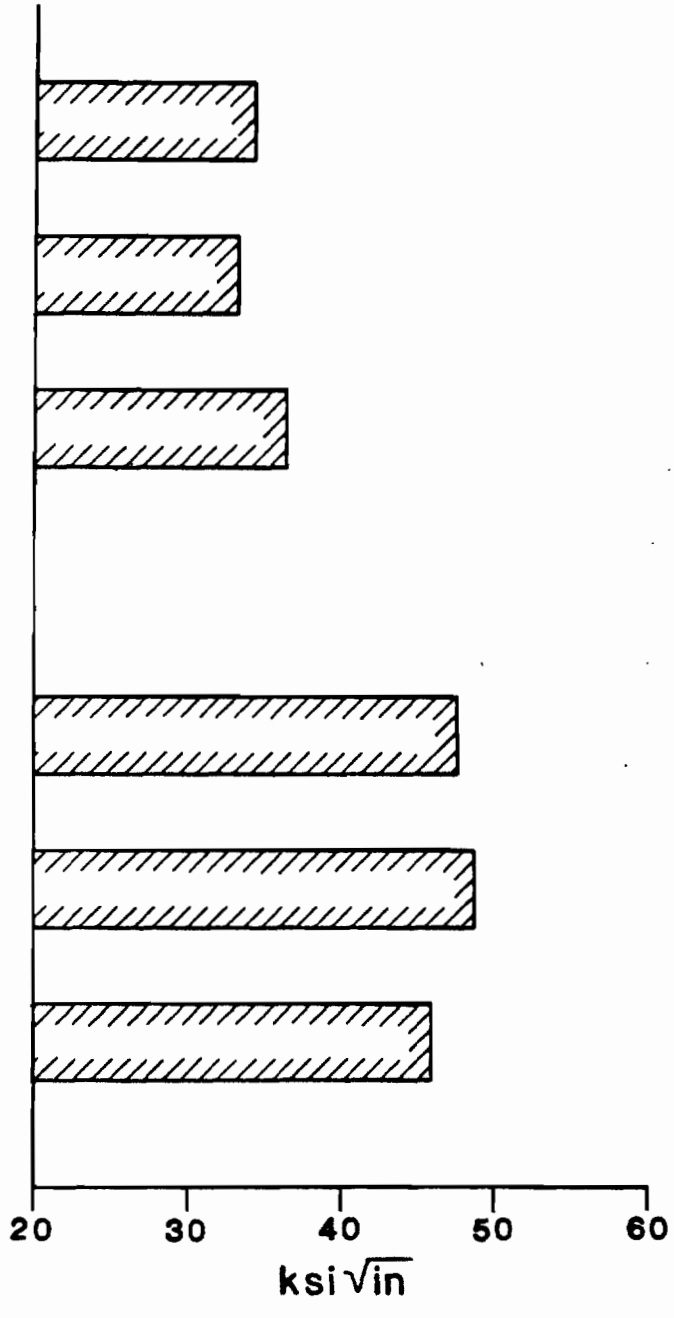

Figure 67. VARIATION IN ROOM TEMPERATURE DYNAMIC FRACTURE TOUGHNESS OF RAIL WELD USING 0.65 wt.% C FILLER WIRE AND HALF-RAIL/HALF-MILD STEEL GUIDE TUBE.

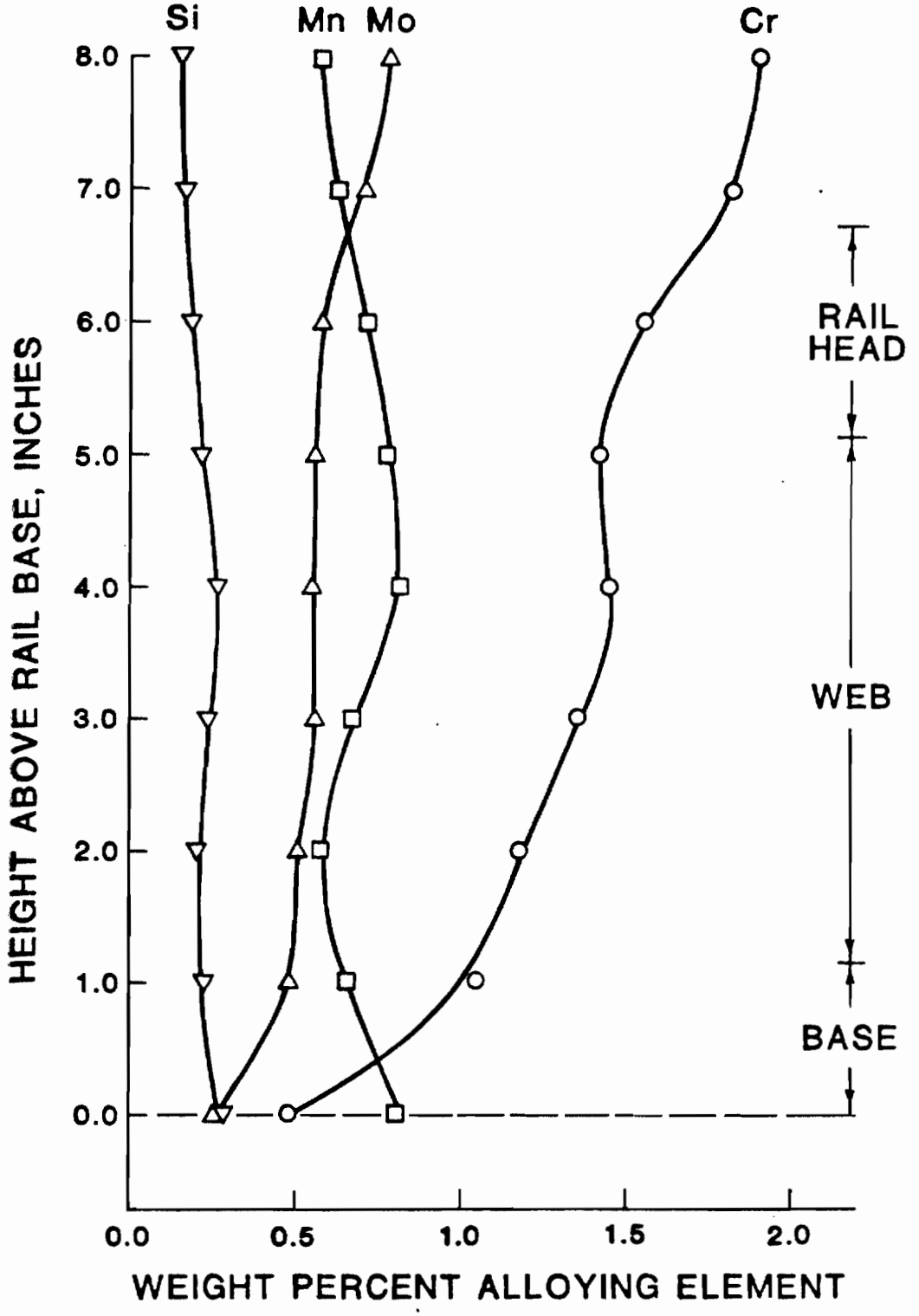

Figure 68. VARIATION IN CHEMICAL ANALYSIS OF ELECTROSLAG RAIL WELD.

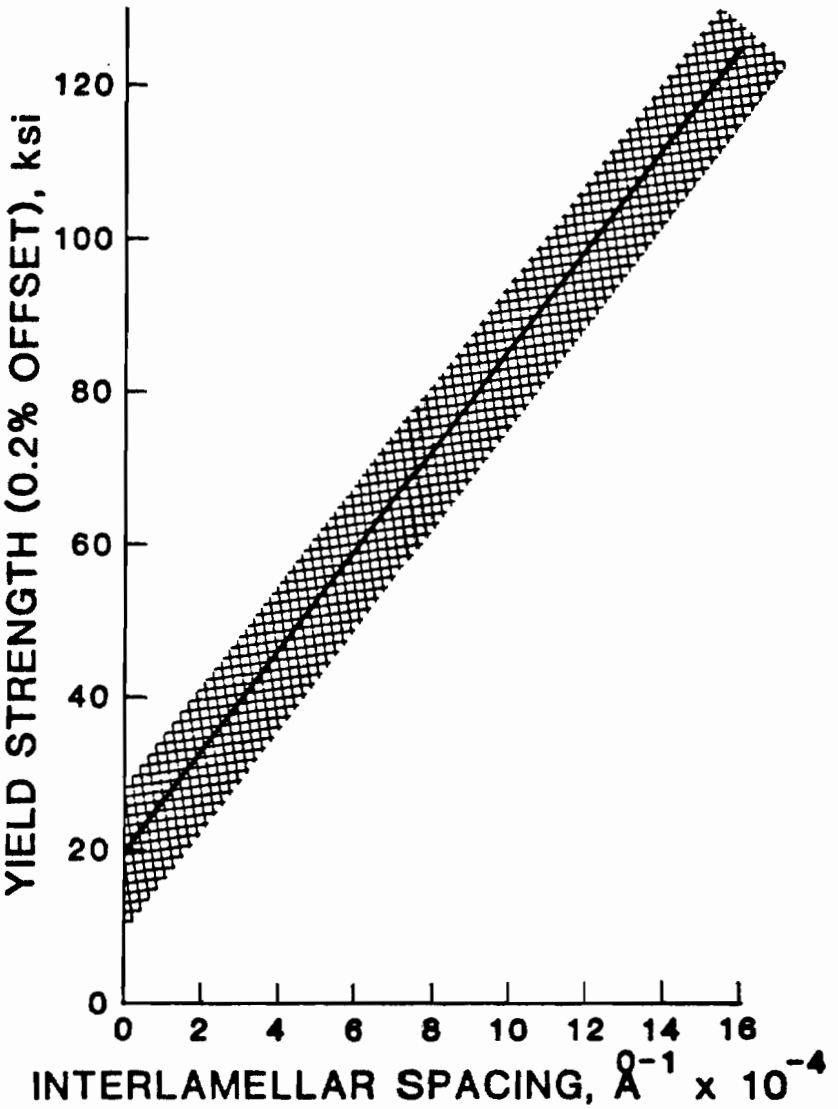

Figure 69. RELATIONSHIP BETWEEN PEARLITE INTERLAMELLAR SPACING AND YIELD STRESS.

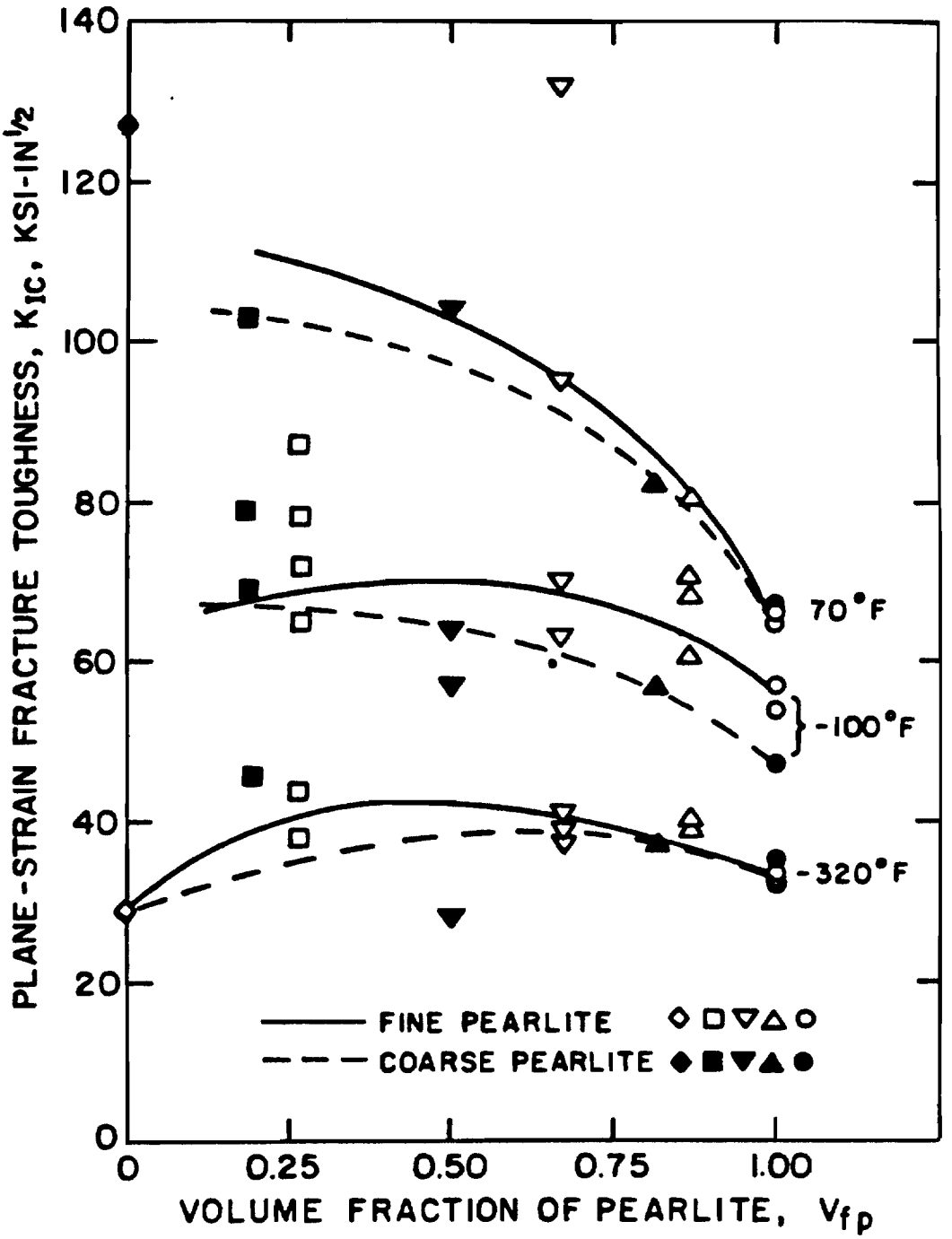

Figure 70. RELATIONSHIP BETWEEN AMOUNT OF PEARLITE AND PLANE-STRAIN FRACTURE TOUGHNESS.

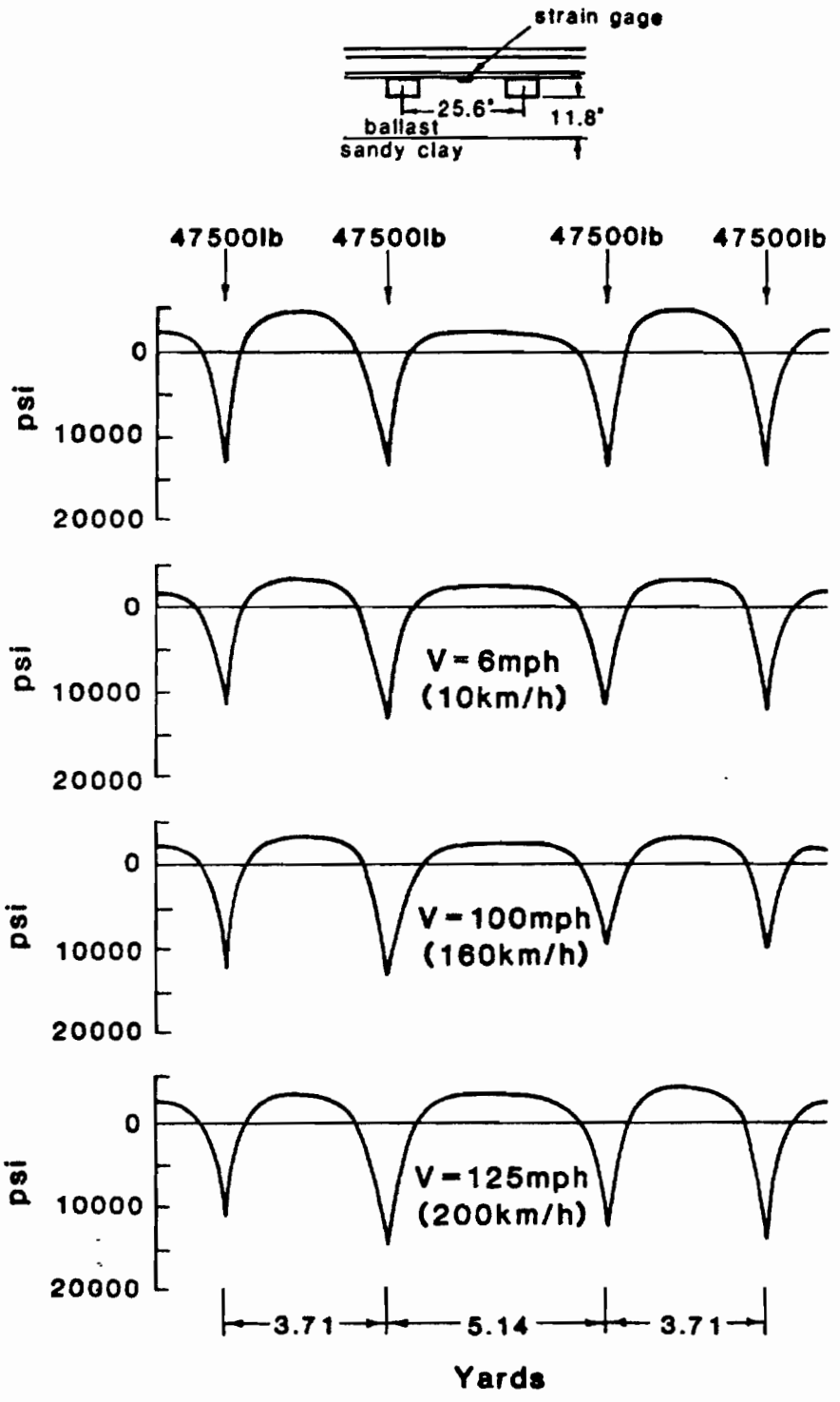

Figure 71. STRESSES SEEN AT THE RAIL BASE IN TRAFFIC.

BIOGRAPHICAL NOTE

The author was raised in the San Diego, California, area with a normal progression through the local schools before going to college at the California Polytechnic State University in San Luis Obispo. There he received his degree as a Bachelor of Science in Metallurgical and Welding Engineering, but not before acquiring a taste for antique engines and tractors and for running.

From Cal Poly, he went on up the coast to the Oregon Graduate Center to work on his Masters Degree, this thesis being the culmination of that activity.